NOPO

NGR-28-004-021

(NASA-CR-146775) PHOTOIONIZATION OF ATOMS AND MOLECULES (Nebraska Univ.) 123 p HC $5.50 CSCL 20H

N76-22000

Unclas
G3/72 21536

PHOTOIONIZATION OF ATOMS AND MOLECULES

James A. R. Samson

Behlen Laboratory of Physics, University of Nebraska,
Lincoln, NE 68588

April 5, 1976

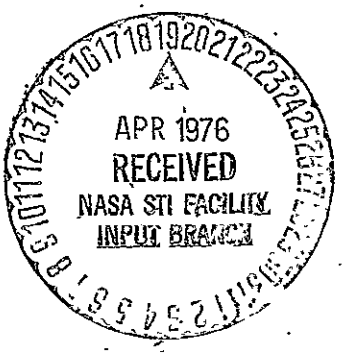

To: PHYSICS REPORTS
North-Holland
Publishing Co.
Amsterdam

PHOTOIONIZATION OF ATOMS AND MOLECULES

		page
1.	Introduction	1
2.	Experimental techniques	3
	2.1. Total absorption cross sections	4
	2.2. Photoionization cross section	7
	2.3. Photoionization mass spectroscopy	8
	2.4. Photoelectron spectroscopy	10
	2.5. Fluorescence spectroscopy	14
3.	Ionization potentials	16
4.	Photoionization of molecules	20
	4.1. Hydrogen	21
	4.2. Dissociative-ionization	26
	4.3. Multiple ionization	29
	4.4. Branching ratios	30
	4.5. Electron impact "photoionization"	31
5.	Photoionization of atoms	33
	5.1. Helium	35
	5.2. Xenon	36
	5.3. Multiple ionization	39
6.	Specialized photoionization	42
	6.1. Positive and negative ions	42
	6.2. Excited states	43
	6.3. Free Radicals	44
7.	Photoelectron angular distribution	46
8.	Discussion	49
9.	References	50

1. Introduction

The field of photoionization is one area of the more general problem of understanding how radiation interacts with atoms and molecules. For most atoms and molecules photoionization occurs for photon energies greater than 10 eV. That is, in the spectral region of the vacuum ultraviolet. Understanding of the interaction mechanisms is important to such fields as plasma physics, atomic and molecular physics, aeronomy, and astrophysics.

The primary processes in photoionization are (a) direct ionization into the continuum, with or without excitation of the ion, (b) direct dissociative ionization, and (c) direct multiple ionization. Secondary processes occur such as, fluorescence from the excited states of the ions, subsequent dissociation from an otherwise stable state of the ion (predissociation), and multiple ionization through Auger processes. Knowledge of both these primary and secondary processes are extremely valuable to many fields of science. The goal in experimental photoionization studies is to determine the absolute interaction cross section for each of the specific processes. From the theoretical point of view it is desired to be able to calculate the probability of any specific photoionization event. In any calculation, however, it is necessary to understand the interaction mechanisms in order to perform reasonable calculations. For example, does the photon field interact simply with one electron in an atom or with several? Is the out-going photoelectron influenced by electrons from within the same

shell or in other shells? From the large body of recent theoretical results it would appear that a single electron model is suitable for inner-shell ionization[1]. However, for lower photon energies where the interactions occur in the valence shells it would appear that collective processes are taking place and calculations based on a many-body theory are necessary. To reconcile the various theoretical approximations it is necessary to obtain results for the partial cross sections. Considerable progress has been made along these lines within the last five years.

It is the purpose of this report to review the current status of Photoionization. A description of the various techniques that have been developed to study photoionization will be given. Selected atoms and molecules will be chosen to illustrate these techniques and to show the present state of our knowledge in this field.

2. Experimental Techniques

The products of photoionization guide us to the various techniques that can be used to determine specific absorption processes. The most important products are the ions and electrons. Mass spectroscopy is used to identify unambiguously the ions that are produced. Measurements of the ion and electron kinetic energies lead to the fields of photoelectron and photoion spectroscopy. Where fluorescence is present it is possible to measure the competing processes of autoionization and fluorescent de-excitation. In determining partial cross sections care must be taken not to count secondary reactions in the primary photoionization partial cross section. For example, the partial cross section for producing a specific ionized state of a molecule can be determined using the technique of photoelectron spectroscopy. However, if the molecular ion then predissociates the partial cross sections obtained by mass spectroscopy should not be considered as a primary process.

Central to the entire process of obtaining partial cross sections σ_j is the precise determination of total absorption cross sections σ_t. This can be expressed by the relation

$$\sigma_j = \sigma_t \cdot \gamma \frac{N_j}{\sum_j N_j} , \qquad (2.1)$$

Where γ is the photoionization yield, defined as ions produced per photons absorbed. N_j represents either the number of electrons

ejected from the state j or the number of fragment ions of mass j, and ΣN_j represents either the total number of primary electrons ejected or the total number of ions of all masses produced. Thus, total absorption cross sections and ionization yields of gases must be measured before it is possible to determine absolute partial cross sections.

2.1. Total Absorption Cross Sections

The traditional method of measuring absorption cross sections is to measure the intensity of the radiation passing through an absorption cell before and after filling the cell with a gas. The absorption cross section is then given by

$$\sigma = (1/nL) \ln (I/I_0), \qquad (2.2)$$

where n is the number density of the gas, L is the path length traversed, I_0 and I are the intensities of the radiation before and after filling the cell with gas, respectively. One drawback of this method is that there is a delay in time in measuring I_0 and then I. During this interval the intensity of the incident radiation may vary. Thus, techniques have been devised to bring the methods of double beam or split beam spectrophotometry, used in the visible region of the spectrum, to operate in the vacuum uv region[2-5]. From the point of view of photoionization this usually means that window materials cannot be tolerated and absorption cells must be used with a continuous flow of gas. Thus, only the split beam types as used by Boursey, et al.[3] and Hudson [5] are suitable for work below 1000 Å. The split beam spectrophotometers consist generally of a mesh placed at 45° in the incident light path and located in front of the entrance to the absorption cell. The mesh is coated with sodium

salicylate[6] and the fluorescent light is observed with a photomultiplier at right angles to the direction of the ionizing radiation. The transmitted radiation is viewed by a second photomultiplier. The two multipliers are matched and adjusted to give similar readings with no gas in the cell. The ratio of the two signals when gas is in the cell is used in eq. (2.2) to determine the total absorption cross section of the gas.

Systematic errors can arise with any method using photomultipliers owing to the possibility of fluorescence being produced in the gas. The fluorescence is usually of wavelengths longer than the ionization potential of the gas and can be detected by the photomultiplier measuring the transmitted radiation. This problem is particularly serious with CO_2.

The above problems can be eliminated by the use of a double ion chamber [7,8]. The experimental arrangement of the double ion chamber is shown in fig. 1. Because the radiation is absorbed exponentially in the gas the ion current produced along the ionizing beam also decreases exponentially. If all the ions produced above a collector electrode are collected by that electrode and if the electrodes are of equal length L, as shown in fig. 1, then the absorption cross section is given by

$$\sigma = (1/nL) \ln(i_1/i_2), \qquad (2.3)$$

where i_1 and i_2 are the ion currents produced above each electrode. The double ion chamber has all the advantages of the split beam method because i_1 and i_2 can be measured simultaneously. It is not only insensitive to fluorescence produced by the absorption process but

it is also much less sensitive to scattered light from the monochromator system. When at all possible the use of the double ion chamber is the most accurate method for measuring absorption cross sections. Of course, when the gas is a vapor that must be produced in a heat pipe or equivalent system it is usually not possible to apply the double ion chamber technique.

The accuracy in determining σ depends primarily on the precision with which the pressure and the ratio (i_1/i_2) can be measured. Probably the most accurate pressure measurements are made with precision micromanometers[9] and with capacitance manometers[10] (e.g., Baratrons). An accuracy of ± 2% or better should be obtainable. The error in $\ln (i_1/i_2)$ is typically 1 or 2 percent. This gives a standard deviation of about 2½% for the error in σ.

Systematic errors can be further minimized by the proper selection of light sources. Where structure is present in the photoionization cross section it is necessary to use a source of continuum radiation such as the Hopfield continuum[11] or synchrotron radiation. However, even with a continuum source of radiation errors will appear if the structure is very fine. This means that measurements must be made with the highest possible resolution. A major problem with continuum sources is the difficulty in determining the effects of scattered light. Thus, when measuring cross sections in the ionization continuum discrete light sources should be used whenever possible. The effects of scattered light can then be easily accounted for.

2.2 Photoionization cross sections

The photoionization cross section σ_i is a measure of the probability that an absorbed photon will produce ionization and is defined as

$$\sigma_i = Y \sigma_t \quad , \tag{2.4}$$

where Y is called the photoionization yield and is defined as the number of primary ions produced per photon absorbed. The value of Y is unity whenever a photon produces an ion regardless whether the ion is singly or multiply charged. Thus, for atoms the photoionization cross sections and total absorption cross sections are synonomous. We are neglecting the effects of scattering because this is only important in the x-ray region of the spectrum. For molecules, however, many more channels are open and the yield is generally less than unity near the ionization threshold.

The measurement of photoionization cross sections requires a measurement of the absolute intensity of the ionizing radiation. In the past this was difficult to do in the vacuum ultraviolet region of the spectrum. Traditionally, a calibrated thermocouple was used to determine radiant energy in the visible and infrared spectral regions. However, in the vacuum uv where the intensity of light sources are generally weaker than in the visible, measurements with a thermocouple are extremely tedious and inaccurate. With the development of the double ion chamber for absolute intensity measurements the situation is very much better [7, 12]. With a carefully constructed double ion chamber, similar to that shown in fig. 1, the absolute intensity of the ionizing radiation is given by

$$I_0 = \left(\frac{1}{Y}\right) \frac{i_1^2/e}{(i_1 - i_2)} \tag{2.5}$$

where Y is the ionization efficiency, defined as the number of charges produced per photon absorbed. For atoms Y = 1 between the thresholds for single and double ionization. Beyond the threshold for double ionization Y > 1.

e is the electronic charge and i_1 and i_2 are the ion currents collected by the two electrodes. Equation (2.5) implies that the efficiency must be known. This is true, however, as mentioned above the ionization efficiency λ of an atom must be unity between the onset for ionization and the double ionization threshold. Normally, the rare gases are used in the double ionization chamber. Thus, in eq. (2.5) we can set $Y = 1$. To extend this technique to shorter wavelengths we must know the effects of multiple ionization. These have been measured down to about 40 Å[13-15].

For convenience, secondary standards such as photo-diodes can be calibrated against the double ion chamber[16]. This is the procedure now adopted by the National Bureau of Standards[17].

The ionization yield of a molecule is measured by flowing the molecular gas under consideration into the double ion chamber. The intensity of the radiation, I_0, can then be determined either with a calibrated photo-diode or simply by repeating the experiment with a rare gas.

2.3 Photoionization Mass Spectrometers

Having determined the probability that a photon will cause ionization the question arises concerning the state of the ion. Did the ionizing event cause single or multiple ionization, did dissociative ionization occur, or was the ion left in some state of excitation? The problem of dissociative and multiple ionization can best be studied with a mass spectrometer.

The use of a photon source to produce ions in the ion chamber of a mass spectrometer dates back to 1930. At that time Terenin and co-workers[18-20] photoionized thallium iodide vapor in the spectral

region of 2000 to 2200 Å. Virtually no more work was done along these lines until 1956 and 1957 when Lossing and Tanaka[21] and Herzog and Marmo[22] used undispersed H_2 light sources with LiF windows to produce ions within a mass spectrometer. This provided an ionizing energy band of about 9 to 11.3 eV (1400 to 1100 Å). Thereafter, photoionization with mass analysis and variable wavelengths developed rapidly[23-33].

A typical arrangement of light source, vacuum monochromator, and mass spectrometer is shown in Fig. 2. Magnetic sector, quadrupole, and time of flight mass spectrometers have all been used with photoionization sources. All have their advantages. However, the prime problem to be solved with any mass analyzer is the discrimination against ions formed with kinetic energy. In the dissociative ionization process the fragment ions can be formed with several electron volts of energy, whereas, the parent ion is formed simply with its room temperature energy of about 0.025 eV. This usually causes severe discrimination in the mass spectrometer. Most of the measurements to date do not correct for this discrimination and the published data must represent a lower limit to the amount of dissociative ionization. The one exception to this is the recent work of Fryar and Browning[33]. Their system was designed and studied with the express purpose of providing absolute branching ratios of the ionized fragments. This is done, essentially, by using a very large extraction field (about 1 to 2 kV).

Another problem in the use of mass spectrometers is the discrimination experienced by the ion detector--usually a windowless electron multiplier. The detection efficiency varies with the amount of charge per ion, mass of the ion, and molecular arrangement (i.e., diatomic, triatomic, etc.). These effects have been studied in detail by

Inghram[34] and Schram, et al[35]. For example, Schram has shown that atomic ions of various charges, but all with the same velocity, will be detected with equal efficiencies.

Photoionization with mass analysis is extremely important even if just to understand what channels are available in the photoionization process. But to determine absolute branching ratios great care must be exercised. To date, very little has been done in this direction. Anothe important but neglected area is the measurement of the kinetic energies of the ion fragments simultaneously with mass analysis. Also, coincidence measurements of the photoelectron energy and ion are extremely useful. A few results have been obtained by Eland[36,37]. In most cases, simply studying the kinetic energy spectrum of the photoelectrons provides a wealth of information. However, coincidences techniques with mass analysis allows information on direct dissociative ionization process in contrast to ionization with subsequent predissociation.

Although mass analysis does provide some information on the various channels open to photoionization it gives no information on the state of excitation produced in the ions. This information can best be determined by the technique of photoelectron spectroscopy.

2.4 Photoelectron Spectroscopy

Photoelectron spectroscopy is a relative new technique. Work in this field was first described by Vilesov, et al[39] in 1961 and independently by Turner[40] in 1962. The principle of this method is as follows. In the photoionization process a photon of energy $h\nu$ will eject an electron with a specific energy. The residual ion will also be given some energy. However, since momentum is conserved the

energy partition between the electron and the ion is in the inverse ratio of their masses. Therefore, practically all of the energy is carried away by the electron. Thus, the energy of a particular photoelectron is given by,

$$E_j = h\nu - I_j, \qquad (2.6)$$

where hν represents the photon energy and I_j represents the j^{th} ionization level of the atom or molecule. This level could be a specific rotational level of a particular vibrational and electronic state of the molecular ion. Therefore, knowledge of both the electron energy and photon energy is sufficient to obtain precise information regarding the energy levels of an atom or molecule. As can be seen from eq. (2.1), once the total absorption cross sections and the photoionization yields are known then all that remains to be measured in order to find the partial photoionization cross sections is the ratio $N_j/\Sigma N_j$. This ratio is known as the Branching Ratio, that is, it is the number of electrons ejected from a specific state divided by the total number of electrons ejected from all states by a photon of a given energy.

Photoelectron spectroscopy is the technique to use in determining the state of excitation produced in the residual ion. When fragmentation or multiple ionization occurs the electrons are ejected with a broad continuum of energy. In many cases these continua are difficult to observe above a scattered electron background, in which case, the technique of mass analysis is best used.

Many types of electron energy analyzers have been described for measuring E_j[40-44]. However, all analyzers sample only a small fraction of the electrons produced, usually in an acceptance cone of 3 to 6°.

One of the most sensitive differential electron energy analyzers is the cylindrical mirror[45-47]. In this case the acceptance angle is 6° x 360°. A schematic of a cylindrical mirror analyzer is shown in fig. 3 with the light beam incident on axis. A typical photoelectron spectrum of O_2 is shown in fig. 4 and illustrates the beautiful way in which the energies of the molecular orbitals are displayed on a linear energy scale. In this case monochromatic radiation of 584 Å (21.22 eV) was used to ionize O_2. But in addition to giving the energies of the vibrational and electronic levels, the peak heights in the spectrum give the transition probabilities for entering each state. However, this is only true provided the collecting efficiency of the analyzer, operating at that specific angle, is constant for all electron energies. In general, this is not the case. There are two main reasons for this. First, low energy electrons are more affected by contact potentials, stray magnetic fields, and fringing electric fields than are the higher energy electrons. Secondly, photoelectrons are ejected with specific angular distributions that depend upon their energy and upon the orbit from which they are ejected (i.e., upon their angular momentum state). Thus, it is necessary to correct for these two problems in order to obtain meaningful branching ratios.

The first correction to be made is for the varying angular distribution of the photoelectrons. It has been shown theoretically[48,49] that for dipole transitions the number of electrons N_j ejected per unit solid angle in a specific direction by plane polarized radiation is given by

$$N_j \propto (\sigma_j/4\pi)[1 + \beta P_2(\cos\theta)], \qquad (2.7)$$

where β is an asymmetry parameter that can take on values ranging from -1 to +2, θ is the angle between the electric vector and the photon direction, and $P_2(\cos\theta) = 3/2\cos^2\theta - \frac{1}{2}$. Equation (2.7) has been generalized[50-52] to include the case of partially polarized or elliptically polarized radiation and takes the form

$$N_j \propto (\sigma_j/4\pi)\left[1+\tfrac{1}{2}\beta\left\{\frac{3}{g+1}\left(g\cos^2\theta_x+\cos^2\theta_y\right)-1\right\}\right] \qquad (2.8)$$

where g is defined by the ration I_x/I_y; I_x being the intensity of the radiation vibrating along the x-axis and I_y the intensity vibrating along the y-axis. The angles θ_x and θ_y refer to the direction of the photoelectron with respect to the x and y-axes, respectively, as shown in fig. 5. Either the x or y axis must be oriented parallel to the direction of maximum polarization. The general expression in eq. (2.8) is necessary because most vacuum ultraviolet monochromators produce partially polarized radiation and synchrotron light sources are all elliptically polarized. When $\theta_x = \theta_y = 54°44'$ the expression containing β in eq. (2.8) vanishes and the number of electrons observed is independent of their angular distribution. Thus, all analyzers should observe electrons at this "magic angle" in order to remove the effects of varying angular distributions. Unfortunately, most measurements reported in the literature have not been made at this angle and care must be taken when comparisons are made between electron groups of quite different energies. If the angle of observation and β are known then eq. (2.8) can be used to correct Nj.

If an electron enrgy analyzer is used at 54°44' then its luminosity, defined as the fraction of the total number of electrons produced that

are detected, can be measured as a function of electron energy by studying the photoionization of the rare gases as a function of wavelength. The ratio of the photoelectron signal to the incident light intensity should be proportional to the known total photoionization cross section[8]. Any deviations constitute the necessary correction factors. This technique has been described in detail by Gardner and Samson[53]. Data produced by a calibrated analyzer can then be used as a secondary standard to calibrate any other type of analyzer. Accurate branching ratios for N_2, CO, CO_2, and O_2 produced by the 584 Å line have been published expressly for use as a secondary standard[54].

If the electron energy analyzer is equipped with a retarding/accelerating lens, as shown in fig. 3 then it is possible to obtain a fairly accurate calibration by the inverted pass curve method[53,55].

2.5 Fluorescence Spectroscopy

Knowledge of the probability for producing fluorescence in a gas by photon bombardment is very valuable for many fields of physics. Although it is a secondary mechanism in the photoionization process fluorescence measurements can aid substantially in our understanding of the photon-atom interaction process. For example, there is a lack of detailed information regarding repulsive states of molecular ions. For a direct transition into a repulsive state the fragments may be in excited states, such as

$$N_2 + h\nu \rightarrow N^+ + N^* + e$$
$$\rightarrow N^{+*} + N + e.$$

Identification of the fluorescent wavelengths uniquely identifies the process taking place. In the case of atoms, super excited states exist

above the ionization threshold. Many of these states autoionize completely. Some do not. A quantitative measure of the fluorescence emitted gives information about the competing processes. Some research has been done in this area, pioneered primarily by Judge and his group [56].

3. Ionization Potentials

The first ionization potentials of virtually all atoms up to Z = 95 have been measured. The only exceptions are At, Fr, Th, Pa, U, and Np. The ionization potentials have been tabulated by Moore[57], not only for the neutral atoms, but for ions in higher states of ionization. These values have been obtained from observed optical spectra both in emission and absorption.

The binding energies of electrons in free atoms have been tabulated by Lotz[58]. Although the data cover all the elements up to Z = 108 many values are calculated, extrapolated, or obtained from elements in the solid state. Thus, the accuracy of the binding energies is less than that for ionization potentials, which is typically 1 to 10 meV. Lotz estimates that the error in the worst case is no more than 2 eV. With the advent of photoelectron spectroscopy it is expected that this error can be reduced.

The most precise method for obtaining the ionization potential of a gas is the spectroscopic method. A series of Rydberg states must be identified and the limit of such a series gives the ionization potential. For a molecule the energy of the series limit, the so called "adiabatic" ionization potential represents the energy between the ground state of the molecule (with v" = 0 and J" = 0). And the specific electronic state of the ion (v' = 0 and J' = 0). The Rydberg formula is

$$T(n) = T(\infty) - \frac{109737.31}{(n-\delta)^2} \ \text{cm}^{-1}, \qquad (3.1)$$

where T(n) is the observed term value or wavenumber of the n th Rydberg State. $T(\infty)$ is the limit of the series $n\to\infty$ and represents the removal of an electron, that is, the ionization potential of the molecule. The quantity δ is called the quantum defect and represents the deviation of the molecular Rydberg series from the ideal case of atomic hydrogen. The constant 109737 cm^{-1} is the Rydberg constant for an infinite mass (R_∞). The most precise value of this constant is given by Cohen and DuMond[59] as R_∞ = 109737.31 cm^{-1}.

An extremely large compendium of molecular ionization potentials and appearance potentials has been given by Franklin, et al[60].

Although spectroscopic values provide the most precise values of the ionization potential large errors have been propogated in the literature because an author will often take the wavelength of a series limit expressed in electron volts (in the original publication) and convert this value to a wavelength expressed in angstroms. Unfortunately, the conversion factor used in the original publication is generally different from that used by a later author to convert electron volts back to angstroms. In some cases an author may report his results in electron volts but omit recording his conversion factor. It is perhaps useful then to tabulate the various values of this conversion factor as it has appeared in the past (see Table 1).

It is not always possible to identify Rydberg series in a molecular absorption spectrum. For example, no such series has yet been observed leading to the first ionization potential of O_2. This is particularly true for higher ionization potentials of more complex molecules. Where no spectroscopic values exist the technique of photoelectron spectroscopy has proved extremely valuable in providing ionization potentials. Further,

this method has provided checks on the reality of Rydberg series limits. With only one exception, Rydberg series analyses have accurately determined ionization potentials. The one exception is the α-series in NO[61]. Photoelectron spectra at many wavelengths show only the β and γ-series limit[62-65]. However, an ionization limit near the α-series limit is observed and presumably represents the limit of the Rydberg series. A photoelectron spectrum of NO taken with radiation of 462 Å is shown in fig. 6 to illustrate this point. In addition, higher ionization potentials are observed in this spectrum at 21.72 and 23.1 eV[65]

As mentioned above no Rydberg series has yet been identified leading to the first ionization potential of O_2. With such a short-coming other techniques must be chosen. For example, ionization potentials can be determined by the cyclic method, namely,

$$I\ (AB) = I\ (A) + D_0\ (AB) - D_0\ (AB^+), \qquad (3.2)$$

where I (AB) represents the first ionization potential of the molecule AB, I (A) is the ionization potential of the atom A, D_0 (AB) and D_0 (AB^+) are the dissociation energies of the neutral molecule and of the ion, respectively. This method requires accurate values of the dissociation energies. The most accurate method to determine ionization potentials in the absence of a Rydberg series analysis is that of photoelectron spectroscopy. Figure 7 illustrates a portion of the photoelectron spectrum of O_2 taken with the NeI line at 736 Å. Xenon gas is included with the O_2 to act as a calibration line. The doublet nature of the $X^2\Pi$ ionic state is clearly evident in each vibrational peak. Figure 8 illustrates the v = o photoelectron peak of O_2 taken with 920 Å radiation. The photoelectron energy resolution was about 8 meV. The position of the

$^2\Pi_{\frac{1}{2}}$ peak could be determined accurately with reference to the Xe calibration line. By analyzing the shape of the peak in terms of unresolved rotational lines the true ionization potential is seen to lie 2 meV lower than the peak value, namely at 12.071 eV.

4. Photoionization of Molecules

Until recently, quantitative measurements on the photoionization of molecules were concerned, primarily, with total photoionization cross sections and ionization potentials. Certainly, qualitative measurements had been carried out on fragmentation processes[24]. However, although these results only gave lower limits to dissociative ionization processes they did reveal some of the channels available to photoionization. Within the last ten years dramatic strides have been made in accurate measurements of the vibrational distributions (Franck-Condon factors), electronic transition probabilities, and dissociative ionization of a few molecules. Also, the role and identification of autoionizing states in molecules is beginning to be understood. This has all come about by a careful application of the experimental techniques described in Section 2. Although each technique is indispensable, the latest technique, namely, photoelectron spectroscopy has proved to be extremely powerful. Without it, it is nearly impossible to measure transition probabilities to vibrational and electronic states of the ion.

Ten years ago very few molecular calculations existed on photoionization[66-69]. With the advent of good experimental data and advanced theoretical methods more analyses are being made[70-80]. However, most of these calculations concern molecular hydrogen.

To illustrate our present knowledge of molecular photoionization some specific molecules and measurements will be discussed in the following sections.

4.1 H_2

Surprisingly, very few measurements of the photoionization cross sections of molecular hydrogen have been made. The pioneering measurements of Wainfan et al[81] show considerable scatter and were made at only a few discrete wavelengths between 480 and 804 Å. More detailed measurements were made by Cook and Metzger[82] from threshold to 600 Å and by Samson and Cairns[83] from 209 to 452 Å. Denne[84] extended the measurements from 80 to 23 Å. Recently, Samson and Haddad[85] have measured the cross sections from threshold to 100 Å with an accuracy of ± three percent. These results are shown in fig. 9 along with the experimental results of Denne[84]. Between 700 and 800 Å a large number of absorption and autoionizing lines exist that mask the vibrational steps in the photoionization spectrum. However, these steps are estimated from known Franck-Condon factors and the maximum cross section at 700 Å. Because a discrete line source was used only a few of the autoionizing lines are observed in this spectrum. For wavelengths shorter than 700 Å the absorption is continuous.

The first significant calculations were made by Flannery and Öpik[70] in the vicinity of the ionization threshold. Compared with the data of fig. 9 their calculated values at the maximum of the curve at 700 Å are about 17% high. More sophisticated calculations by Kelly[77] are only 6% too high at 700 Å when the dipole length form is used in his calculations. Over the entire range of his calculations (threshold to 400 Å) the experimental data are bounded by the dipole length and velocity approximations.

The most recent calculation and the one that agrees most closely with experiment is that by Martin et al[75] (see fig. 9). Their calculation was based on the random phase approximation. At 700 Å there is

precise agreement with experiment, namely, 9.7×10^{-18} cm^2. There is excellent agreement over the whole spectral range within ± seven percent. However, this deviation is significant considering the absolute error in the experimental data is quoted at ± three percent.

The photoelectron spectrum of H_2 provides the vibrational intensity distribution or Franck-Condon factors. To observe all the vibrational levels photon energies in excess of 18.1 eV are required. Usually the 584 Å HeI line is used (21.22 eV). A typical 584 Å spectrum, taken with 30 mV resolution, is shown in fig. 10. Vibrational quanta up to v = 15 can be observed. Several such spectra have been reported in the literature[86-90]. However, it is important to have a calibrated electron energy analyzer to determine accurately the Franck-Condon factors over such a large energy range. Table 2 gives the observed intensity distribution after the calibration has been applied[90]. Higher resolution reveals the rotational structure. Figure 11 shows a spectrum with a resolution of 8 mV taken with the NeI 736 Å line. Because a monochromator was used the second line of NeI, namely the 744 Å line, did not interfere with the spectrum. The rotational spectrum has also been obtained by Åsbrink[89] and by Niehaus and Ruf[91] using undispersed Ne radiation. The rotational lines are seen more clearly in fig. 12 for the v = 5 and 6 vibrational lines. The Q-branch ($\Delta N = 0$) dominates the transitions. The photoelectron spectrum verifies the rotational selection rule of $\Delta N = 0$ or 2 for the photoionization of H_2 as derived from analysis of H_2 absorption spectra[92]. Rotational selection rules have not been enunciated, in general, for photoionization of molecules. Unfortunately, the separation of rotational lines in most molecules is too small to be clearly resolved in photoelectron spectra.

The vibrational intensity distribution should be practically insensitive to the energy of the exciting radiation. However, when transitions into the ionization continuum proceed via autoionizing transitions the normal Franck-Condon factors do not hold. This is the case for the 736 Å radiation.

Numerous absorption lines exist in H_2 between 700 and 804 Å but not all of them autoionize. Photoionization yield measurements can determine the fraction of photons absorbed by a line that will produce ions. However, the fate of H_2 can be further determined by observing the fluorescence produced by the non-autoionizing lines. These absorption processes tend to cause dissociation of the molecule leaving one atom of hydrogen excited to radiate the Lyman alpha line at 1216 Å [93, 94].

Mass analysis has been applied to the photoionization of H_2 [33, 95-101]. This provides information on the fragmentation process and on autoionization near threshold. Considering first the study of the autoionizing structure, it would seem unnecessary to use mass analysis, especially near the ionization threshold. This is indeed true. However, by using mass analysis any problem of impurity ionization is eliminated. The most detailed study of the autoionizing structure has been carried out by Chupka and Berkowitz [98, 99] and by Chupka and Dehmer [100]. With a wavelength resolution of 0.04 to 0.016 Å and a continuum light source, rotational structure was clearly resolved. Ordinary hydrogen and para-hydrogen were studied, both at room temperature and at 78°K. This allowed accurate identification of rotational levels and Rydberg series. The most striking observation is the weakness of the direct continuum ionization in contrast to the autoionizing structure. Some of the results are reproduced in figs. 13-15. Figure 13 show the spectral region near

the ionization threshold of 803.7 Å. The lower spectrum shows the relative photoionization cross section and the upper shows the relative total absorption cross section. Ionization appears before the threshold because of a lowering of the ionization potential by the P and Q branches for transitions starting from J values > 0. A more extended spectrum of the relative photoionization cross section is shown in Fig. 14 for ordinary H_2 at 78°K. This eliminates rotational levels with J > 1 in the ground state of H_2 and thus removes some of the ionization observed before the true threshold. However, because in ordinary H_2 three-fourths of the molecules are in odd levels (ortho-H_2) and one-fourth in even levels (para-H_2) the transitions with J = 1 are not eliminated and a group of autoionizing lines are observed in the vicinity of 804 Å. However, when pure para-H_2 is ionized at 78°K as shown in Fig. 15, only J = 0 states are available and the group of autoionizing lines at 804 Å disappear, clearly indicating the origin of these transitions. The detailed analyses of the structure observed provides valuable and complimentary data to the absorption spectral analysis of Namioka[102] and Monfils[103] in the same spectral region.

The second application of mass analysis to the photoionization of H_2 is the study of dissociative ionization. Figure 16 gives the potential energy curves of H_2 and H_2^+ illustrating the Franck-Condon region of most probable transitions. There is a small probability of dissociative ionization occuring from the $X\ ^2\Sigma_g^+$ ($1s\sigma_g$) starting at about 18.0 eV. However, higher photon energies are necessary to reach the repulsive curves $^2\Sigma_u^+$ ($2p\sigma_u$) or $^2\Pi_u$ ($2p\pi_u$). Typically, the photon energy threshold is > 30 eV for transitions into the repulsive states. Direct measurements of H^+ have been made by Browning and Fryar[33, 101] with a mass spectrometer designed to collect the true ratio H^+/H_2^+. Over most of

the photon energy range up to 30.5 eV the ratio was constant at about two percent. At 30.5 eV the ratio increased rapidly to 5% as the $2p\sigma_u$ channel opened up and at 304 Å (40.8 eV) the ratio was 10.8% [101].

Although mass analysis unambiguously identifies that dissociative ionization is taking place and also the magnitude of dissociation it does not distinguish between transitions into the various repulsive curves. After the initial photoionization occurs electrons and ions of specific energies are emitted that are characteristic of the final levels produced in the ion. Thus, the use of both photoelectron and photoion spectroscopy can further identify the primary absorption process. Both these techniques have been used at one or two wavelengths[104,105].

The photoelectron spectrum[104] was obtained at 247 Å (50.2 eV) and clearly shows a new ionization channel opening up at about 30 eV in agreement with transitions into the $2p\sigma_u$ state. The spectra are necessarily broad because of the continuous nature of the repulsive states and details of transitions into higher lying repulsive curves are lost.

The photoion curves[105] have been deconvoluted and they suggest that at 304 Å transitions into the $2p\sigma_u$ and $2p\pi_u$ states are about of equal probability. Application of the technique of fluorescence spectroscopy at these high incident photon energies would be very valuable to further elucidate the photoionization process. For example, transitions into the $2p\pi_u$ state should produce excited H atoms radiating at 1216 Å. This area remains to be investigated.

Another type of dissociative ionization occurs in some molecules. Namely, the production of positive and negative ion pairs. This was first observed with mass analysis by Morrison et al. [106] for molecular iodine and more recently by McCulloh and Walker [107] and by Chupka et al. [108] for H_2. Measuring the threshold for ion-pair formation by the use of msss spectrometry the value of the electron affinity of atomic hydrogen has been measured accurately. A value of 0.7542 eV was obtained in the photoionization experiments in excellent agreement with the theoretical value of 0.75421 eV [109].

4.2 Dissociative Ionization

The dissociative ionization of H_2 has been discussed above under the overall context of the photoionization of H_2. However, the only transitions possible in H_2 to produce dissociative ionization are transitions to repulsive states. In this section the more general aspect of dissociative ionization will be discussed wherein stable electronic states may predissociate into ion fragments. The dissociative ionization of CO_2 will be discussed in detail.

The lowest threshold for dissociative ionization of CO_2 is 19.071 eV. This results in the formation of O^+ (^4S) and $CO(X\ ^1\Sigma^+, v = 0)$. An energy level diagram of CO_2^+ is shown in fig. 17 illustrating the relationship of several dissociation limits relative to the electronic states of CO_2^+.

The first mass analysis study of the photoionization of CO_2 was carried out by Weissler et al.[24] at several discrete emission lines between 430 and 900 Å. Both the O^+ and CO^+ fragments were observed. More recently McCulloh [110] and Dibeler and Walker [111] have studied the fragmentation with a continuum light source (600 - 900 Å). Fryar and Browning[33] have reported data at 584 and 304 Å and Van Brunt et al [112] at 44, 9.9, and 8.2 Å.

The continuum ionization results of Dibeler and Walker and of McCulloh are shown in figs. 18 and 19, respectively. In fig. 18 the relative photoionization efficiency curve for the production of CO_2^+ ions is shown from the ionization threshold down to 600 Å. A large number of autoionizing lines are observed that form Rydberg series terminating on the various electronic states of the ion. In addition, the appearance of O^+ ions are also shown. The fragmentation at threshold can be more easily followed from fig. 19. A weak signal of O^+ ions appears at 19.07 eV. At higher energies the yield of O^+ ions is modulated with

a Rydberg series leading up to the $C(^2\Sigma_g^+)$ state. Thus, the appearance of fragment O^+ ions exactly at the dissociation limit of CO_2^+ must be caused by an initial transition into high lying neutral Rydberg states that subsequently autoionize into dissociative continuua yielding $O^+(^4S) + CO(v = o)$ fragments. The dashed levels in Fig. 17 represent schematically these Rydberg states. Then precisely at 19.39 eV the yield of O^+ ions dramatically increases. This is the threshold for production of the C molecular ionic state. The interpretation of this sudden increase is that the primary absorption process is a direct ionization into the lowest vibrational level of the $C(^2\Sigma_g^+)$ state of CO_2^+, which is stable for a short period of time, then predissociation occurs giving $O^+ + CO\ (v = o)$. The C-state is stable enough to produce a photoelectron spectrum. A spectrum taken at 584 Å is shown in Fig. 20. The predissociation of the C-state was long suspected because no radiative transitions had ever been observed from this state [113]. However, predissociation was elegantly proved by a photoelectron - photoion coincidence experiment by Eland [114], who showed that the C-state completely predissociates. He estimated that the ratio O^+/CO_2^+ was 0.033. If the C-state completely predissociates but still gives a photoelectron spectrum then the photoelectron branching ratio of this state can be equated to the total fragmentation ratio $(O^+ + CO^+)/CO_2^+$. We have recently obtained a value of 0.047 for the $C\ ^2\Sigma_g^+$ branching ratio [115].

The most series problem in obtaining accurate ratios of the fragment ions with mass spectrometers is that of discrimination of ions formed with kinetic energy. So far very few measurements have been made of ion kinetic energies. The mass spectrometers used by all of the references cited above, with the exception of Fryar and Browning, are likely to discriminate against

energetic ions. However, the fragmentation of CO_2 by 584 Å obtained by these authors are compared in Table 3 along with data obtained by indirect methods. Eland's ion kinetic energy measurements show that the O^+ ions have an energy of about 0.2 eV, which is what is expected if the 584 Å radiation produces O^+ through predissociation of the C-state and not directly from a repulsive state. From Table 3 it would appear as if the fragment kinetic energies in this case are not causing too much trouble. The average of the 584 Å measurements for O^+/CO_2^+ is 4.4% and for CO^+/CO_2^+ it is 1.7 percent. At 304 Å the total fragment ratio is 36% as obtained by Fryar and Browning and 34.2% as obtained from our recent branching ratio measurements. At the higher photon energies Van Brunt et al. find a total fragmentation ratio of 36% at 44 Å, 54% at 9.9 Å, and 53% at 8.8 Å. Without knowing the kinetic energy of the fragments produced it is difficult to asses if any losses occured in their mass spectrometer. Thus, these high energy ratios can be considered as lower limits.

As we have discussed above, dissociative ionization of CO_2 proceeds most strongly through predissociation of electronic states that lie above the dissociation limits rather than by direct transitions into repulsive states. This may be a rather general phenomena. Danby and Eland [116] show that the B $^2\Sigma_g^-$ state of O_2^+ predissociates when O_2 is ionized by 584 Å. This is confirmed by photoion spectra [117, 118], which indicate complete predissociation of the B-state. In addition, photoion spectra [117] taken at 304 Å indicate predissociation of the c $^4\Sigma_u^-$ state as well as the B-state. Thus, it would appear that detailed mass analysis of photo-ionized fragments could predict the possibility of electronic states of an ion predissociating. A possible prediction can be made for NO. In

the early mass analysis study made by Weissler et al.[24] N^+ fragments were observed with a ration N^+/NO^+ of 5% with a very rapid onset at 21.8 eV. Later photoelectron spectra showed a new ionization level in NO at 21.7 eV[65]. The threshold for the process

$$NO(X\ ^2\Pi) \rightarrow N^+(^3P) + O(^3P)$$

is 21.03 eV. Thus, it would appear that no N^+ is produced until the dissociative channel at 21.7 eV opens up.

4.3 Multiple Ionization

Studies of multiple ionization of molecules have been made only at wavelengths shorter than 44 Å[112, 119]. The molecules studied were O_2, N_2, NO, CO, and CO_2. The absolute abundance of the parent ion produced at these wavelengths was small. The vast majority of the products were fragment ions. Although multiple ions were observed the absolute numbers initially formed is hard to determine because of subsequent dissociation of these ions. Table 4 lists the abundance observed for the singly and doubly charged ions. According to theoretical predictions by Hurley and Maslen[120, 121] the ground states of doubly ionized O_2, N_2, and NO are stable. Thus, observation of multiple ionization could be expected. No photoionization measurements have been reported yet near the threshold for double ionization, typically between 30 and 40 eV. However, preliminary measurements in our laboratory indicate that if double ionization occurs the population of these states must be less than one or two percent. Several electron impact measurements have been made[122, 126]. All measurements indicate a small percentage of double ionization.

4.4 Branching Ratios

The branching ratio is defined as the ratio of the number of electrons N_j ejected from a specific state j relative to the total number of electrons ejected from all states, that is, the ratio $N_j/\Sigma_j N_j$. The partial cross section σ_j is then obtained by multiplying the branching ratio with the photoionization cross section [see eq. (2.1)].

The determination of the number of electrons of a given energy is clearly the field of photoelectron spectroscopy. In this section we will describe its application to identifying ions in specific states of excitation.

In fig. 4 the photoelectron spectrum of O_2 was given for 584 Å radiation showing the production of all allowed states of O_2^+ up to 21.2 eV. In fig. 21 the spectrum is extended by using the 304 Å line of He II. Integrating the contribution of each vibrational line within an electronic state the branching ratios can be determined for direct transitions into the continuum. The intensity distribution of the vibrational levels within a given electronic state are seen to be similar for both the 584 and 304 Å spectra. They are also close to the calculated Franck-Condon factors. This is to be expected when the transitions are directly into the continuum. Quite differeat and unpredictable vibrational distributions are found when an ionic transition proceeds first into a high lying (super excited) state and then autoionizes into the continuum. This occurs when O_2 is ionized by the 736 Å NeI line (see fig. 22). Vibrational levels in the $X^2\Pi_g$ ground state of the ion can be seen from v = 0 to v = 24. The varying intensity of the vibrational envelope should provide information about the high lying neutral state of O_2 at 736 Å. The branching ratios for the two accessible states in this case are $X^2\Pi_g$ (55.8%) and $a^4\Pi_u$ (44.2%).

To accumulate branching ratios for the various states of molecules photoelectron spectra, such as those shown in figs. 4, 21, and 22, must be taken as a function of wavelength with carefully calibrated electron energy analyzers. In absorption regions, where there is a great deal of structure, continuum sources should be used. In other regions line sources are suitable. Few data have been taken with a variable wavelength [127-129]. Recently, O_2, N_2, CO and CO_2 have been studied using a line source, from their ionization threshold to 304 Å [115]. The results for CO are shown as an example [127]. The branching ratios are illustrated in fig. 23 and compared with the electron impact data of Van der Weil and Brion [130] (under certain conditions electron impact experiments can simulate photoionization data. This technique will be discussed briefly in the next section). The partial cross sections are shown in fig. 24(a) and 24(b) along with measurements obtained from fluorescent spectroscopy by Judge and Lee [131].

4.5 Electron Impact "Photoionization"

A "photon" source of variable energy is simulated by observing the energy loss of fast electrons that are scattered through a small angle after ionization of a gas. When the resulting ions are charge analyzed, and detected in coincidence with the scattered electrons it is possible to extract the relative optical oscillator strengths by applying the Born relation for electron scattering at small momentum transfers. This, in effect, simulates the total photoionization cross section [132, 133]. If instead of detecting the ions the ejected electrons are energy analyzed and detected in coincidence with the incident high energy electrons (typically 10 keV) the result is to simulate photoelectron spectroscopy and hence obtain branching ratios for the various excited states of the ions produced [130]. Finally, if the ions and photons emitted by the excited ions are detected in triple coincidence with the primary electrons fluorescence spectroscopy is simulated [134].

Hamnet et al. [135] have recently published the "photoelectron" branching ratios and partial "photoionization" cross sections for CO and N_2 by use of this technique. Their results are in excellent agreement with those obtained by a conventional photon source. The main advantage of the electron impact "optical" source is that it simulates a continuum light source and can readily be used at high energies without the necessary recourse to synchrotron radiation.

5. Photoionization of atoms

The first measurements of photoionization date back to the 1920's [136-141]. Quite naturally the first measurements were made with the alkali metals because their ionization potentials all lie between 2000 and 3000 Å. This is a straightforward spectral region in which to conduct measurements. However, serious problems arise that hinder accurate photoionization cross section measurements. Because a furnace must be used to vaporize the materials there is the problem of maintaining a uniform pressure over the absorption path length and in determining the end effects of the furnace on the path length. In addition, one requires accurate vapor pressure data to determine the number density of the atoms. Finally, there is the problem that atomic and molecular species of the vapor exist simultaneously in the absorption cell. Most of these problems have been considered by the various workers in the field [142-144], however, large error bars remain in the experimental data making it difficult for theory to decide on the various approximations that should or should not be included in a calculation.

After the basic techniques of vacuum ultroviolet spectroscopy had been developed for work below 1000 Å a start was made on the photoionization of the rare gases in the 1950's [145, 146]. Since that period the rare gases have been studied extensively. Measurements have been made from 1.5 Å to the ionization threshold for Ne, Ar, Kr, and Xe, and from 44 Å to threshold for He. This work has been reviewed up to 1966 by Samson [8]. Measurements of partial and total cross sections, of multiple ionization, and of the angular distributions of the ejected photoelectrons have been made. This large body of experimental data encouraged more detailed theoretical calculations. It was soon clear that the single electron theory and imprecise wavefunctions were insufficient to explain the experimental data in the low energy region near the photoionization threshold. Modern calculations must consider the interaction of all the electrons within

a shell and even should consider the correlations effects between different shells. The many body calculations have been making steady progress in the last ten years with different approaches to the problem by Amusia [147], Kelly [148], and Burke [149]. Overall agreement with experiment has been obtained within the 20% range. However, the absolute accuracy of the experimental data is, in some cases, in the region of ± 5%. This allows theory to contrast the effect on the cross section by including (or excluding) specific physical processes such as the polarization of the atom as the ejected electron leaves, and core relaxation, etc.

Photoionization measurements on many of the elements are difficult mainly because of the high temperatures needed to vaporize them. Where atomic beams are used the resulting low number density along with low light intensity create difficulties. The problem of low light intensity is less severe now with the availability of synchrotron radiation. Progress, however, is being made with the elements of lower melting points, such as, the alkaline earth metals, Cd, Zn, Hg, etc. and has been reviewed by Marr [150]. Fewer problems exist in obtaining photographic absorption spectra, particularly now that synchrotron radiation is available as a continuum background extending from the infrared down into the x-ray region. Spectra have been taken for nearly all the rare earths, the halides, and a few other selected atoms such as Be, Sr, U, Mn, Cu, Ag, and Cr. Most of these atoms have been studied in the spectral region from 320 to 1000 Å [151] except the halide group, which covers the region 600 to 1500 Å [152].

Quantitive measurements on the photoionization cross sections of a variety of atoms with different shell configurations (closed shells, open shells, etc.) is desirable to test the theoretical approximations. The rare gases, characterized by closed shells, have been thoroughly investigated and are, at present, the best group to compare with theory. Figure 25 presents a summary of the

cross sections for the rare gases. In the following sections two representitive atoms are chosen, namely, He and Xe to illustrate the progress that has been made both in theory and in experiment.

5.1. Helium

The photoionization cross sections of He were first measured near threshold by Lee and Weissler in 1955 [153]. Since that time numerous measurements have been made [154-159] including an evaluation made by the electron energy loss technique [160]. The precision of the measurements has been improving. However, systematic errors are always of concern and are more difficult to evaluate. Nevertheless, agreement between several research groups are within $\pm$ 5 percent of each other. Figure 26, illustrates our latest and unpublished results between 100 and 504 Å. The absolute accuracy of these results are estimated to be within $\pm$ 3%. At 206 Å and below, resonance series appear caused by two electron excitations leading to the production of He^+ ($n = 2, 3 \ldots$) [161]. The present experimental data were obtained with a source of discrete emission lines and hence do not give the actual cross sections within the resonances. This has been determined by Madden and Codling [161] using synchrotron radiation as a continuum background. Their results are shown in fig. 27 as the continuous line. The present results are shown by the discrete data points. Almost precise agreement is obtained although the techniques used were vastly different (photographic vs double ion chamber). A detailed theory for the profiles of these autoionizing transitions has been given by Fano [162].

No definitive calculation of the photoionization cross section of He has yet been made. Many calculations have been made each taking into account specific approximations for the continuum wave functions [147, 163-168]. In all cases correlations between the two electrons have been taken into account to

some degree. Several of the calculations lie within the experimental error bars, especially at threshold. A summary of some of the theoretical cross sections is shown in fig. 28. Two enclosed areas are shown, the lower one represents the dipole length (DL) and dipole velocity (DV) limits of the Hartree-Fock calculations of Stewart and Webb [163]. The upper area represents the DV and DL limits of Bell and Kingston's calculation[165]. The dashed curve with the data points is the present experimental curve (see fig. 26). Not shown in the figure are the theoretical curves of Burke and McVicar[164], which have a very small spread between the DL and DV approximations and lie wholly within the lower area curve of Stewart and Webb. Also not shown in the figure are the RPAE data of Amusia. They are in excellent agreement with experiment near threshold. However, they tend to deviate at about 400 Å and are about 10% higher than experiment at 300 Å, which is well outside of the experimental accuracy in this region. The RPA treatment of Wendin appears to give excellent results except in the immediate vicinity of threshold. All of the calculations appear to lie within ± 10% of the experimental data at all wavelengths. However, it seems desirable at this point to make a more accurate calculation of the photoionization of helium to assess the importance of some of the approximations.

There is now general agreement between the theoretical and experimental photoionization cross sections for all of the rare gases. This is particularly true of the pioneering calculations in the Random Phase approximation used by Amusia and colleagues [147]. To illustrate the progress that has been made in understanding the specific photoionization processes that can take place in a many electron atom we have chosen xenon as an example to discuss in detail.

5.2. Xenon

Figure 29 illustrates the experimental total absorption cross section of xenon as a function of wavelength from the ionization threshold down to a few Ångstrom units. Only the continuum cross sections are shown with the exception

of one datum point that coincided with a window type autoionizing resonance. In general, there are numerous autoionizing lines that lie at wavelengths shorter than 600 Å. An extensive tabulation of the position of these lines has been given by Codling and Madden [169]. Of interest is how the photon energy is shared when several channels are open to photoionization and also the explanation given by theory of the interaction process.

Calculations based on the single particle approximation show no agreement with experiment. However, calculations that include the interaction between the out-going electron and the remaining electrons within the shell show immediately good agreement with experiment. Calculations by Wendin [170] are shown in fig. 30 for both the single particle approximation and the random phase approximation involving electron correlations. There is very good agreement with experiment [8]. Better agreement is to be expected if the out-going electron is correlated with the electrons in the $5s^2$ and $4d^{10}$ shells. Amusia [147] has shown that such intershell correlations can be very important as discussed below.

In the vicinity of 524 Å it is possible to eject an outer s-shell electron from xenon. The single particle approximation predicts an almost zero s-shell cross section at this threshold. However, experimentally it is a maximum at threshold and decreases to a minimum at higher photon energies [171, 172]. By considering the interaction of the $5p^6$ and $4d^{10}$ electrons on the s-shell electrons Amusia showed that theory indeed agrees with experiment. Figure 31 shows his theoretical curves for the single particle model, the RPAE model with $4d^{10}$ intershell interaction, and the RPAE model with both the $4d^{10}$ and $5p^6$ intershell interaction. The data points are experimental data [171, 172]. There is dramatic agreement between theory and experiment only after the interaction is considered between both neighboring shells. At higher photon energies, theory predicts a

rise in the s-shell cross section in the energy range where d-shell electrons can be ejected. Figure 29 shows the extremely large total cross section associated with d-shell electron ejection. In fig. 32 Amusia's calculation of this total cross section is shown along with experimental data [173]. Good overall agreement exists between the data but discrepencies exist in some details. Notably, the theoretical maximum appears to be too high and the onset of the broad absorption peak is shifted to shorter wavelengths. RPAE calculations by Wendin [174] produce similar results except there is better agreement at the maximum and he has shown that by including core relaxation there results in a shift of the low energy part of the 4d shell absorption cross section towards lower energies. But what are the specific processes that take place within this broad resonance? By the use of photoelectron spectroscopy the partial cross sections for ejection of s, p, and d-shell electrons can be determined. This has been done by West et al [175] and their results are reproduced in fig. 33. As can be seen from the figure both the s and p-shell electrons show an increase in cross section in this energy range rather than continuing their monotonic decrease in cross section. Although the amount of increase is less than theory predicts, especially for the s-shell electrons, nevertheless it is clear evidence of the influence of the d-shell on the probability of photoionization from the s and p-shells. Further experimental evidence comes from the electron impact method of "photoionization"(see section 4.5). Here the results of Van der Wiel and Wight [176] give the partial cross sections of the $5p^6$ electrons across the 4d resonance. Their results are in substantial agreement with those of West et al.

Finally, further studies of the specific photoionization processes taking place within the 4d resonance reveals that multiple ionization competes with the other processes [177-179]. This is true particularly near the threshold for double ionization where a single photon ejects two electrons simultaneously,

whereas, at higher photon energies Auger processes take place after the ejection of a d-shell primary electron. This will be discussed briefly below.

5.3. Multiple ionization

When measuring the partial photoionization cross sections care must be taken to insure that an interaction is not considered twice. A problem can present itself in the case of multiple ionization. For example, when a 4d electron is ejected from xenon there is a high probability that as the ion relaxes an Auger electron will be ejected. This leaves a doubly charged ion. If the process is being studied with a mass spectrometer there is no way of knowing whether two $5p^6$ electrons were ejected or whether an Auger process took place. Once Auger processes are possible one needs to use photoelectron spectroscopy to sort out the various processes. This can be difficult because in a direct double ionization process the two electrons ejected will share their energy and a rather broad continuum of energies is produced. This continuum can be difficult to observe in the presence of a scattered electron background. There is, of course, no difficulty in observing the Auger electrons and identifying that process [180]. If the photon energy is less than the 4d ionization threshold then there is no ambiguity in the mass spectrometer results and true partial cross section can be obtained.

In the rare gases the production of multiple ionization is surprisingly large. For xenon, near the 4d threshold, 43% of the ions produced are doubly charged and in krypton 28% are doubly charged [178]. In figs. 34 and 35 the results of several authors for the ratio of double to single ionization is shown for He and Ar, respectively. Previously, there had been a disagreement between photon impact results and the electron impact "photoionization" technique, especially for He, Ne, and Ar [181]. This problem has now been resolved by modification of the electron impact experiments [182]. The earlier electron im-

pact data for multiple ionization of Kr and Xe [183] was in better agreement with the photoionization results than the authors realized. They had erroneously assumed that the photoionization data [8] measured the total charge produced rather than the total absorption cross section as was measured in their experiment. Thus, all discrepencies between the two methods appear to be resolved.

Few calculations of multiple ionization in the threshold region have been made. To date some calculations have been performed for He [184-186] and for Ne [187, 188]. So far there is poor agreement between theory and experiment for He. However, the Many Body Perturbation Theory approach used by Chang and Poe for Ne is in good agreement with the experimental data. A comparison of the theoretical and experimental results is shown in fig. 36. The theoretical results take into account core rearrangement, ground state correlations within the 2p-shell and between the 2s and 2p-shells, virtual Auger transitions, and inelastic internal collisions. Refinements in the theory still appear necessary to take into account the small discrepency between theory and experiment near the maximum of the curve. The various experimental data are all in excellent agreement in this region [178, 179, 182].

Multiple photoionization of atoms may be quite a probable event. The fact that very few observations of multiple ionization have been reported is probably caused by a lack of research in this area. Mass spectroscopy or photoelectron spectroscopy techniques must be used with the appropriate photon energy. Few atoms can be doubly ionized with the popular 584 Å line (21.2 eV) used in photoelectron spectroscopy. To use more energetic photons requires a more elaborate experimental arrangement, consisting of vacuum monochromators and spark light sources or synchrotron radiation. However, this is not necessary for barium, which has a single ionization threshold at 5.2 eV and a double

ionization threshold at 15.2 eV. Brehm and Buckner [189] studied the ionization of barium with a mass spectrometer and undispersed radiation from a He resonance lamp (21.2 eV photons) and a Ne resonance source (16.7 and 16.9 eV photons). They obtained the startling result that the ratio of Ba^{++}/Ba^{+} was 2.4 with the He source and only 0.25 with the Ne source. Subsequently, Brehm and Höfler and others [190-192] studied Ba with a photoelectron spectrometer. No continuum electrons were observed. However, Hotop and Mahr [191] observed Auger electrons indicating the presence of double ionization. The photoelectron spectrum of Ba at 584 Å is complicated. A large number of peaks can be explained by Ba^{+} being formed in excited states. The entire spectrum is, however, not typical in the sense that the interaction of the 584 Å photon with Ba does not simply produce ionization directly into the continuum. Instead, as can be seen from photographic absorption spectra [151] the 584 Å line falls on a large discrete absorption peak. The classification of this line is unknown at present but clearly autoionization occurs and is responsible for the complex spectrum and abnormally large quantity of Ba^{++}. Further studies of Ba^{++} need to be made as a function of wavelength.

The only other study of double photoionization was made by Parr and Inghram for ytterbium [193]. They studied the threshold behavior of double ionization for about 3 eV above the onset (18.35 eV). They found that the ionization efficiency increased linearly with photon energy, which agrees with the more recent results obtained with the rare gases [178]. A single measurement of the double ionization of ytterbium at 584 Å yielded a ratio of 6.7% for Yb^{++} relative to Yb^{+}.

6. Specialized photoionization

This is the area where the target gases are not in stable states. For example, atoms in excited states, positive or negative ion, and atoms or free radicals like atomic oxygen and OH radicals, etc. Because of the problems in producing these species little research has been accomplished in this area. Yet there are strong motives to obtain results. Data are needed for Astrophysics, upper atmosphere studies, plasma physics, and to aid theory in understanding the mechanisms of the photon interaction with the atomic electrons and the interaction of the out-going electron with the residual ion.

A brief description is given below of the present progress in photoionization of unstable species.

6.1 Positive and negative ions

A few theoretical calculations have been made on the photoionization cross sections of posivive and negative atomic ions [109, 194-198]. Because many of these calculations have not included the effects of electron correlation the results must be suspect. In the case of He^+ an exact calculation is possible and Bates [195] quotes the cross section at the ionization threshold as 1.6×10^{-18} cm^2. No experimental verifications exist. In fact no data have been obtained on the experimental cross sections of positive ions with the exception of Xe^+. Cairns and Weissler [199] obtained the cross section of Xe^+ at the single wavelength of 555 Å and quoted a value of, approximately, 16×10^{-18} cm^2.

The ionization threshold for most positive ions lies above 15 eV and, therefore, the vacuum uv spectral region must be used. In contrast, most negative ions can be ionized with photons of energy less than 2 eV. This is particularly advantageous because of the availability of lasers in this spectral region. Consequently, considerable progress has been made in the study of negative ions.

Photoionization of negative ions is generally called photodetachment. Photodetachment studies were first introduced by Branscomb and Fite [200] in 1954 using carbon arc light sources. The results obtained with these techniques have been reviewed up to the 1960's by Branscomb [201] and Smith [202]. The main results obtained were the photodetachment cross sections and electron offinities of H^- [203], O^- [204], and O_2^- [205]. The photodetachment cross sections of O^- are particularly important because practically all subsequent measurements are relative and many are put on an absolute basis by comparison with the O^- data.

From about 1967 lasers have been used frequently to study photodetachment [206-215]. One of the most important applications of lasers to this field is in photoelectron spectroscopy. A negative ion beam is irradiated with a fixed laser frequency and the resluting photoelectrons are energy analyzed. Thus, the electron affinity of the atom or molecule is obtained immediatly with a high degree of accuracy. In addition, tunable lasers have been invaluable in the study of photodetachment relative cross sections in the vicinity of threshold.

To date, studies have been made on the negative ions of O, O_2, OD, OH, H, C, CH, NH, NH_2, NO_2, SO_2, S_2, S, Si, SiH, SiH_2, Li, Na, K, Rb, Cs, Ar, He, Au, Pt, Ag, and I. However, all measurements have been made within a few eV from the ionization threshold. No measurements have yet been performed in the vacuum uv region.

6.2 Excited states

Again, the availability of lasers has made it practical to study the photoionization of atoms in excited states. Stebbings et al. [216] have measured the photoionization cross sections of metastable He and Ar near threshold, Gallagher and York [217] have studied metastable Ba, and Bradley et al [218] have investigated autoionization of excited Ba and Mg. The only non-laser studies have been those by Nygaard et al. [219] who photoionized the excited 6 ^2P states of Cs by use of

a Hg-Xe lamp.

From the theoretical side most interest has centered around He. The earliest calculations were carried out by Goldberg in 1939 [220] for transitions from the $2\,^1S$ and $2\,^3S$ metastable states of helium into the ground state of He^+. More recently, numerous calculations have been carried out [221-227], not only for transitions into the 1s state of He^+ but also into the 2s and 2p states of the ion. The calculations by Jacobs [227] predict the resonance features in the cross section for transitions from the $2\,^1S$ state into the (2s, 2p) ^1P state between 350 and 365 Å. The resonance is asymmetric and similar to that obtained by Madden and Codling [161] for ground state helium atoms at 206 Å. The experimental results of Stebbings et al. [216] only covered the threshold region (2500 to 3100Å). However, their results are in good agreement with theory and establish a threshold cross section for the He $(2\,^1S)$ state of approximately, 9.5×10^{-18} cm^2. The He $(2\,^3S) \rightarrow He^+$ cross section is about 6.5×10^{-18} cm^2.

The production of molecular excited states in large quantities is somewhat easier than in atoms. Thus, the photoionization of the lowest excited state of molecular oxygen, the O_2 $(^1\Delta_g)$ state, was first obtained by Cairns and Samson [228] by the use of conventional vacuum uv light sources. The O_2 $(^1\Delta)$ was produced with a 10% concentration by a microwave discharge in a mixture of O_2 + He. The vacuum uv absorption spectrum has been obtained by Huffman et al. [229] and the photoionization cross sections near threshold have been measured by Clark & Wayne [229(a)]. The photoelectron spectrum of O_2 $^1\Delta$ has been obtained by Jonathan and co-workers [230-232]. Dyke et al. [233] have studied the P. E. spectrum of vibrationally excited H_2 and N_2.

6.3 Free radicals

Under this heading we consider briefly transient spieces other than those described in the last two sections.

Probably the best technique for studying transient species is that of photo-

electron spectroscopy. In 1970 Jonathan and colleagues published the first photoelectron spectrum of N, O, and H [234]. All these species were produced in small quantities in the presence of the parent molecular species. Since that beginning several transient species have been studied [235-243], for example, CH_3, SO, CS, etc. and the progress in this area has been reviewed by Frost [244] up to 1974. Figure 37 shows the 584 Å P. E. spectrum of discharged O_2 clearly revealing the spectrum of atomic oxygen [243]. The relative transition probabilities can be obtained for transitions into the various excited states of the ion provided that the electron energy analyzer has been calibrated for the transmission of electrons as a function of their kinetic energies. This is the case for the spectrum shown if fig. 37. Excellent agreement is obtained with theory at this wavelength [245].

Many elements are not in the vapor phase at room temperature. Thus, a high temperature source is required to produce the desired vapors. However, an element like atomic sulpher is not readily formed when solid sulpher is vaporized unless the temperature is extremely high. Berkowitz and co-workers [246-247] formed S_2, S_3, S_5, S_6, and S_8 by heating mercury sulphide and studying the photoionization products with a mass spectrometer and more recently they have obtained a photoelectron spectrum of S_2 [248]. Dyke et al. [242] have also obtained a P. E. spectrum by simply vaporizing flowers of sulpher to a temperature of approximately 600 K. No spectrum of atomic S was obtained. The results of Dyke et al. are shown in fig. 38.

Berkowitz and co-workers have made a continuing study of high-temperature molecular vapors [248-253]. Figure 39 shows the results of the 584 Å P. E. spectrum of Cs I [250]. The $^2\Pi_{1/2,\ 3/2}$ states, caused by spin-orbit coupling, are clearly seen in the 7 to 9 eV region of the spectrum. However, vibrational structure is not resolved.

7. Photoelectron angular distribution

The direction in which a photoelectron is ejected from an atom or moecule, with respect to the direction of the incident photon, is influenced by the orbital angular momentum of the electron, the space orientation of the atom or molecule, the excess energy between the photon energy and the orbital binding energy of the electron, and on the degree of polarization of the ionizing radiation. Taking all these factors into account and using linearly polarized radiation, the angular distribution of photoelectrons ejected from atoms, randomly oriented, is described by the differential cross section [254, 255],

$$\frac{d\sigma_j}{d\Omega} = \frac{\sigma_j}{4\pi}\left[1+\beta P_2(\cos\theta)\right], \qquad (7.1)$$

where σ_j is the photoionization cross section for ejection of an electron from the jth orbital, β is the asymmetry parameter, and $P_2(\cos\theta)$ is the second order Legendre polynomial given by,

$$P_2(\cos\theta) = \tfrac{3}{2}\cos^2\theta - \tfrac{1}{2}. \qquad (7.2)$$

θ is the angle between the electric vector and the direction of the incident light. Tully et al. [256] have shown that eq. (7.1) also holds for randomly oriented molecules in the electric-dipole approximation. Samson [50-52] has generalized eq. (7.1) for ionizing radiation of any degree of polarization (including elliptically polarized radiation), namely,

$$\frac{d\sigma_j}{d\Omega} = \frac{\sigma_j}{4\pi}\left\{1-\frac{\beta}{2}\left[1-\frac{3}{2}\cos^2\theta_x\,(1+p)-\frac{3}{2}\cos^2\theta_y\,(1-p)\right]\right\}, \qquad (7.3)$$

where, p is the degree of polarization of the incident light and the angles θ_x and θ_y are defined in fig. 5. The degree of polarization p is related to g in eq. (2.8) as follows; $p = (g - 1)/(g + 1)$.

11 One of the important reasons for measuring the asymmetry parameter β is to

look for deviations from the theoretical values predicted by the one-electron approximation. Deviations are expected when electron correlations are important. Dill et al. [257] have shown that for most open-shell atoms β is further influenced by anisotropic electron-ion interactions. Dill [258] has also shown that the photoelectron angular distribution should show pronounced variations with energy across autoionizing resonances. The prediction applies to both atomic and molecular autoionization. Finally, Manson [259] has shown that oscillations in β are expected as a function of the electron kinetic energy.

From the above discussion it is obvious that the β-parameter should be measured as a function of the photoelectron energy (and hence as a function of the ionizing wavelength). While measurements of β have been made for numerous molecules at the single wavelength of 584Å [260-262] there have been no measurements made to date as a function of wavelength. For atoms the situation is different. Numerous measurements have been made at a few discrete wavelengths, including the 584Å line. However, for comparison with theory the most significant measurements have been made with continuum radiation producing electrons with energies between 0 and 70 eV from the rare gases [263-270]. These results clearly show the variation of β with electron energy. The recent work of Houlgate et al. [266, 268] verifies Manson's prediction that oscillations in β are to be expected. The data of Houlgate et al. for argon are shown in fig. 40. The solid curves are the single-electron Hartree-Fock length and velocity (HF-L and HF-V) calculations of Kennedy and Manson [271]. The dashed curve is the RPAE calculations of Amusia et al. [272], which includes electron correlation effects in the ground and excited states. Both calculations predict oscillations as a function of photoelectron energy. However, the RPAE calculation, which agrees more closely with experiment, shows the importance of including electron correlation effects. The oscillations in β have also been seen by use of the electron impact "photoionization" technique [273, 274].

The prediction of Dill [258] that the photoelectron angular distribution should show oscillations across discrete autoionizing resonances has been verified by Samson and Gardner [275] for xenon in the wavelength range of 950 to 1020 Å that is, between the $^2P_{1/2,\ 3/2}$ ionization thresholds. The experimental results and theoretical predictions are shown in fig. 41. Measurements of β across resonant structures provide a new and independent method to probe atomic and molecular dynamics.

8. Discussion.

Most of the basic tools for studying the photoionization of atoms and molecules have now been developed. Undoubtedly, the future will provide more sophisticated instrumentation and techniques. However, the present techniques allow us to measure, quantitatively, all the specific photon absorption processes. For example, single and multiple photoionization, dissociative ionization, and the partial photoionization cross sections for producing specific electronic and vibrational states. The application of photoelectron spectroscopy to this field has been mainly responsible for the accumulation of reliable and accurate partial cross sections.

The accuracy of the experimental data is now sufficiently good that meaningful comparisons can be made with the various theoretical approximations. In general, theory has not been able to predict molecular photoionization cross sections reliably. However, theory has been making substantial progress with atoms. Its progress to date clearly indicates the collective nature of the bound electrons and the necessity for using the various aspects of the many body theory. However, to aid theory in evaluating the importance of different approximations it is desirable to obtain experimental results on atoms of various types and in various conditions. For example, photoionization measurements should be made on selective open and closed shell atoms, on atoms in excited states, and on ions. Because of the problems involved in producing atoms normally in the solid state at room temperature most experimental work has been involved with closed shell atoms, that is, the rare gases.

Acknowledgement

It is with pleasure that we acknowledge the National Aeronautics and Space Administration, under Grant # NGR28-004-021, for support of our program on

References

1. J. W. Copper, Atomic Inner-Shell Processes, Vol. I (Academic Press, New York, 1975) p. 159.

2. R. G. Schmitt and R. K. Brehm, Applied Opt. 5 (1966) 1111.

3. E. Boursey, J. -Y. Roncin, H. Damany, and N. Damany, Rev. Sci. Instr. 42 (1971) 526.

4. M. Castex, J. Romand, and B. Vodar, Rev. Sci. Instr. 39 (1968) 331.

5. R. D. Hudson, Phys. Rev. 135A (1964) 1212.

6. J. A. R. Samson, Techniques of Vacuum Ultraviolet Spectroscopy (John Wiley and Sons, 1967) Chap. 7.

7. J. A. R. Samson, J. Opt. Soc. Am. 54 (1964)

8. J. A. R. Samson, Advances in Atomic and Molecular Physics, Vol. 2 (Academic Press, New York, 1966) p. 177.

9. A. M. Thomas and J. L. Cross, J. Vac. Sci. and Tech. 4 (1967) 1.

10. G. Loriot and T. Moran, Rev. Sci. Instr. 46 (1975) 140.

11. R. E. Huffman, Y. Tanaka, and J. C. Larrabee, Appl. Optics 2 (1963) 617.

12. J. A. R. Samson and G. N. Haddad, J. Opt. Soc. Am. 64 (1974) 46.

13. T. A. Carlson, Phys. Rev. 156 (1967) 142.

14. J. A. R. Samson and G. N. Haddad, Phys. Rev. Letters 33 (1974) 875.

15. V. Schmidt, N. Sander, H. Kuntzemuller, P. Dhez, F. Wuilleumier, and E. Kallne,

ref. (cont.)

Phys. Rev. A (to be published).

16. R. B. Cairns and J. A. R. Samson, J. Opt. Soc. Am. 56 (1966) 1568.

17. E. B. Saloman and D. L. Ederer, Appl. Optics. 14 (1975) 1029.

18. A. Terenin, Phys. Rev. 36 (1930) 147.

19. A. Terenin and B. Popov, Z. Physik 75 (1932) 338.

20. A. Terenin and B. Popov, Physik Z. Sowjetunion 2 (1932) 299.

21. F. P. Lossing and I. Tanaka, J. Chem. Phys. 25 (1956) 1031.

22. R. F. Herzog and F. F. Marmo, J. Chem. Phys. 27 (1957) 1202.

23. H. Hurzeler, M. G. Inghram, and J. D. Morrison, J. Chem. Phys. 28 (1958) 76.

24. G. L. Weissler, J. A. R. Samson, M. Ogawa, and G. R. Cook, J. Opt. Soc. Am. 49 (1959) 338.

25. F. J. Comes and W. Lessman, Z. Naturforsch. 19a (1964) 65.

26. F. J. Comes, Adv. Mass Spectrosc. 4 (1968) 737.

27. K. E. McCulloh, J. Chem. Phys. 59 (1973) 4250

28. P. Warneck, J. Soc. Photo-Opt. Instr. Engnrs. 9 (1971) 149.

29. G. R. Parr and J. W. Taylor, J. Mass. Spectrosc. and Ion Phys. 14 (1974) 467.

30. G. R. Parr and J. W. Taylor, Rev. Sci. Instr. 44 (1973) 1578.

31. J. Berkowitz and W. A. Chupka, J. Chem. Phys. 45 (1966) 1287.

32. V. H. Dibeler, R. M. Reese, and M. Kraus, Adv. Mass Spectrosc. 3 (1966) 471.

ref. (cont.)

33. F. Fryar and R. Browning, Planet. Space Sci. 21 (1973) 709.

34. M. G. Inghram and R. J. Hayden, A Handbook on Mass Spectroscopy, National Research Council, Washington, 1954 (Nuclear Science Series, Report No. 14).

35. B. L. Schram, A. J. H. Boerboom, W. Kleine, and J. Kistemaker, Physica 32 (1966) 749.

36. J. H. D. Eland, J. Mass Spectrosc. and Ion. Phys. 8 (1972) 143.

37. C. J. Danby and J. H. D. Eland, J. Mass Spectrosc. and Ion Phys. 8 (1972) 153.

38. F. I. Vilesov, B. L. Kurbatov, and A. N. Terenin, Dokl. Akad. Nauk. SSSR 138 (1961) 1329; 140 (1961) 797. [English transl.: Soviet Phys.—Doklady 6 (1961) 490 and 6 (1962) 883, respectively].

39. D. W. Turner, J. Chem. Phys. 37 (1962) 3007.

40. D. W. Turner, C. Baker, C. R. Brundle, Molecular Photoelectron Spectroscopy (Wiley-Interscience, New York, 1970).

41. A. D. Baker and D. Betteridge, Photoelectron Spectroscopy (Pergamon Press, New York, 1972).

42. J. H. D. Eland, Photoelectron Spectroscopy, (Halsted Press, Division of Wiley & Sons, New York, 1974).

43. K. D. Sevier, Low Energy Spectrometry (Wiley-Interscience, New York, 1972).

44. K. Sieghbahn et al. ESCA Applied to Free Molecules (North-Holland, Amsterdam, 1969).

45. M. Karras, M. Pessa, and S. Aksela, Ann. Acad. Sci. Fennical A VI, No. 289, 1968.

ref. (cont.)

46. S. Aksela, M. Karras, M. Pessa, and E. Suoninen, Rev. Sci. Instr. 41 (1970) 351.

47. D. W. O. Heddle, J. Phys. E, 4 (1971) 589.

48. C. N. Yang, Phys. Rev. 74 (1948) 764.

49. J. Cooper and R. N. Zare, Lectures in Theoretical Physics, Vol 2c (Gordon and Breach, New York, 1969) p. 317.

50. J. A. R. Samson, J. Opt. Soc. Am. 59 (1969) 356.

51. J. A. R. Samson and J. L. Gardner, J. Opt. Soc. Am. 62 (1972) 856.

52. J. A. R. Samson and A. F. Starace, J. Phys. B. 8 (1975) 1806.

53. J. L. Gardner and J. A. R. Samson, J. Electron. Spectrosc. 6 (1975) 53.

54. J. L. Gardner and J. A. R. Samson, J. Electron. Spectrosc. (to be published, 1976).

55. R. T. Poole, R. C. G. Leckey, J. Liesgang, and J. G. Jenkin, J. Phys. E 6 (1973) 226.

56. L. C. Lee, R. W. Carlson, D. L. Judge, and M. Ogawa, Chem. Phys. Letters 19 (1973) 183; J. Chem. Phys. 61 (1974) 3261; J. Chem. Phys. 63 (1975) 3987; J. Phys. B (1975).

57. C. E. Moore, Ionization Potentials and Ionization Limits Derived from the Analyses of Optical Spectra, NSRDS-NBS 34, 1970 (Superintendent of Documents, Washington, D. C. 20402).

58. W. Lotz, J. Opt. Soc. Am. 60 (1970) 206.

ref. (cont.)

59. E. R. Cohen and J. W. M. DuMond, Revs. Mod. Phys. 37 (1965) 537.

60. J. L. Franklin, J. G. Dillard, H. M. Rosenstock, J. T. Herron, K. Draxl, and F. H. Field, Ionization Potentials, Appearance Potentials, and Heats of Formation of Gaseous Positive Ions, NSRDS-NBS 26, 1969 (Superindendent of Documents, Washington, D. C. 20402).

61. Y. Tanaka, Sci. Papers I. P. C. R. 39 (1942) 456.

62. M. I. Al-Joboury and D. W. Turner, J. Chem. Soc. (1964) 4434.

63. D. W. Turner and D. P. May, J. Chem. Phys., 45 (1966) 471.

64. W. C. Price, Advances in Atomic and Molecular Physics, Vol. 10 (Academic Press, New York, 1974) p. 148.

65. J. A. R. Samson, Phys. Letters, 28A (1968) 391.

65a. J. A. R. Samson and J. L. Gardner, Can. J. Phys. 53 (1975) 1948.

66. D. R. Bates, U. Öpik, and G. Poots, Proc. Phys. Soc. (London) A66 (1953) 1113.

67. A. Dalgarno, Proc. Phys. Soc. (London) A65 (1952) 663.

68. S. Geltman, Phys. Rev. 112 (1958) 176

69. M. Shimizu, J. Phys. Soc. Japan, 15 (1960) 1440.

70. M. R. Flannery and U. Öpik, Proc. Phys. Soc. (London), 86 (1965) 491.

71. I. G. Kaplan and A. P. Markin, Doklady Akad. Nauk. SSSR 184 (1969) 66. English translation, Soviet Physics-Doklady 14 (1969) 36.

72. I. G. Kaplan and A. P. Markin, Optics and Spectrosc. 24 (1968) 475 and 25 (1968) 275.

ref, (cont.)

73. S. P. Khare, Phys. Rev. 173 (1968) 43.

74. J. P. Hernandez, Phys. Rev. 167 (1968) 108.

75. P. H. S. Martin, T. N. Rescigno, V. McKoy, and Henneker, Chem. Phys. Letters, 29 (1974) 496.

76. T. E. H. Walker and H. P. Kelly, Chem. Phys. Letters 16 (1972) 511.

77. H. P. Kelly, Chem. Phys. Letters, 20 (1973) 547.

78. H. C. Tuckwell, J. Phys. B3 (1970) 293.

79. H. C. Tuckwell, J. Quant. Spectrosc. Radiat. Transfer 11 (1971) 391.

80. C. Buzy and R. S. Berry, Phys. Rev. (in press 1976).

81. N. Wainfan, W. C. Walker, G. L. Weissler, Phys. Rev. 99 (1955) 542.

82. G. R. Cook and P. H. Metzger, J. Opt. Soc. Am. 54 (1964) 968.

83. J. A. R. Samson and R. B. Cairns, J. Opt. Soc. Am. 55 (1965) 1035.

84. D. R. Denne, J. Phys. D, 3 (1970) 1392.

85. J. A. R. Samson and G. N. Haddad, to be published (1976).

86. D. C. Frost, C. A. McDowell, and D. A. Vroom Proc. Roy. Soc. (London) A296 (1967) 566.

87. D. W. Turner, Proc. Roy. Soc. (London) A307 (1968) 15.

88. J. Berkowitz and R. Spohr, J. Electron Spectrosc. 2 (1973) 143.

89. L. Åsbrink, Chem. Phys. Letters. 7 (1970) 549.

ref. (cont.)

90. J. L. Gardner and J. A. R. Samson, J. Electron Spectrosc. 8 (1976) 123.

91. A. Niehaus and M. W. Ruf, Chem. Phys. Letters 11 (1971) 55.

92. G. Herzberg and Ch. Jungen, J. Molec. Spectrosc. 41 (1972) 425.

93. F. J. Comes and H. O. Wellern, Z. Naturforsch. 23a (1968) 881.

94. J. E. Mentall and E. P. Gentieu, J. Chem. Phys. 52 (1970) 5641.

95. V. Dibeler, R. M. Reese, M. Krauss, J. Chem. Phys. 42 (1965) 2045.

96. F. J. Comes and W. Lessmann, Z. Naturforsch. 19a (1964) 508.

97. F. J. Comes, Phys. Letters, 24a (1967) 465.

98. W. A. Chupka and J. Berkowitz, J. Chem. Phys. 48 (1968) 5726.

99. W. A. Chupka and J. Berkowitz, J. Chem. Phys. 51 (1969) 4244.

100. W. A. Chupka and P. M. Dehmer, to be published.

101. R. Browning and J. Fryar, J. Phys. B, 6 (1973) 364.

102. T. Namioka, J. Chem Phys. 40 (1964) 3154; 41 (1964) 2141; and 43 (1965) 1636.

103. A. Monfils, J. Mol. Spectrosc. 15 (1965) 265 and 25 (1968) 513.

104. J. A. R. Samson, Chem. Phys. Letters, 12 (1972) 625.

105. J. L. Gardner and J. A. R. Samson, Phys. Rev. A 12 (1975) 1404.

106. J. D. Morrison, H. Hurzler, M. G. Inghram, and H. E. Stanton, J. Chem. Phys. 33 (1960) 821.

ref. (cont.)

107. K. E. McCulloh and J. A. Walker, Chem. Phys. Letters 25 (1974) 439.

108. W. A. Chupka, P. M. Dehmer, and W. T. Jivery, J. Chem. Phys. 63 (1975) 3929.

109. C. L. Pekeris, Phys. Rev. 126 (1962) 1470.

110. K. E. McCulloh, J. Chem. Phys, 59 (1973) 4250.

111. V. H. Dibeler and J. A. Walker, J. Opt. Soc. Am. 57 (1967) 1007.

112. R. J. Van Brunt, F. W. Powell, R. G. Hirsch, and W. D. Whitehead, J. Chem. Phys. 57 (1972) 3120.

113. J. E. Hesser, J. Chem. Phys. 48 (1968) 2518.

114. J. H. D. Eland, J. Mass Spectrosc. and Ion Phys. 9 (1972) 397.

115. J. A. R. Samson and J. L. Gardner (unpublished data, 1975).

116. C. J. Danby and J. H. D. Eland, J. Mass Spectrosc. and Ion Phys. 8 (1972) 153.

117. J. L. Gardner and J. A. R. Samson, J. Chem. Phys. 62 (1975) 4460.

118. P. H. Doolittle, R. I. Schoen, and K. E. Schubert, J. Chem. Phys. 49 (1968) 5108.

119. T. A. Carlson and M. O. Krause, J. Chem. Phys. 44 (1972) 4510.

120. A. C. Hurley and V. W. Maslen, J. Chem. Phys. 34 (1961) 1919.

121. A. C. Hurley, J. Mol. Spectrosc. 9 (1962) 18.

122. H. D. Smyth, Proc. Roy. Soc. (London) A104 (1923) 121.

123. T. R. Hogness and R. W. Harkness, Phys. Rev. 32 (1928) 936.

124. A. L. Vaughan, Phys. Rev. 38 (1932) 1687.

ref. (cont.)

125. F. H. Dorman and J. D. Morrison, J. Chem. Phys. 35 (1961) 575 and 39 (1963) 1906.

126. St. Halas and B. Adanczyk, J. Mass Spectrosc. and Ion Phys. 10 (1972/1973) 157.

127. J. A. R. Samson and J. L. Gardner, J. ELectron Spectrosc. 8 (1976) 35.

128. R. I. Schoen, J. Chem.Phys. 40 (1964) 1830.

129. J. L. Bahr, A. J. Blake, J. H. Carver, J. L. Gardner, and V. Kumar, J. Quant. Spectrosc. Radiat. Transfer, 12 (1972) 59.

130. M. J. Van der Wiel and C. E. Brion, J. Electron Spectrosc. 1 (1973) 309.

131. D. L. Judge and L. C. Lee, J. Chem.Phys. 57 (1972) 455.

132. M. J. Van der Wiel, Physica 49 (1970) 411.

133. Th. M. El-Sherbini and M. J. Van der Wiel, Physica, 59 (1972) 433.

134. C. Backx, M. Klewer, and M. J. Van der Wiel, Chem. Phys. Letters 20 (1973) 100.

135. A. Hamnett, W. Stoll, and C. E. Brion, J. Electron Spectrosc. (in press, 1976).

136. G. R. Harrison, Phys. Rev. 24 (1924) 466.

137. B. Trumpy, Z. Physik 47 (1928) 804.

138. R. W. Ditchbum, Proc. Roy. Soc. (London) A117 (1928) 486.

139. F. L. Mohler and C. Boeckner, J. Res. Nat. Bur. Std. (US) 3 (1929) 303.

140. F. L. Mohler, P. D. Foote, and R. L. Chenault, Phys. Rev. 27 (1926) 37.

ref. (cont.)

141. E. O. Lawrence and N. E. Edlefsen, Phys. Rev. 34 (1926) 947.

142. R. W. Ditchburn , J. Tunstead, and J. G. Yates, Proc. Roy. Soc. (London) A181 (1943) 386.

143. G. V. Marr and D. M. Creek, Proc. Roy. Soc. (London) A304 (1968) 233.

144. R. D. Hudson and V. Carter, Phys. Rev. 139 (1965) A1426.

145. P. Lee and G. L. Weissler, Phys. Rev. 99 (1955) 540.

146. N. Axelrod and M. P. Givens, Phys. Rev. 115 (1959) 97.

147. M. Ya. Amusia and N. A. Cherepkov, Case Studies in Atomic Physics, 5 (1975) 47, and in Vacuum ultraviolet radiation physics, eds. E. Koch, R. Haensel, and C. Kunz (Pergamon-Vieweg, Braunschweig, Germany, 1974) p. 205.

148. H. P. Kelly, Adv. Theor. Phys. 2 (1968) 75 and Adv. Chem Phys. 14, (1969) 129.

149. P. G. Burke and W. D. Robb, in Adv. At. Molec. Phys. Eds. D. R. Bates and B. Bederson (Academic Press, N. Y., 1975) Vol. 11, p 144.

150. G. V. Marr, Photoionization Process in Gases (Academic Press, New York, 1967).

151. J. P. Connerade, Private communication, 1975.

152. R. E. Huffman, J. C. Larrabee, and Y. Tanaka, J. Chem. Phys. 47 (1967) 856.

153. Po Lee and G. L. Weissler, Phys. Rev. 99 (1955) 540.

154. N. N. Axelrod and M. P. Givens, Phys. Rev. 115 (1959) 97.

155. D. J. Baker, Jr., D. E. Bedo, and D. H. Tomboulian, Phys. Rev. 124 (1961) 1471.

156. J. F. Lowry, D. H. Tomboulian, and D. L. Ederer, Phys. Rev. 137 (1965) A1054.

157. F. J. Comes and A. Elzer, Z. Naturforschg. 19a (1964) 721.

ref. (cont.)

158. A. P. Lukirskii, I. A. Brytov, and T. M. Zimkina, Optics and Spectroscopy 17 (1964) 234.

159. J. A. R. Samson, J. Opt. Soc. Am. 54 (1964) 876.

160. C. E. Kuyatt and J. A. Simpson, Atomic Collision Processes, Ed. M. R. C. McDowell (North-Holland Pub. Co. Amsterdam, 1964) p. 191.

161. R. P. Madden and K. Codling, Astrophys. J. 141 (1965) 364.

162. U. Fano, Phys. Rev. 124 (1961) 1866.

163. A. L. Stewart and T. G. Webb, Proc. Phys. Soc. 82 (1963) 532.

164. P. G. Burke and D. D. McVicar, Proc. Phys. Soc. 86 (1965) 989.

165. K. L. Bell, A. E. Kingston, Proc. Phys. Soc. 90 (1967) 31.

166. E. McGuire, Phys. Rev. 161 (1967) 51 and 175 (1968) 20.

167. G. Wendin, Phys. Letters 33 A (1970) 16.

168. T. N. Rescigno, C. W. McCurdy, Jr., and V. McKoy, Phys. Rev. A 9 (1974) 2409.

169. K. Codling and R. P. Madden, J. Res. Natl. Bur. Std. 76A (1972) 1.

170. G. Wendin, J. Phys. B, 5 (1972) 110.

171. J. A. R. Samson and R. B. Cairns, Phys. Rev. 173 (1968) 80.

172. J. A. R. Samson and J. L. Gardner, Phys. Rev. Letters 33 (1974) 671.

173. R. Haensel and G. Keitel, P. Schreiber, and C. Kunz, Phys. Rev. 188 (1969) 1375.

174. G. Wendin, J. Phys. B, 6 (1973) 42.

ref. (cont.)

175. J. B. West, P. R. Woodruff, K. Codling, and R. G. Houlgate, J. Phys. B. (in press '76

176. M. J. Van der Wiel and G. R. Wight, Phys. Letters, 54A (1975) 83.

177. R. B. Cairns, H. Harrison, and R. I. Schoen, Phys. Rev. 183 (1969) 52.

178. J. A. R. Samson and G. N. Haddad, Phys. Rev. Letters 33 (1974) 875.

179. V. Schmidt, N. Sander, H. Kuntzemüller, P. Dhez, F. Wuilleumier, and E. Källne, Phys. Rev. A (to be published).

180. M. O. Krause, in Atomic Inner-Shell Processes, Vol. II (Academic Press, New York, 1975) p. 33.

181. M. J. Van der Wiel, and G. Wiebes, Physica 53 (1971) 225 and 53 (1971) 411.

182. G. R. Wight and M. J. Van der Wiel, J. Phys. B (to be published).

183. Th. M. El-Sherbini and M. J. Van der Wiel, Physica 62 (1972) 119.

184. F. W. Byron and C. J. Joachain, Phys. Rev. 164 (1967) 1.

185. R. L. Brown, Phys. Rev. A1 (1970) 586.

186. M. Ya. Amusia, E. G. Drukarev, V. G. Gorshkov, and M. P. Kazachkov, J. Phys. B8 (1975) 1248.

187. T. N. Chang, T. Ishihara, and R. T. Poe, Phys. Rev. Letters, 27 (1971) 838.

188. T. N. Chang and R. T. Poe, Phys. Rev. A 12 (1975) 1432.

189. B. Brehm and A. Bucher, Int. J. Mass Spectrom. Ion Phys. 15 (1974) 463.

190. B. Brehm and K. Höfler, Int. J. Mass Spectrom. Ion Phys. 17 (1975) 371.

ref. (cont.)

191. H. Hotop and D. Mahr, J. Phys. B8 (1975) L301.

192. S. T. Lee, S. Süzer, E. Matthias, and D. A. Shirley, J. Chem. Phys. Letters (to be published).

193. A. C. Parr and M. G. Inghram, J. Chem. Phys. 52 (1970) 4916.

194. D. R. Bates, Monthly Notices Roy. Astron. Soc. 106 (1946) 423.

195. D. R. Bates, Monthly Notices Roy. Astron. Soc. 106 (1946) 432.

196. M. B. Hidalgo, Astrophys. J. 153 (1968) 981.

197. S. Chandrasekhar, Revs. Mod. Phys. 16 (1944) 301.; Astrophys. J. 102 (1945) 395; and Astrophys. J. 98 (1943) 205.

198. S. Geltman, Astrophys. J. 136 (1962) 935.

199. R. B. Cairns and G. L. Weissler, Bull. Am. Phys. Soc. 7 (1962) 129.

200. L. M. Branscomb and W. L. Fite, Phys. Rev. 93 (1954) 651A.

201. L. M. Branscomb, Atomic and Molecular Processes, Ed. D. R. Bates (Academic Press Inc., New York, 1962).

202. S. J. Smith, Methods of Experimental Physics, Vol. 7, Ed. B. Bederson and W. L. Fite (Academic Press, New York, 1968) Chp. 2.

203. S. J. Smith and D. S. Burch, Phys. Rev. Letters 2 (1959) 165 and Phys. Rev. 116 (1959) 1125.

204. L. M. Branscomb, S. J. Smith, and G. Tiscome, J. Chem. Phys. 43 (1965) 2906.

205. D. S. Burch, S. J. Smith, and L. M. Branscomb, Phys. Rev. 112 (1958) 171, and 114 (1959) 1652.

ref. (cont.)

206. B. Brehm, M. A. Gusinow, and J. L. Hall, Phys. Rev. Letters 19 (1967) 737.

207. W. C. Lineberger and B. W. Woodward, Phys. Rev. Letters 25 (1970) 424.

208. H. Hotop, T. A. Patterson, and W. C. Lineberger, Phys. Rev. A 8 (1973) 762.

209. H. Hotop and W. C. Lineberger, J. Chem. Phys. 58 (1973) 2379.

210. E. Herbst, T. A. Patterson, and W. C. Lineberger, J. Chem. Phys. 61 (1974) 1300

211. R. J. Celotta, R. A. Bennett, and J. L. Hall, J. Chem. Phys. 60 (1974) 1740.

212. H. Hotop and T. A. Patterson, J. Chem. Phys. 60 (1974) 1806.

213. T. A. Patterson, H. Hotop, A. Kasdan, and D. W. Norcross, Phys. Rev. Letters 32 (1974) 189.

214. A. Kasdan and E. Herbst, J. Chem. Phys. 62 (1975) 541.

215. A. Kasdan, E. Herbst, and W. C. Lineberger, Chem. Phys. Letters 31 (1975) 78.

216. R. F. Stebbings, F. B. Dunning, F. K. Tittel, and R. D. Rundel, Phys. Rev. Letters 30 (1973) 815, and Phys. Rev. A 8 (1973) 665.

217. A. C. Gallagher and G. York, Rev. Sci. Instr. 45 (1974) 662.

218. D. J. Bradley, P. Ewart, J. V. Nicholas, and J. R. D. Shaw, J. Phys. B 6 (1973) 1594 and Phys. Rev. Letters 31 (1973) 263.

219. K. J. Nygaard, R. E. Hebner Jr., J. D. Jones, and R. J. Corbin, Phys. Rev. A12 (1975) 1440.

220. L. Goldberg, Astrophys. J. 90 (1939) 414.

221. A. Burgess and M. J. Seaton, Monthly Notices Roy. Astron. Soc. 120 (1960) 121.

ref. (cont.)

222. D. W. Norcross, J. Phys. B4 (1971) 652.

223. V. L. Jacobs, Phys. Rev. A3 (1971) 289 and A4 (1972) 939.

224. V. L. Jacobs and P. G. Burke, J. Phys. B5 (1972) L67 and B5 (1972) 2272.

225. H. A. Hyman, V. L. Jacobs, and P. G. Burke, J. Phys. B5 (1972) 2282.

226. K. L. Bell, A. E. Kingston, and I. R. Taylor, J. Phys. B6 (1973) 2271.

227. V. L. Jacobs, Phys. Rev. A9 (1974) 1938.

228. R. B. Cairns and J. A. R. Samson, Phys. Rev. 139 (1966) A1403.

229. D. H. Katayama, R. E. Huffman, and Y. Tanaka, J. Chem. Phys. 62 (1975) 2939.

229a. I. D. Clark and R. P. Wayne, J. Geophys. Res. 75 (1970) 699, and Molec. Phys. 18 (1970) 523.

230. N. Jonathan, D. J. Smith, and K. J. Ross, J. Chem. Phys. 53 (1970) 3758.

231. N. Jonathan, A. Morris, K. J. Ross, and D. J. Smith, J. Chem. Phys. 54 (1971) 4954.

232. N. Jonathan, A. Morris, M. Okuda, K. J. Ross, and D. J. Smith, J. Chem. Soc. Faraday Trans. II, 70 (1974) 1810.

233. J. Dyke, N. Jonathan, A. Morris, and T. Sears, J. Chem. Soc. Faraday Trans. II, 72 (1976) 597.

234. N. Jonathan, A. Morris, D. J. Smith, and K. J. Ross, Chem. Phys. Letters 7 (1970) 497.

235. D. C. Frost, S. T. Lee, and C. A. McDowell, Chem. Phys. Letters 17 (1972) 153.

236. N. Jonathan, D. J. Smith, K. J. Ross, Chem. Phys. Letters 9 (1971) 217.

ref. (cont.)

237. N. Jonathan, A. Morris, M. Okuda, D. T. Smith, and K. J. Ross, Chem. Phys. Letters 13 (1972) 334.

238. N. Jonathan, A. Morris, M. Okuda, K. J. Ross and D. J. Smith, Faraday Disc. Chem Soc. 54 (1972) 48.

239. L. Golob, N. Jonathan, A. Morris, M. Okuda, and K. J. Ross, J. Electron Spectrosc. 1 (1972/1973) 506.

240. J. M. Dyke, L. Golob, N. Jonathan, A. Morris, M. Okuda, and D. J. Smith, J. Chem. Soc. Faraday Trans. II 70 (1974) 1818.

241. J. M. Dyke, L. Golob, N. Jonathan, A. Morris, and M. Okuda, J. Chem. Soc. Faraday Trans. II 70 (1974) 1828.

242. J. M. Dyke, L. Golob, N. Jonathan, and A. Morris, J. Chem. Soc. Faraday Trans. II 71 (1975) 1026.

243. J. A. R. Samson and V. Petrosky, Phys. Rev. A 9 (1974) 2449.

244. D. C. Frost, J. Electron Spectrosc. 5 (1974) 99.

245. A. F. Starace, Phys. Rev. A. 9 (1974) 2453.

246. J. Berkowitz and C. Lifshitz, J. Chem. Phys. 48 (1968) 4346.

247. J. Berkowitz and W. A. Chupka, J. Chem. Phys. 50 (1969) 4245.

248. J. Berkowitz, J. Chem. Phys. 61 (1974) 407.

249. J. Berkowitz, J. Chem. Phys. (in press, 1976).

250. J. Berkowitz, J. L Dehmer, and T. E. H. Walker, J. Chem. Phys. 59 (1973) 3645.

251. J. L. Dehmer, J. Berkowitz, L. C. Cusachs, J. Chem. Phys. 58 (1973) 5681.

252. J. L. Dehmer, J. Berkowitz, L. C. Cusachs, A. S. Aldrich, J. Chem. Phys. 61 (1974) 594.

253. J. Berkowitz, Proceedings of the IV Int. Conf. VUV Radiation Phys., Eds. E. Koch, R. Haensel, and C. Kuntz (Pergamon and Vieweg, German, 1974) p 107.

254. J. Cooper and R. N. Zare, J. Chem. Phys. 48 (1968) 942, and in Lectures in theoretical physics, eds. S. Geltman, K. Mahanthappa, and W. E. Brittin (Gordon and Breach, New York, 1969), vol. II, p. 317.

255. J. W. Cooper and S. T. Manson, Phys. Rev. 177 (1969) 157.

256. J. C. Tully, R. S. Berry, and B. J. Dalton, Phys. Rev. 176 (1968) 95.

257. D. Dill, S. T. Manson, and A. F. Starace, Phys. Rev. Letters 32 (1974) 971.

258. D. Dill, Phys. Rev. A 7 (1973) 1976.

259. S. T. Manson, Phys. Rev. Letters 26 (1971) 219.

ref. (cont.)

260. T. A. Carlson, G. E. McGuire, A. E. Jonas, K. L. Cheng, C. P. Anderson, C. C. Lu, and B. P. Pullen, in Electron Spectroscopy, ed. D. A. Shirley (North-Holland, Amsterdam, 1972) p. 207.

261. R. Morgenstern, A. Niehaus, and M. W. Ruf, Proceeding VII ICPEAC, Amsterdam, July 1971.

262. W. H. Hancock and J. A. R. Samson, J. Electron Spectrosc. to be published.

263. M. J. Lynch, A. B. Gardner, and K. Codling, Phys. Letters 40A (1972) 349.

264. P. Mitchell and K. Codling, Phys. Letters 38A (1972) 31.

265. M. J. Lynch, K. Codling, and A. B. Gardner, Phys. Letters 43A (1973) 213.

266. R. G. Houlgate, J. B. West, K. Codling, and G. V. Marr, J. Phys. B 7 (1974) L470.

267. W. S. Watson and D. T. Stewart, J. Phys. B 7 (1974) L466.

268. R. G. Houlgate, J. B. West, K. Codling, and G. V. Marr, J. Electron Spectrosc. to be published.

269. A. Niehaus and M. W. Ruf, Z. Physik 252 (1972) 84.

270. J. L. Dehmer, W. A. Chupka, J. Berkowitz, and W. T. Jivery, Phys. Rev. A12 (1975) 1966.

271. D. J. Kennedy and S. T. Manson, Phys. Rev. A 5 (1972) 227.

ref. (cont.)

272. M. Ya. Amusia, N. A. Cherepkov, and L. V. Chernysheva, Phys. Letters, 40A (1972) 15.

273. M. J. Van der Wiel and C. E. Brion, J. Electron Spectrosc. 1 (1972/73) 443.

274. G. R. Branton and C. E. Brion, J. Electron Spectrosc. 3 (1974) 123.

275. J. A. R. Samson and J. L. Gardner, Phys. Rev. Letters 31 (1973) 1327.

Table 1

CONVERSION FACTOR TO CONVERT ELECTRON VOLTS TO ANGSTROMS AS REPORTED SINCE 1929

$V\lambda$ (eV Å)	Year	Reference
12336.1 ± 5.00	1929	a
12395.4 ± 2.10	1941	b
12397.80 ± 0.50	1953	c
12397.67 ± 0.22	1955	d
*12398.10 ± 0.13	1965	e
12398.54 ± 0.04	1969	f

(a) R. T. Birge, Revs. Mod. Phys. 1 (1929) 1.

(b) R. T. Birge, Revs. Mod. Phys. 13 (1941) 233.

(c) J. W. M. DuMond and E. R. Cohen, Revs. Mod. Phys. 25 (1953) 691.

(d) E. R. Cohen, J. W. M. DuMond, T. W. Layton and J. S. Rollet, Rev. Mod. Phys. 27 (1955) 363.

(e) E. R. Cohen and J. W. M. DuMond, Revs. Mod. Phys. 37 (1965) 537.

(f) B. N. Taylor, W. H. Parker, and D. N. Langenberg, Revs. Mod. Phys. 41 (1969) 375.

*This is the value currently recommended by the National Academy of Sciences - National Research Council.

Table 2

OBSERVED AND CALCULATED VIBRATIONAL DISTRIBUTIONS

	Experiment		Theory	
v'	(a)	(b)	Case B	Case C
0	44.8±0.9	46.3	46.8	44.6
1	92.2± 0.7	86.3	87.4	85.3
2	100.0±1.1	100.0	100.0	100.0
3	96.9±1.2	88.4	91.8	94.0
4	71.3±0.9	70.0	74.8	78.3
5	57.2±0.8	57.9	56.9	60.8
6	42.3±0.5	47.2	41.6	45.4
7	30.8±0.5	31.3	29.8	33.0
8	20.8±0.4	24.1	21.2	23.8
9	13.2±0.3	13.7	15.0	17.0
10	8.9±0.2	----	10.6	12.2
11	5.8±0.1	----	----	----
12	3.9±0.1	----	5.4	6.3
13	2.4±0.1	----	----	----
14	1.5±0.1	----	2.7	3.2
15	0.5±0.1	----	----	----

a. J. L. Gardner and J. A. R. Samson, J. Electron Spectrosc. 8 (1976) 123.

b. J. Berkowitz and R. Spohr, J. Electron Spectrosc. 2 (1973) 143.

c. Y. Itikawa, J. Electron Spectrosc. 2 (1973) 125.

Table 3

FRAGMENTATION RATIOS FOR CO_2^+ AT 584 Å

Reference	O^+/CO_2^+	CO^+/CO_2^+	$(O^+ + CO^+)/CO_2^+$
[a] Weissler et al.	0.064	0.022	0.086
[b] Dibeler and Walker	0.040	0.010	0.050
[c] Fryar and Browing	0.039	0.018	0.057
[d] McCulloh	0.018*	0.004*	0.022*
[e] Eland	0.033	-----	-----
[f] Samson and Gardner	-----	-----	0.050

*These measurements were made at 625 Å and are expected to be about 30% lower than data at 584 Å. [24]

a. ref. [24]

b. ref. [107]

c. ref. [33]

d. ref. [106]

e. ref. [110]

f. ref. [111]

Table 4

TOTAL ABUNDANCES OF SINGLE AND DOUBLE CHARGED MOLECULAR IONS OBSERVED BY MASS SPECTROSCOPY

Gas	44 Å[a] (%)	13.3 Å[b] (%)	8.2 Å[a] (%)
NO^+	21.0	5.6	0.7
NO^{+2}	3.2	2.3	2.1
CO^+	22.0	5.0	0.6
CO^{+2}	0.4	0.8	0.3
CO_2^+	18.0	5.4	0.8
CO_2^{+2}	0.8	1.1	1.3

a. ref. [108]

b. ref. [114]

Figure Captions

1. Double ion chamber absorption cell. The exit slit of the monochromator is held at the same potential as the repeller electrode. A grounded guard electrode at the end of the ion chamber provides a uniform field at the end of the second collector electrode. Thus, all the ions formed under a given electrode will be collected by that electrode (Samson, ref. 8).

2. Vacuum monochromator and mass spectometer. A, electron multiplier ion detector; B, photomultiplier radiation monitor; C, ion beam; D, G, I, O, to pumping systems; E, ion chamber; F, permanent magnet; H, monochromator exit slit; J, light source; K, monochromator entrance slit; L, grating turntable; M, grating; N, Seya type vacuum monochromator (Weissler, et al., ref. 24).

3. Schematic cross section of a cylindrical mirror electron energy analyzer. A, inner cylinder; B, collimating slit; C, D, retarding slits; E, boron nitride insulator; F, photocathode; G, collimating slit; H, detector; I, outer cylinder.

4. The 584 Å photoelectron spectrum of O_2 showing count rate vs ionization potential.

5. Orientation of the photoelectron with respect to the x, y, and z-axes. The photon $h\nu$ is incident along the z-axis. The azimuthal angle of the photoelectron with respect to the x-axis is $\tilde{\phi}$.

fig. captions

6. The 462 Å (26.84 eV) photoelectron spectrum of NO. The labeled arrows represent ionization potentials obtained spectroscopically. New ionization potentials are shown at 21.72 and 23.1 eV (Samson, ref. 65).

7. The 736 Å (NeI) photoelectron spectrum of O_2. The first seven vibrational bands are shown, including the Xe doublet $^2P_{1/2, 3/2}$ used for calibrating the energy scale. Vibrational bands of the ground state of O_2^+ continue to $v' = 24$. Analyzer resolution was 9 meV (Samson and Gardner, ref. 65a).

8. The 920 Å (ArII) photoelectron spectrum of the $v' = 0$ band of O_2^+. The solid curve is the calculated shape of the band taking into account the rotational structure. Data points are shown as open circles. Analyzer resolution was 7 meV (Samson and Gardner, ref. 65a).

9. Photoionization cross section of H_2 as a function of wavelength: Solid points (•), present experimental data. Dashed line, theoretical data of Martin et al. (Ref. 75). Open circles, data of Denne (Ref. 84). Crosses, data of

10. The 584 Å photoelectron spectrum of H_2 (corrected for analyzer response). Analyzer resolution was 15 meV.

11. The 736 Å photoelectron spectrum of H_2 taken with a resolution of 8 meV to reveal the rotational fine structure.

12. The 736 Å photoelectron spectrum of H_2 showing the rotational structure in the $v' = 5$ and 6 vibrational bands.

fig. captions

13. Ionization and absorption cross sections of ordinary H_2 at room temperature in the neighborhood of the threshold, with some rotational assignments. Not shown are assignments for the $D' - X$ (2, 0) system, no lines of which are autoionized but which include the strong absorptions at 805.72, 805.93, and 806.45 Å [coinciding with P(2) of B''] and at 806.63 Å (Chupka and Berkowitz, ref. 99).

14. Photoionization efficiency spectrum of ordinary H_2 taken at 78K with a wavelength resolution of 0.016 Å (Chupka and Dehmer, ref. 100).

15. Photoionization efficiency spectrum of para-H_2 at 78K taken with a wavelength resolution of 0.016 Å (Chupka and Dehmer, ref. 100).

16. Potential energy curves of H_2 and H_2^+. The shaded area represents the Franck-Condon region.

17. Energy level diagram of CO_2^+. The dashed levels are autoionizing states.

18. Photoionization-efficiency curves for the CO_2^+ and O^+ ions of carbon dioxide. The ordinate scale for the molecule ion is 20 times that of the atom ion (Dibeler and Walker, ref. 111).

19. Photoion-yields of O^+ and CO^+, compare with CO_2^+. Ordinates for the fragment ions are expanded forty-fold relative to CO_2^+. Two predissociating Rydberg series converging to 19.39 eV and an autoionizing Rydberg series converging to 19.75 eV are indicated (McCulloh, ref. 110).

20. The 584 Å photoelectron spectrum of CO_2.

21. The 304 Å, (HeII) photoelectron spectrum of O_2, corrected for the transmission of the analyzer. No transitions could be detected in the omitted portion of the spectrum (Gardner and Samson, ref. 117).

fig. captions

22. The 736 Å (NeI) photoelectron spectrum of O_2.

23. Branching ratios as a function of wavelength for photoionization of CO ($X^1\Sigma^+$), to the $CO^+(X^2\Sigma^+)$, $(A^2\Pi)$, and $(B^2\Sigma^+)$ states. The solid data points represent results of Samson and Gardner (Ref. 127). The open circles represent the data of Van der Wiel and Brion (Ref. 130).

24(a). Partial photoionization cross sections as a function of wavelength for the production of the $CO^+(X\ ^2\Sigma^+)$ state (Samson and Gardner, ref. 127).

(b). Partial photoionization cross section as a function of wavelength for the production of the CO^+ A and B states. The solid data points represent results of Samson and Gardner (Ref. 127). The open circles represent the fluorescent data of Judge and Lee (Ref. 131).

25. Experimental photoionization continuum cross sections of the rare gases as a function of wavelength. The vertical lines indicate the positions of the discrete window type resonances in Ar, Kr, and Xe, caused by (ms-np) type transitions (Samson, ref. 8).

26. Experimental photoionization cross section of He as a function of wavelength. The dashed vertical line at 206 Å represents the first autoionizing resonance level of the series caused by double electron excitation. The limit of the series is shown by the shaded area He^+ (n = 2).

27. Photoionization cross section of He in the vicinity of the autoionizing resonances. The solid continuous line represents the data of Madden and Codling (Ref. 161). The solid point represents the present data.

28. Summary of published theoretical photoionization cross sections of He. See text for details. The dashed curve with the data points represents the present experimental data.

29. Experimental photoionization cross sections of xenon as a function of wavelength (Samson, ref. 8).

30. Theoretical photoionization cross sections for the 5p-ns (^1P) channel in Xe. -----, single particle approximation; -•-•-•-, random phase approximation (RPA) without ground state correlations; -•-•-, RPA with correlations; •••••, single particle approximation for the 5p-ns channel (Wendin, ref. 170). The solid curve is the experimental total photoionization cross section (Samson, ref. 8).

31. Partial photoionization cross sections for the 5s subshell in Xe. -----, RPAE with 5s-4d intershell correlations; •••••, single particle approximation; ———, RPAE with 5s-(4d + 5p) intershell correlations. (Amusia, ref. 147). ●, experimental data points (Samson and Gardner, ref. 172).

32. Total photoionization cross section of Xe in the region of 4d shell ionization. ———, RPAE calculations (Amusia, ref. 147); ----- experimental results (Haensel et al., ref. 173).

33. Partial photoionization cross section of Xe for the ejection of electrons from (a) the 4d-shell, (b) the 5s-shell, and (c) the 5p-shell (West et al., ref. 175). The dashed curves represent the theoretical data of Amusia et al., ref. 147

34. Ratio of double to single ionization for He. Electron-ion coincidence technique: ●, Wight and Van der Wiel, ref. 182. Photoionization technique: △, Schmidt et al. ref. 15; □, Carlson, ref. 13.

35. Ratio of double to single ionization for Ar. Electron-ion coincidence technique: ●, Wight and Van der Wiel, ref. 182. Photoionization technique: △, Schmidt et al. ref. 15; □, Carlson, ref. 13; ○, Samson and Haddad, ref. 14.

fig. captions

36. Partial photoionization cross section of Ne for double ionization: ⊙, Samson and Haddad, ref. 14; x, Carlson, ref. 13. The dashed curve is the best fit to the experimental data. The solid curve represents the theoretical results of Chang and Poe, ref. 188.

37. The 584 Å photoelectron spectrum of O_2, $O_2\,^1\Delta$, and O (Samson and Petrosky, ref. 243).

38. The 584 Å photoelectron spectrum of S_2 ($^3\Sigma_g^-$). (Dyke et al. ref. 241).

39. The 584 Å photoelectron spectrum of CsI: (a) full spectrum, (b) threshold region.

40. The angular distribution parameter β plotted as a function of the photoelectron energy for the 3p electron in argon. ———, Kennedy and Manson, ref. 271; Amusia et al., ref. 272; ○, Houlgate et al., ref. 268; ●, Dehmer et al., ref. 270.

41. Asymmetry parameter β as a function of wavelength. (a) Experimental β value shown in relation to the experimental autoionizing resonances (dashed curve). (b) Theoretical β values (solid-line curve) shown in relation to the theoretical photoionization cross sections (dashed curve).

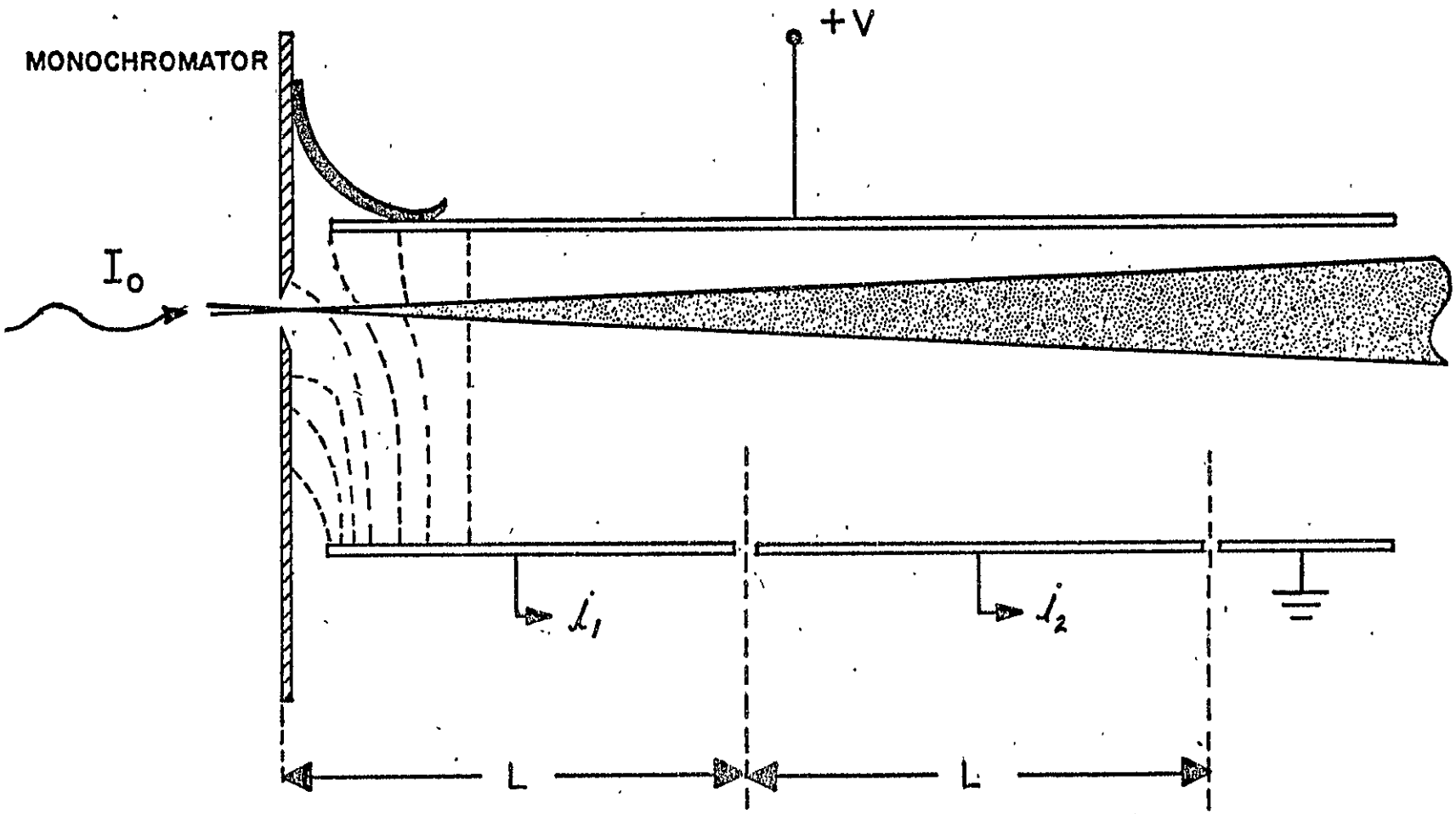
MONOCHROMATOR
+V
I_o
i_1
i_2
L
L

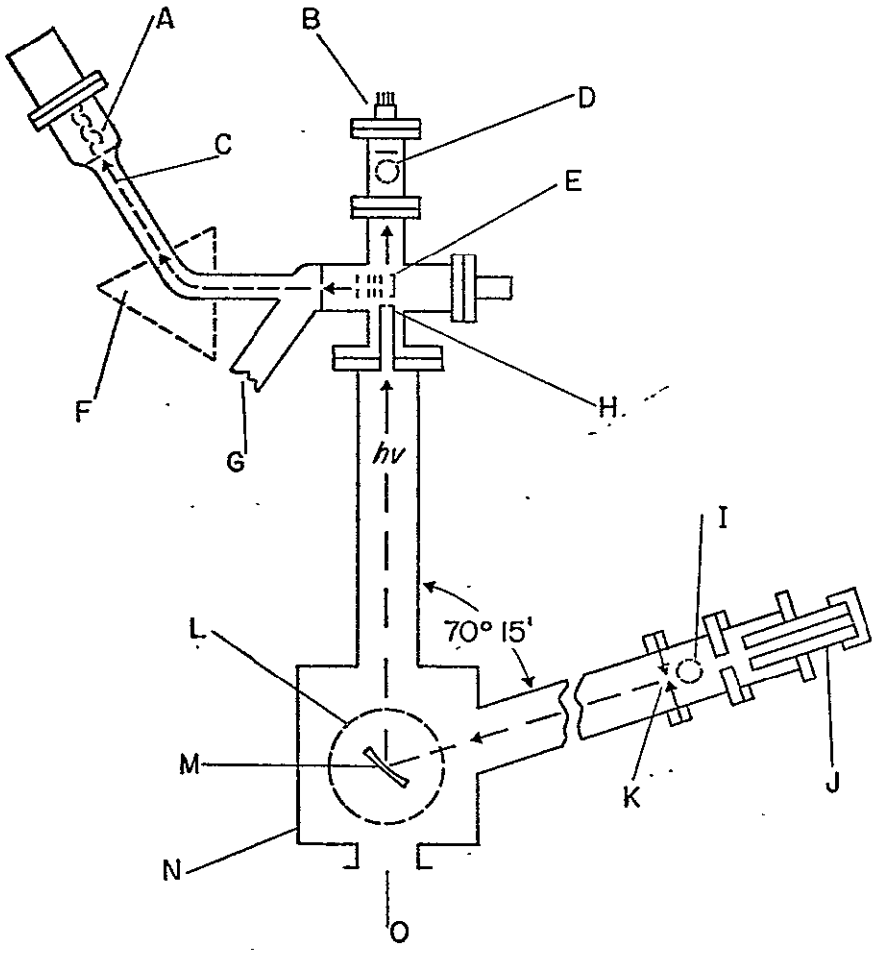
A
B
C
D
E
F
G
H
hv
I
70° 15'
L
M
N
O
K
J

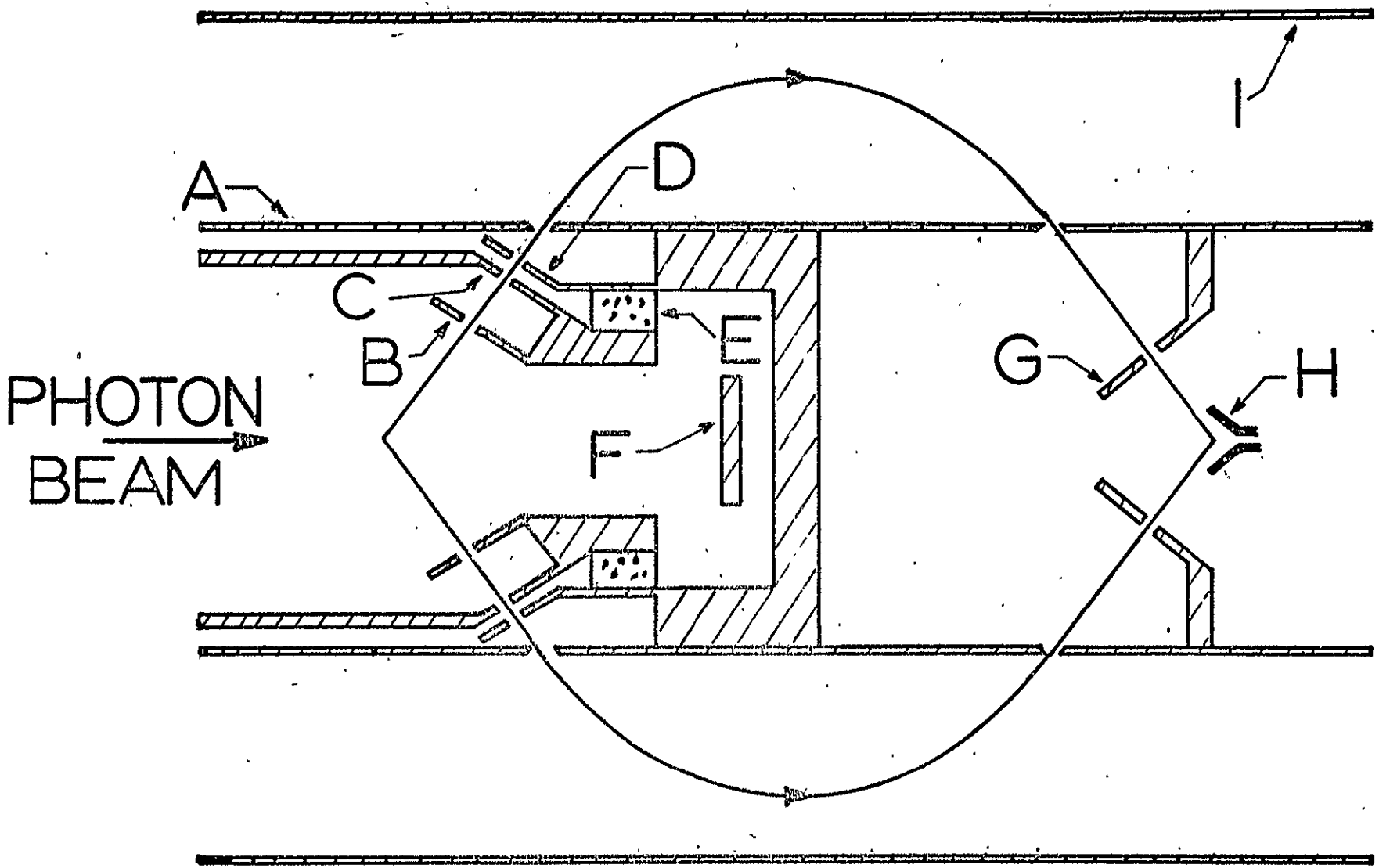
I
A
D
C
B
E
G
H
PHOTON
BEAM
F

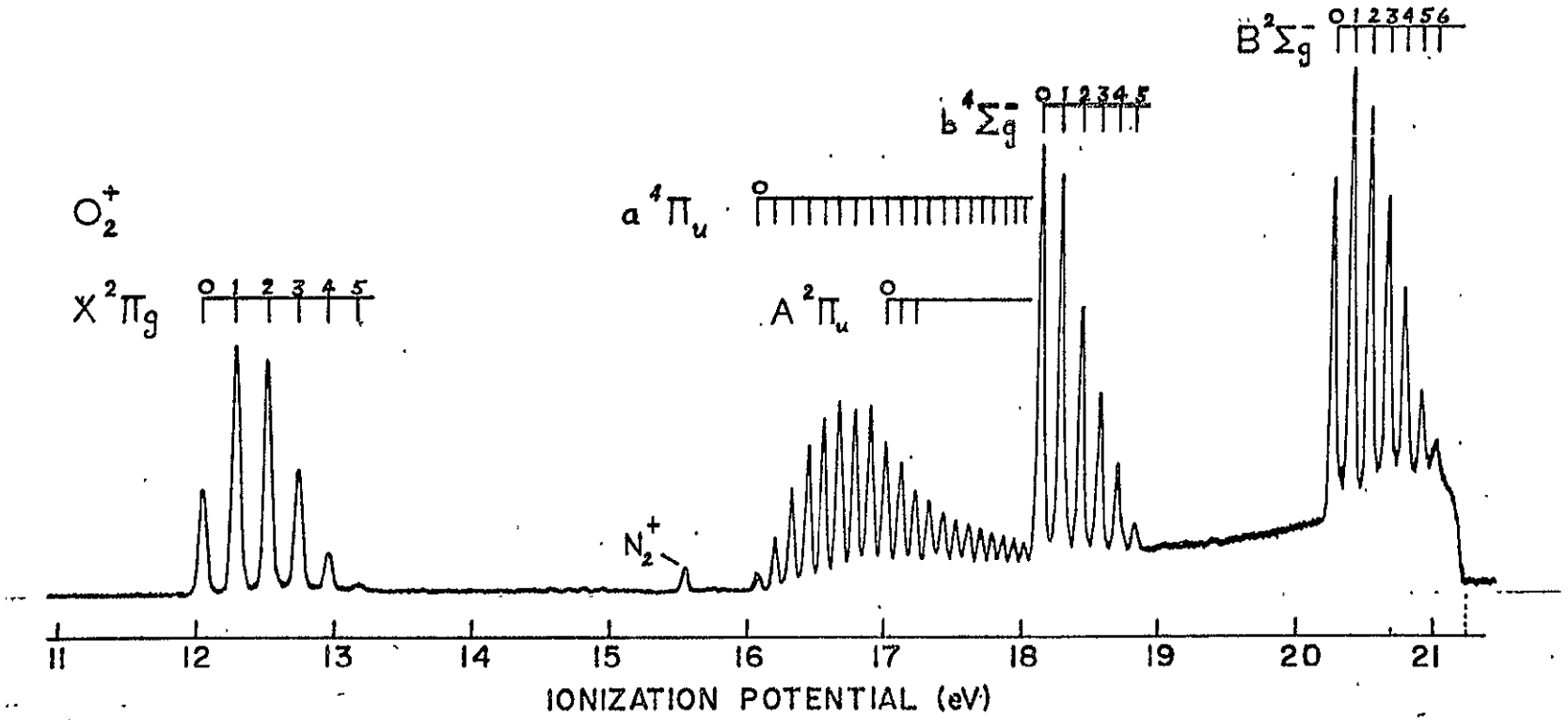

4. Samson, Phys. Reports

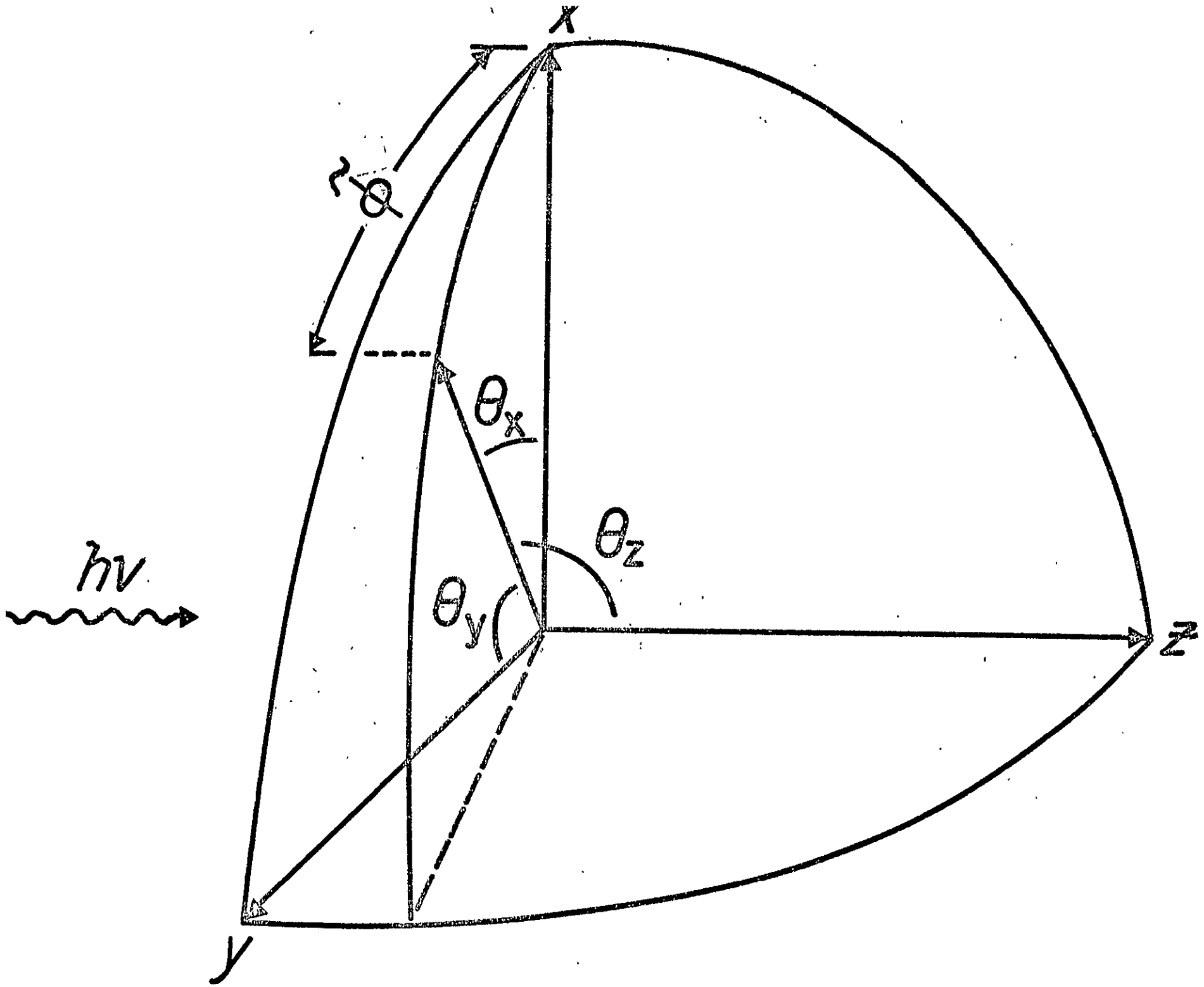
x
α
θ_x
θ_z
θ_y
hν
z
y

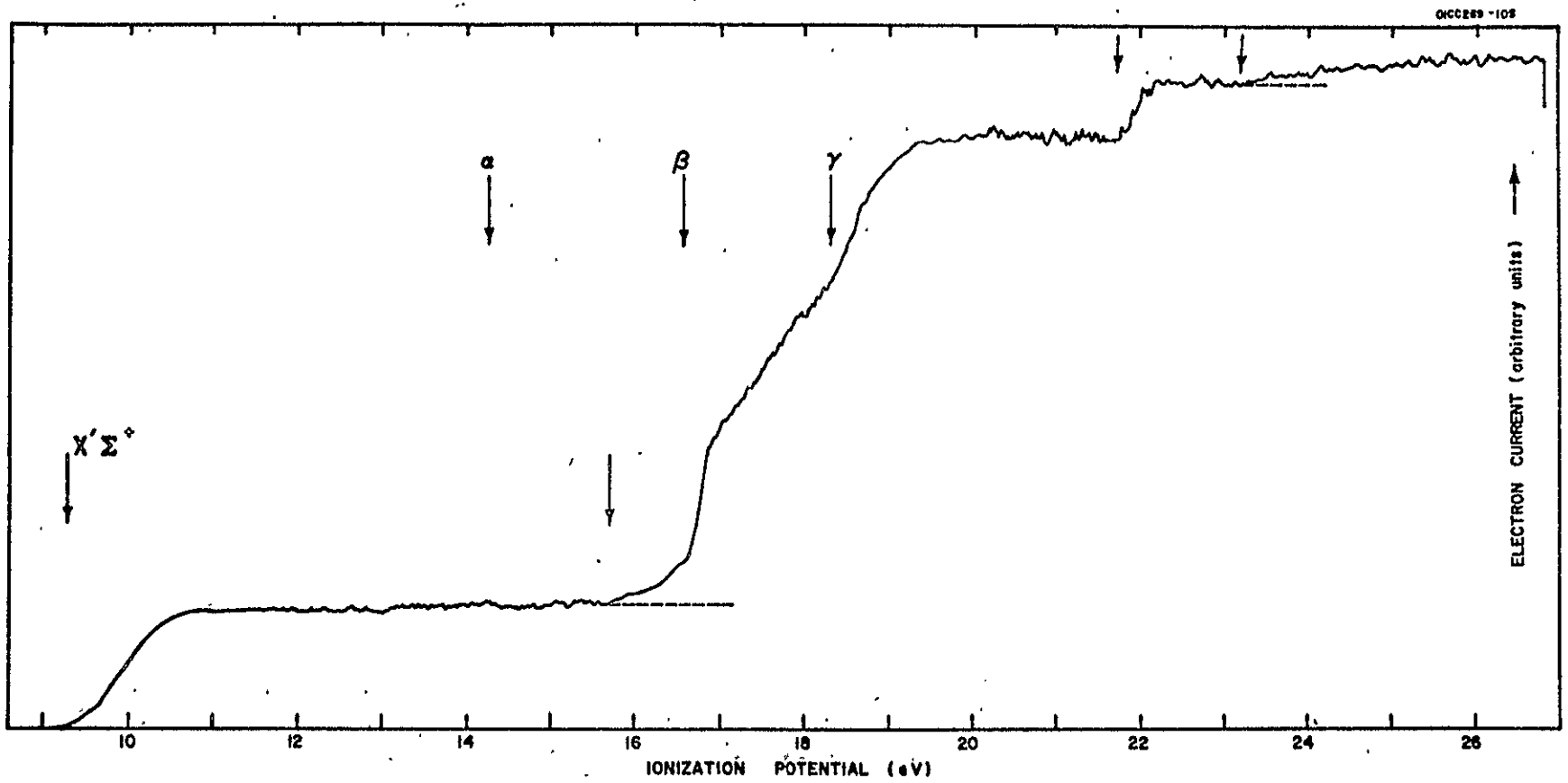
α
β
γ
X'Σ⁺
10
12
14
16
18
20
22
24
26
IONIZATION POTENTIAL (eV)
ELECTRON CURRENT (arbitrary units)

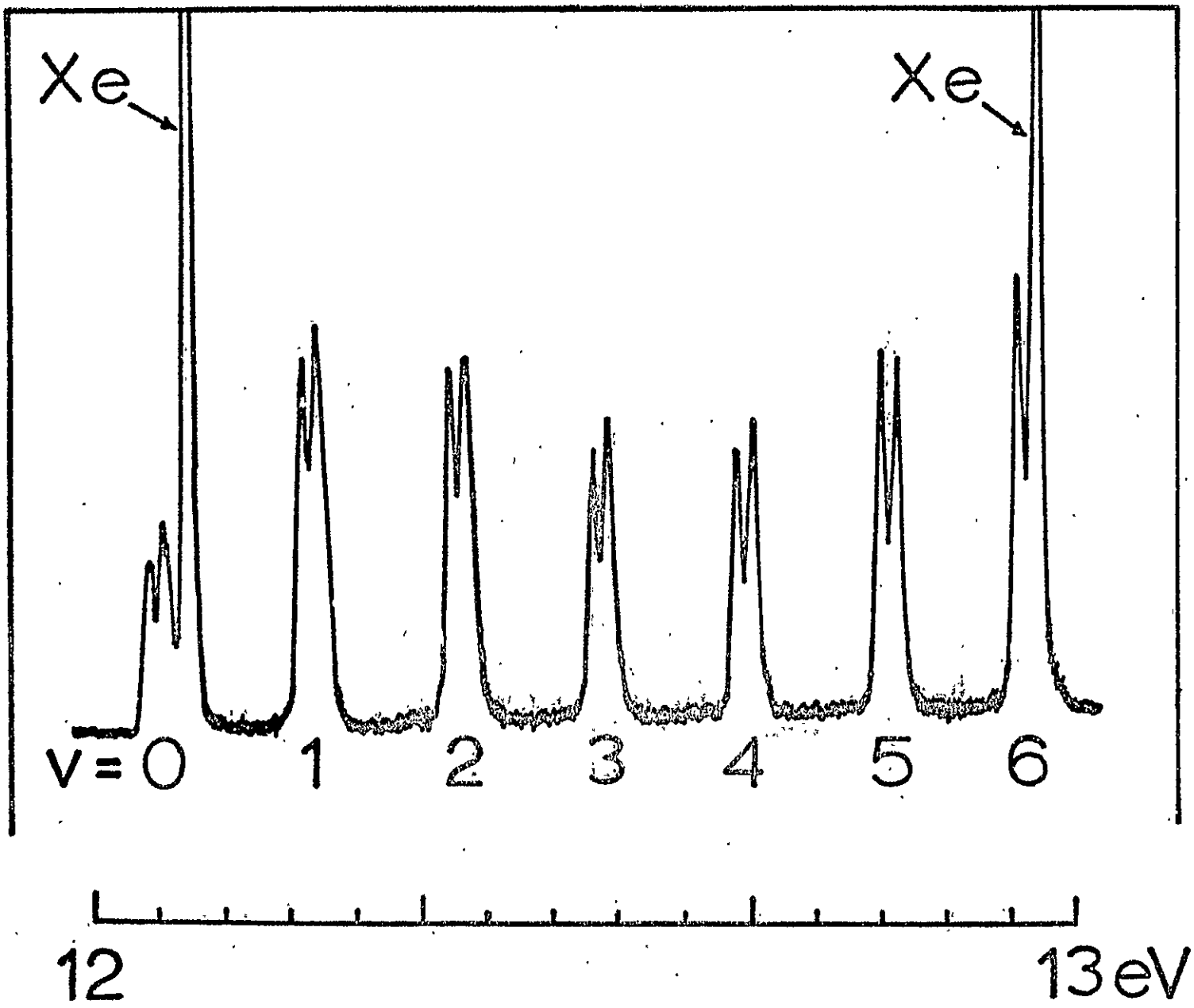
Xe
Xe
v=0
1
2
3
4
5
6
12
13eV

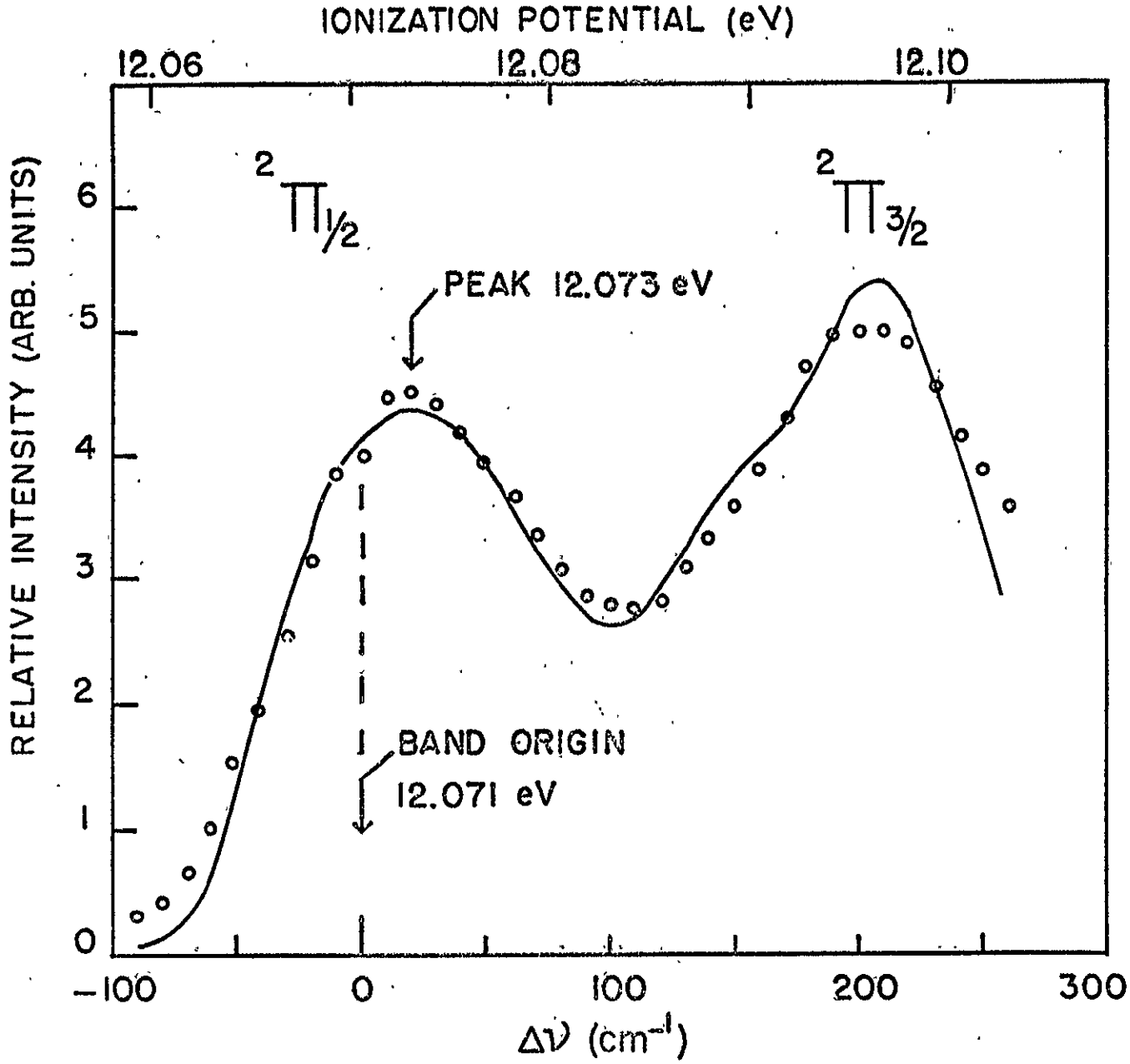
IONIZATION POTENTIAL (eV)
12.06
12.08
12.10
RELATIVE INTENSITY (ARB. UNITS)
0
1
2
3
4
5
6
$^2\Pi_{1/2}$
$^2\Pi_{3/2}$
PEAK 12.073 eV
BAND ORIGIN
12.071 eV
-100
0
100
200
300
$\Delta\nu$ (cm^{-1})

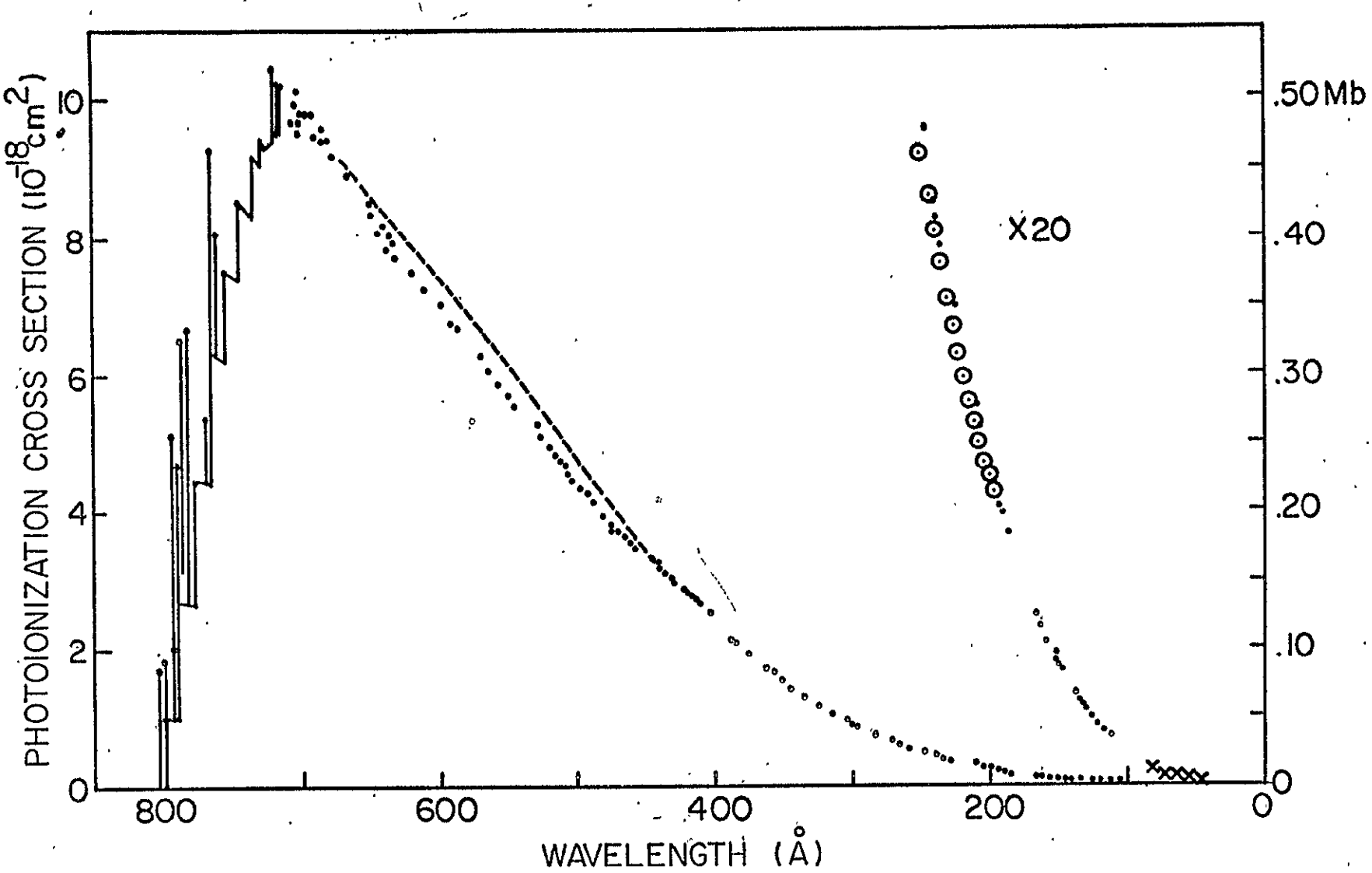
PHOTOIONIZATION CROSS SECTION (10^{-18}cm^2)
0
2
4
6
8
10
.50 Mb
.40
.30
.20
.10
0
X20
800
600
400
200
0
WAVELENGTH (Å)

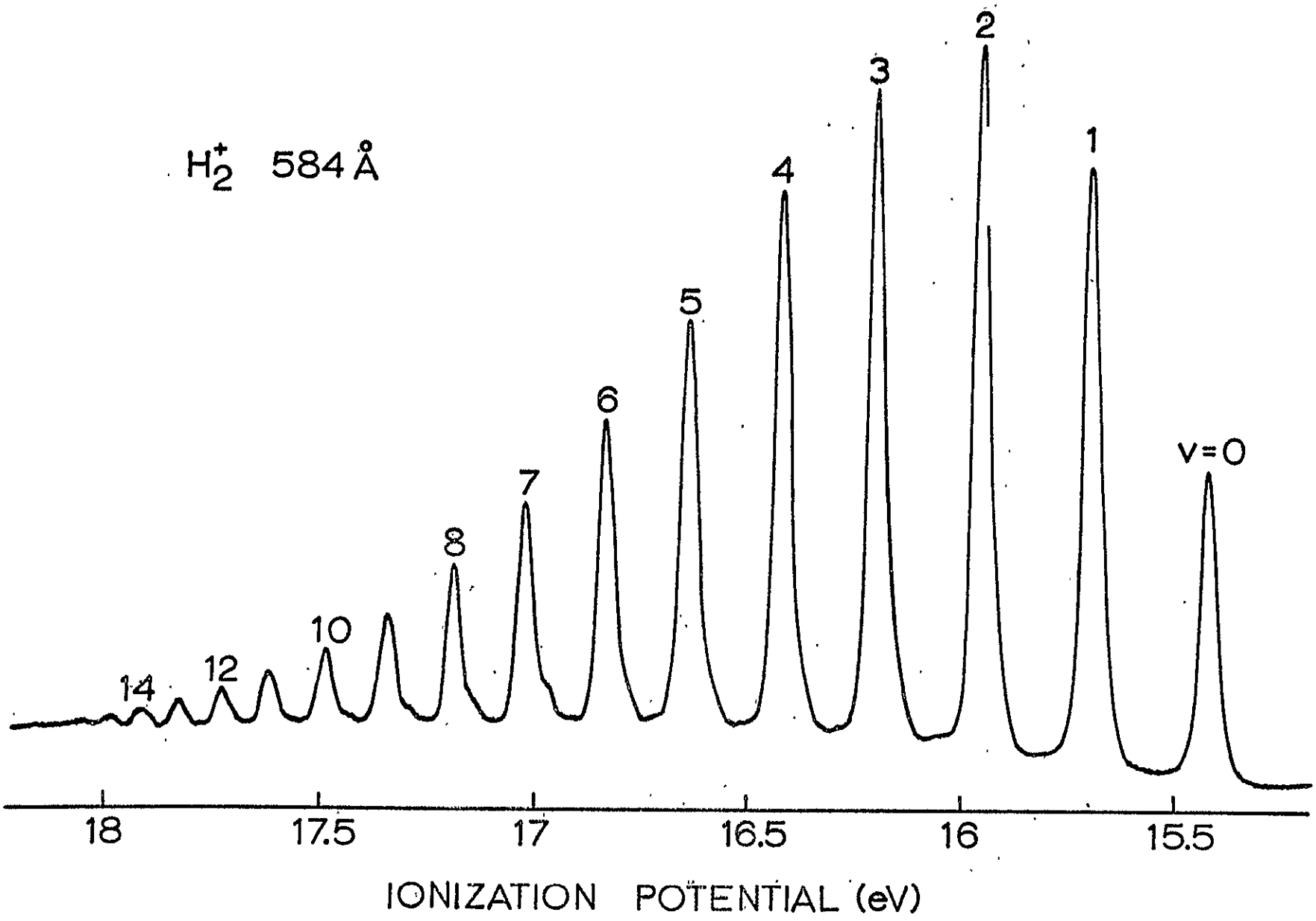
H_2^+ 584 Å
v=0
1
2
3
4
5
6
7
8
10
12
14
18
17.5
17
16.5
16
15.5
IONIZATION POTENTIAL (eV)

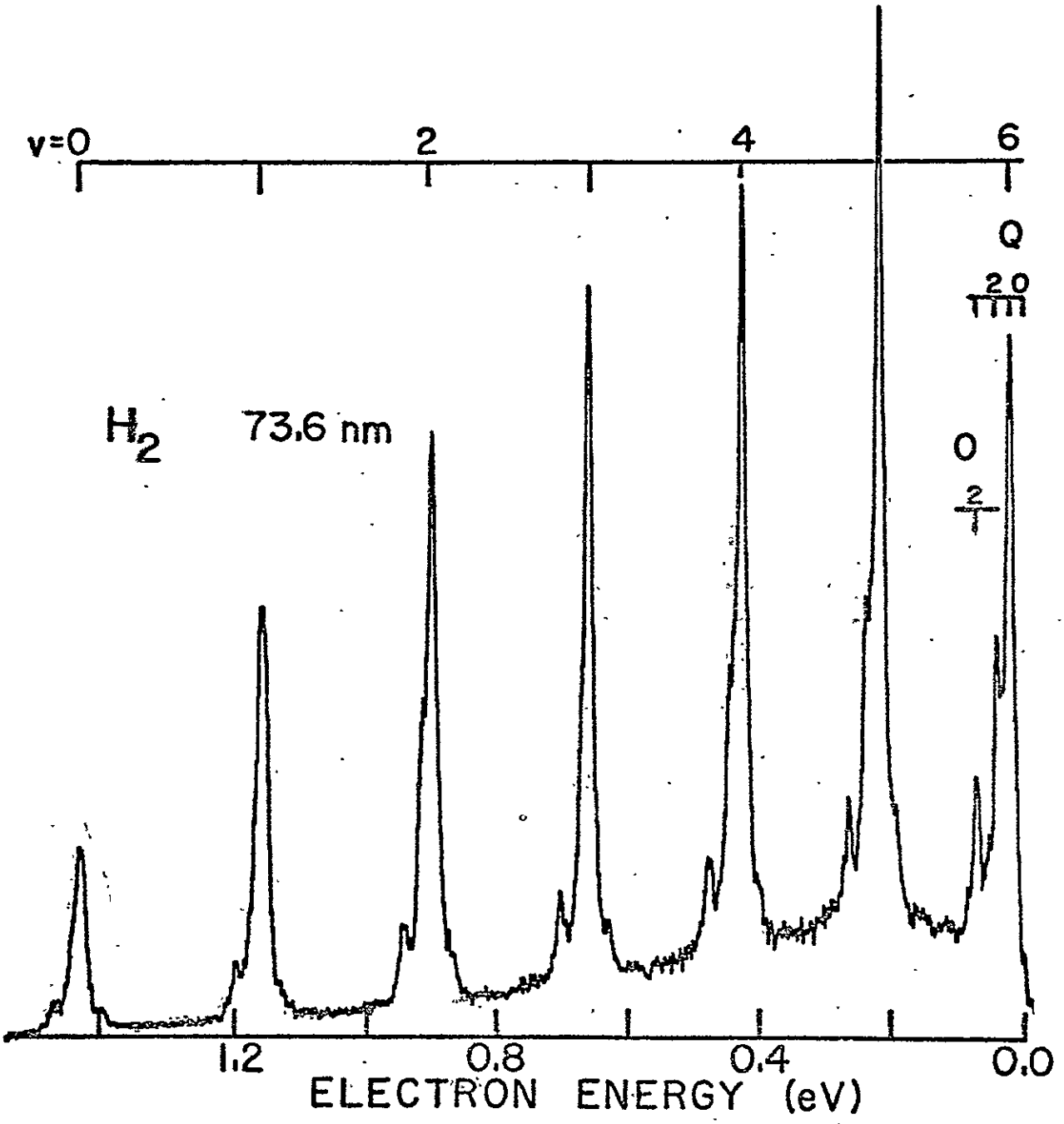
v=0
2
4
6
Q
20
1m
H_2
73.6 nm
O
2
1
1.2
0.8
0.4
0.0
ELECTRON ENERGY (eV)

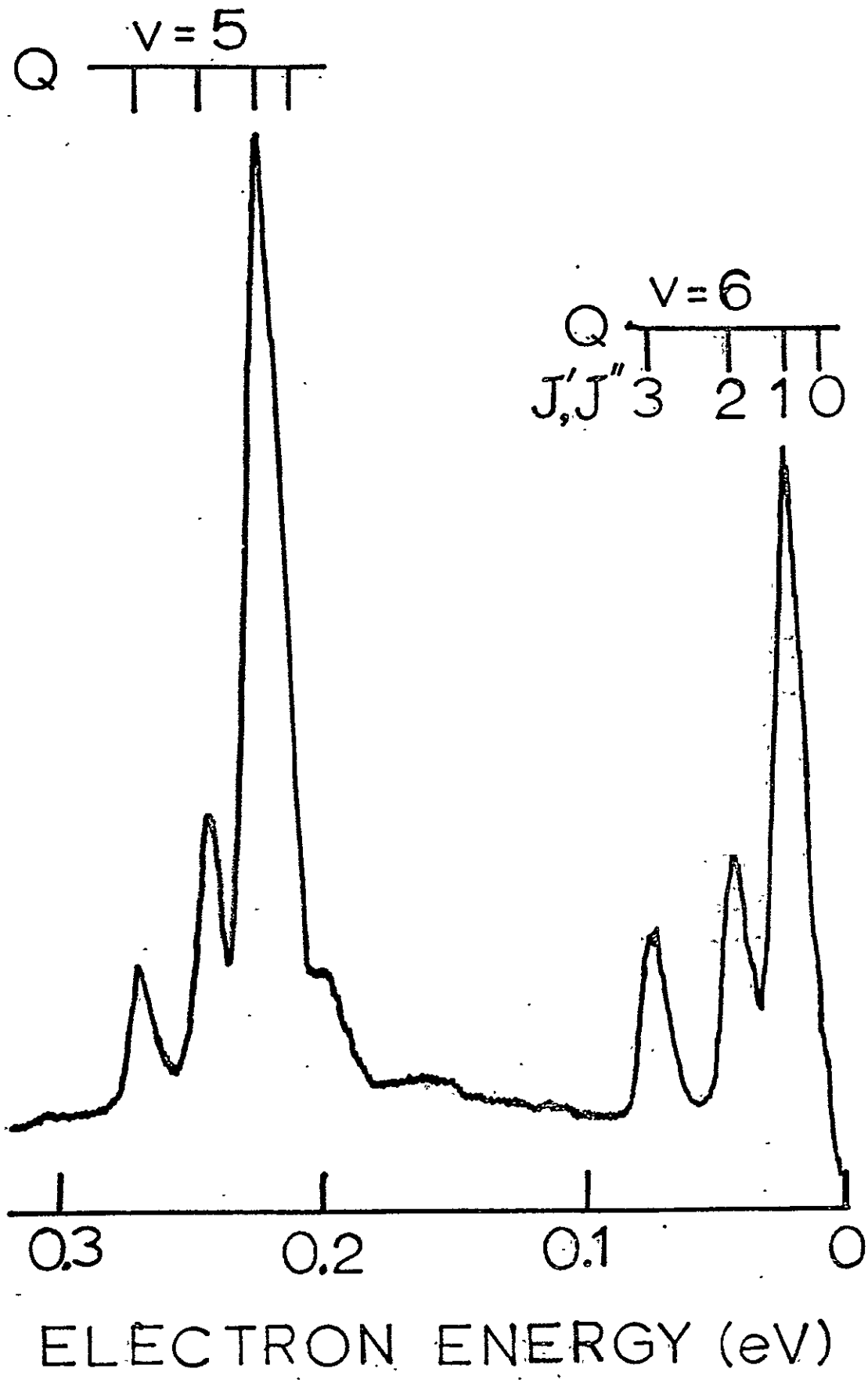
v = 5
Q
v = 6
Q
J', J"
3
2
1
0
0.3
0.2
0.1
0
ELECTRON ENERGY (eV)

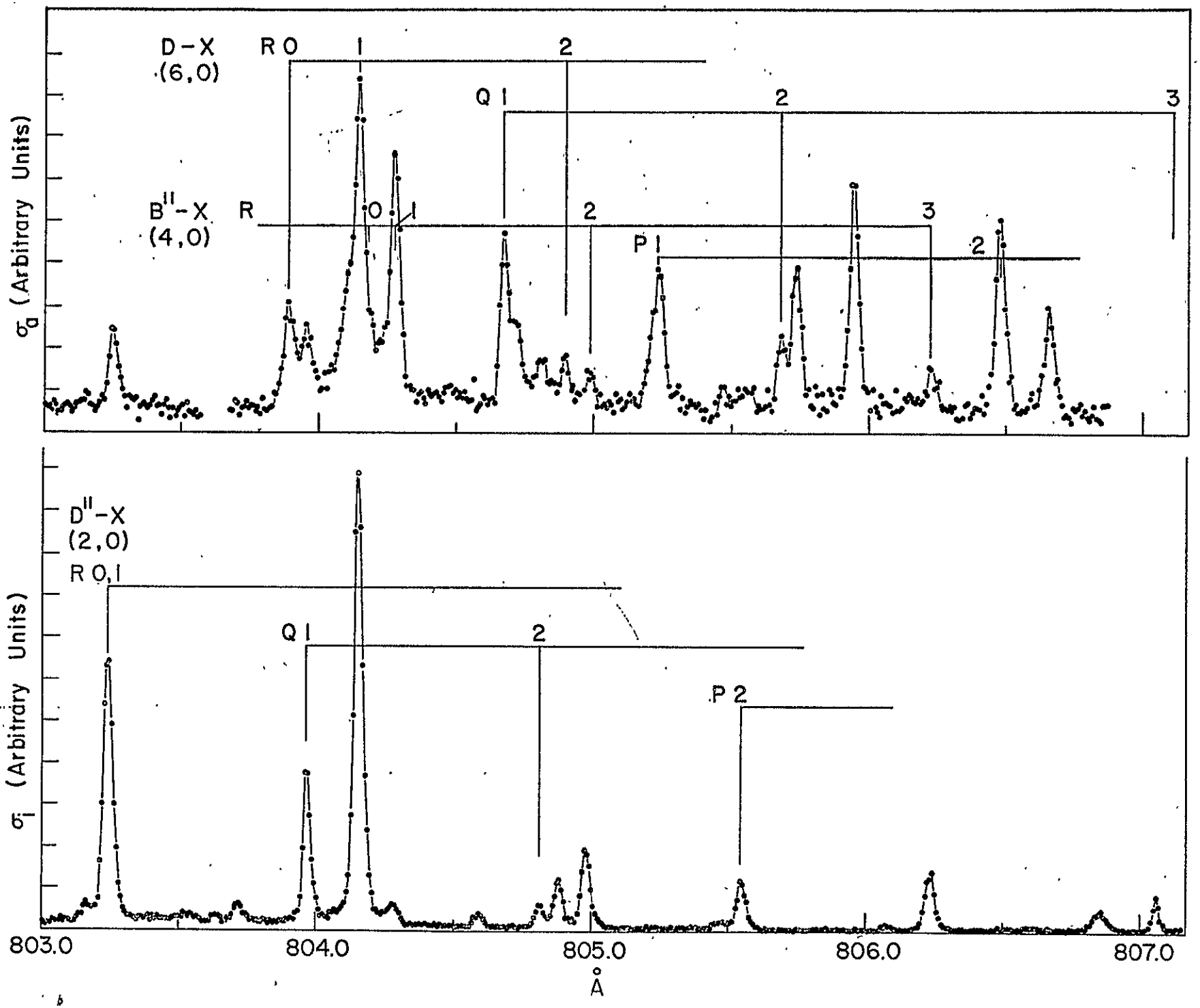
D-X
(6,0)
R 0
1
2
Q 1
2
3
B^{II}-X
(4,0)
R
0
1
2
3
P 1
2
σ_a (Arbitrary Units)
D^{II}-X
(2,0)
R 0,1
Q 1
2
P 2
σ_i (Arbitrary Units)
803.0
804.0
805.0
806.0
807.0
Å

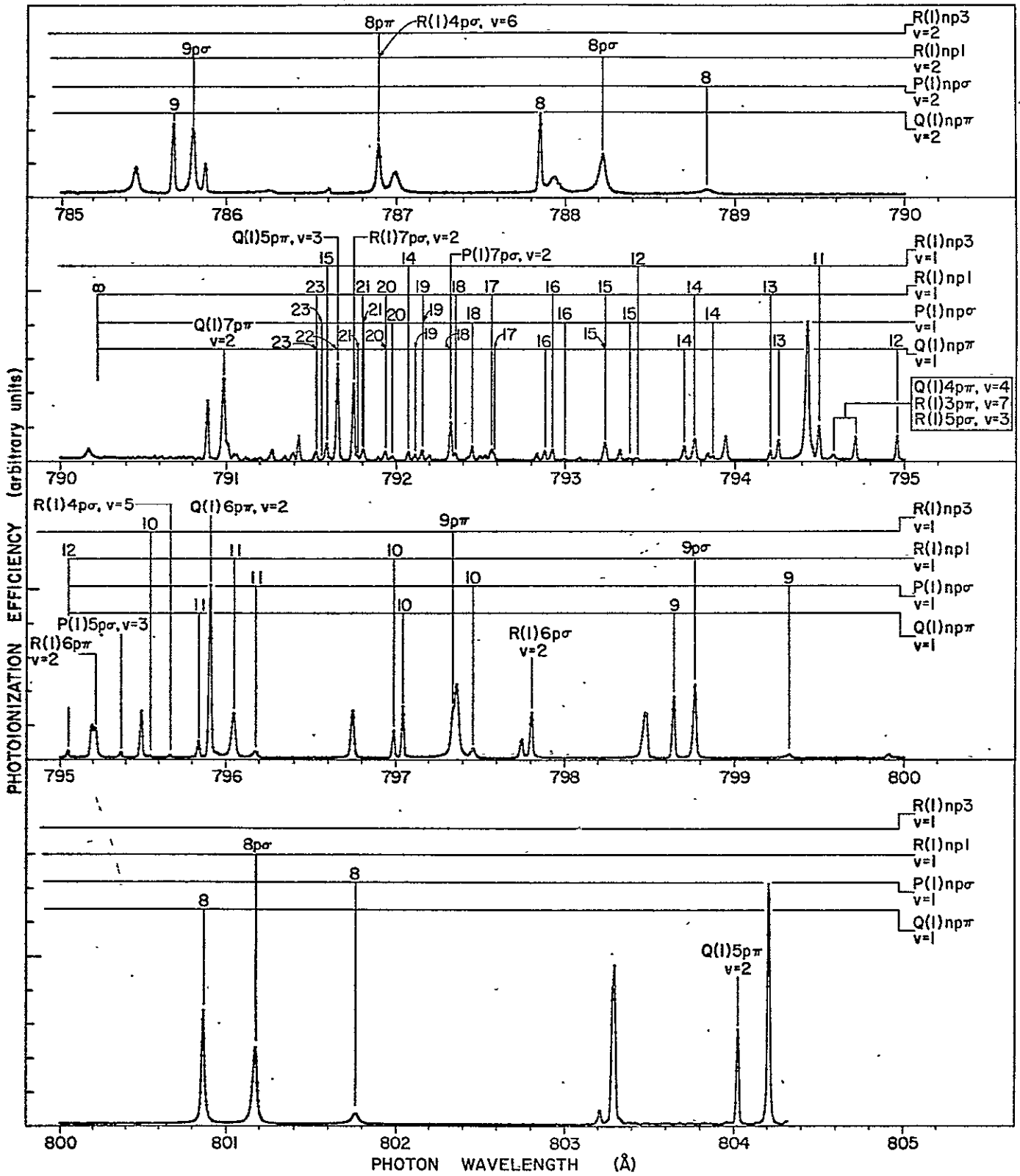

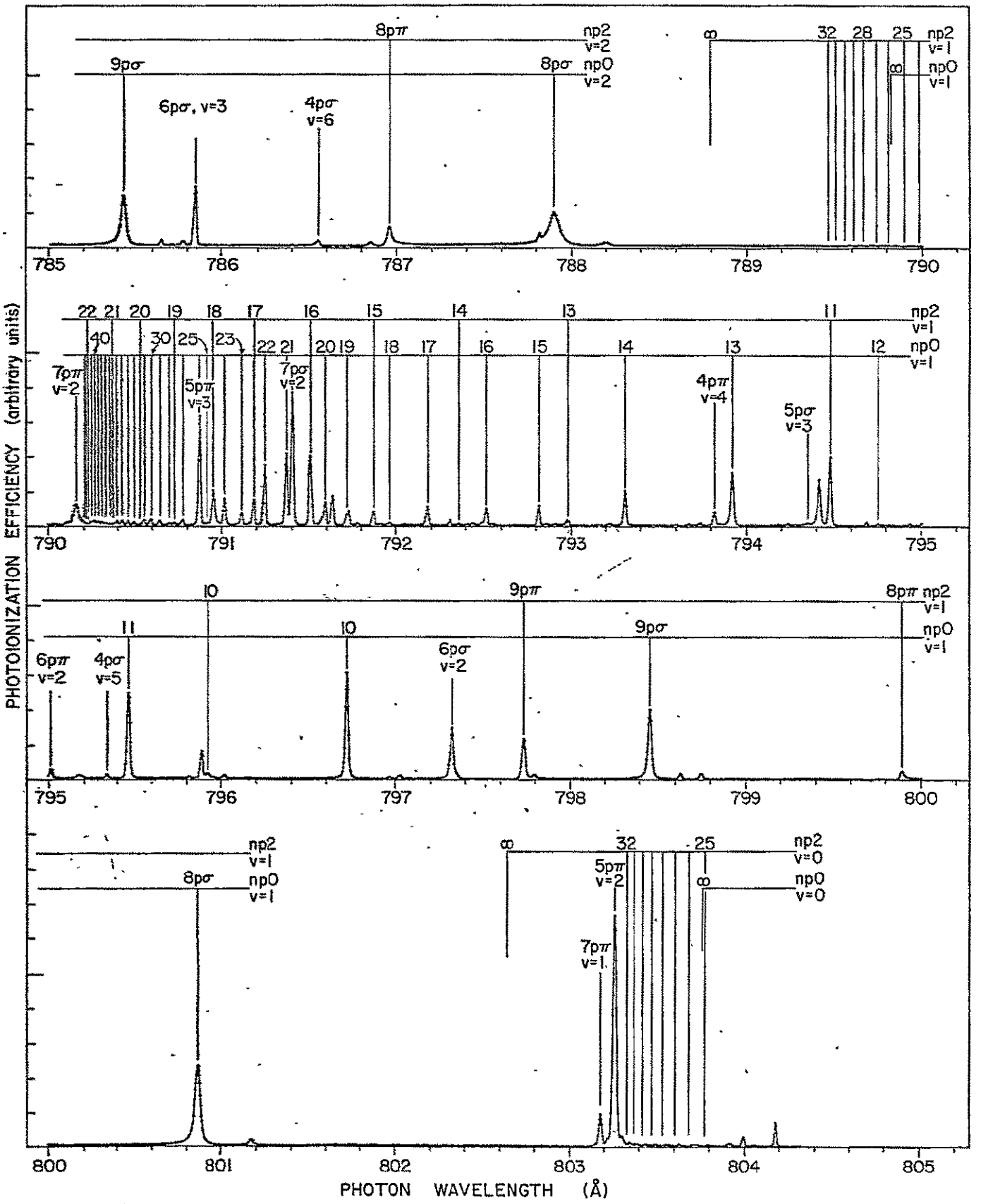
8pπ
np2 v=2
9pσ
8pσ
npO v=2
6pσ, v=3
4pσ v=6
∞
32 28 25
np2 v=1
∞
npO v=1
785 786 787 788 789 790
22 21 20 19 18 17 16 15 14 13 11
np2 v=1
40 30 25 23 22 21 20 19 18 17 16 15 14 13 12
npO v=1
7pπ v=2
5pπ v=3
7pσ v=2
4pπ v=4
5pσ v=3
790 791 792 793 794 795
10
9pπ
8pπ np2 v=1
11 10 9pσ
npO v=1
6pπ v=2
4pσ v=5
6pσ v=2
795 796 797 798 799 800
np2 v=1
8pσ
npO v=1
∞ 32 25
np2 v=0
5pπ v=2
∞
npO v=0
7pπ v=1
800 801 802 803 804 805
PHOTON WAVELENGTH (Å)
PHOTOIONIZATION EFFICIENCY (arbitrary units)

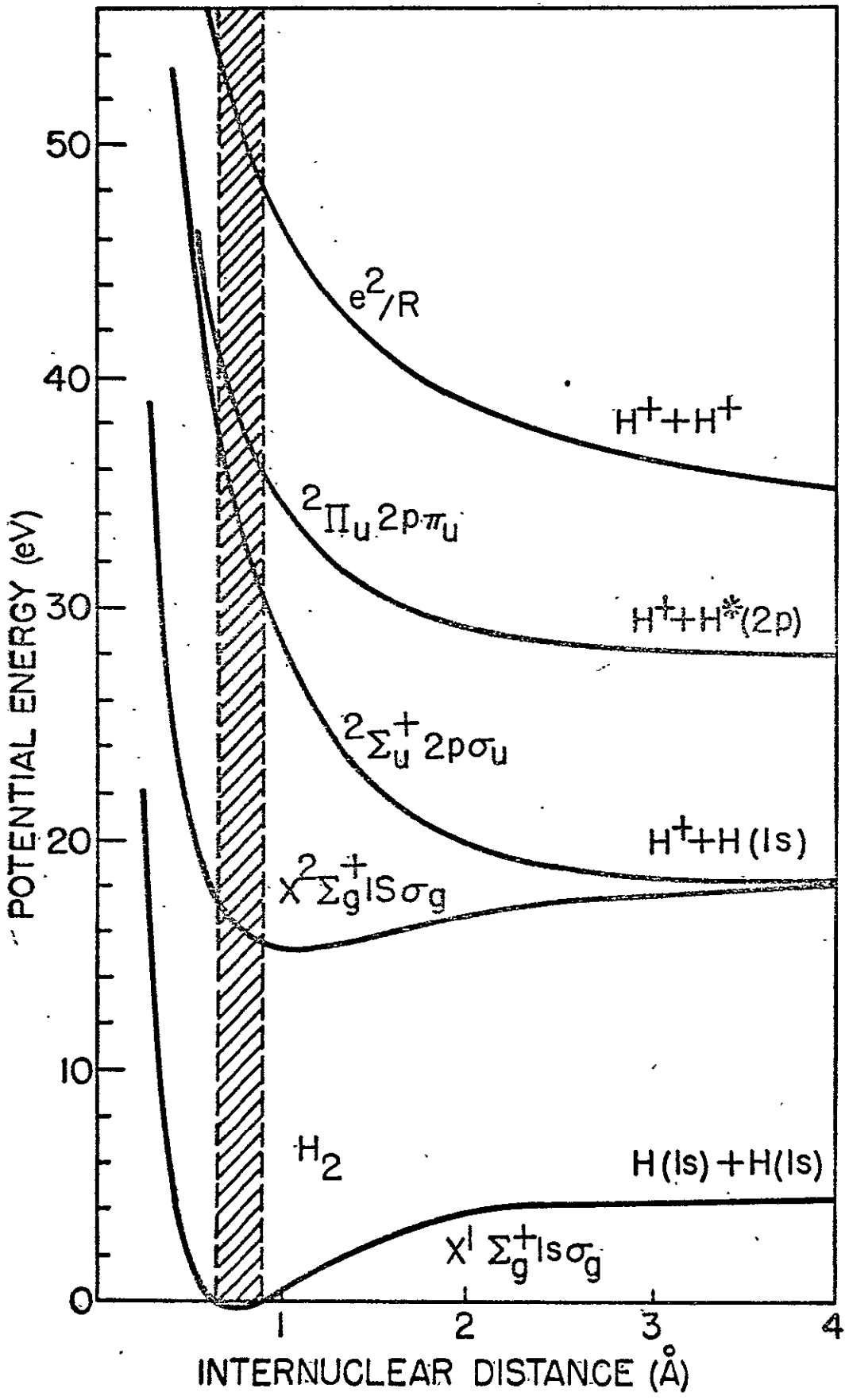
POTENTIAL ENERGY (eV)
0
10
20
30
40
50
1
2
3
4
INTERNUCLEAR DISTANCE (Å)
e^2/R
$H^+ + H^+$
$^2\Pi_u 2p\pi_u$
$H^+ + H^*(2p)$
$^2\Sigma_u^+ 2p\sigma_u$
$H^+ + H(1s)$
$X^2\Sigma_g^+ 1s\sigma_g$
H_2
$H(1s) + H(1s)$
$X^1\Sigma_g^+ 1s\sigma_g$

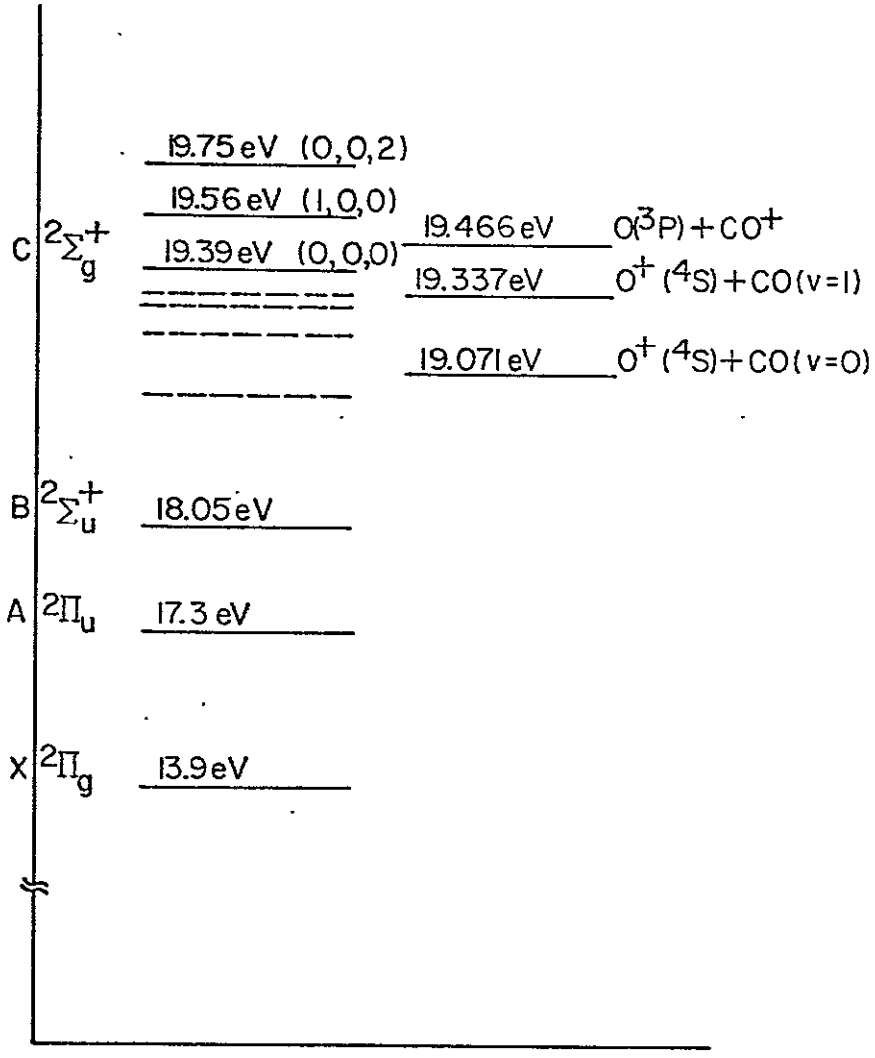
19.75 eV (0,0,2)
19.56 eV (1,0,0)
C $^2\Sigma_g^+$
19.39 eV (0,0,0)
19.466 eV
$O(^3P) + CO^+$
19.337 eV
$O^+(^4S) + CO(v=1)$
19.071 eV
$O^+(^4S) + CO(v=0)$
B $^2\Sigma_u^+$
18.05 eV
A $^2\Pi_u$
17.3 eV
X $^2\Pi_g$
13.9 eV

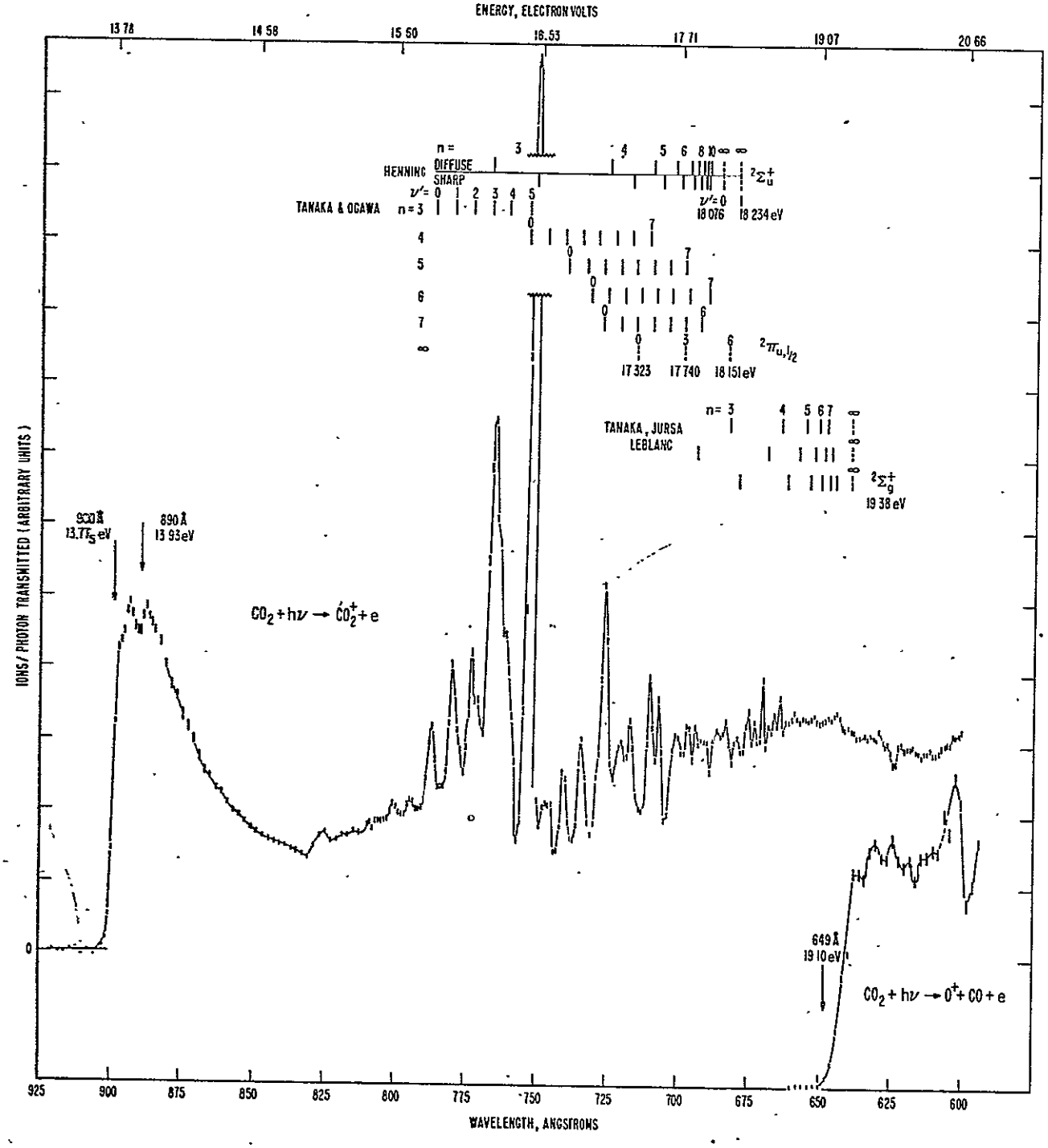

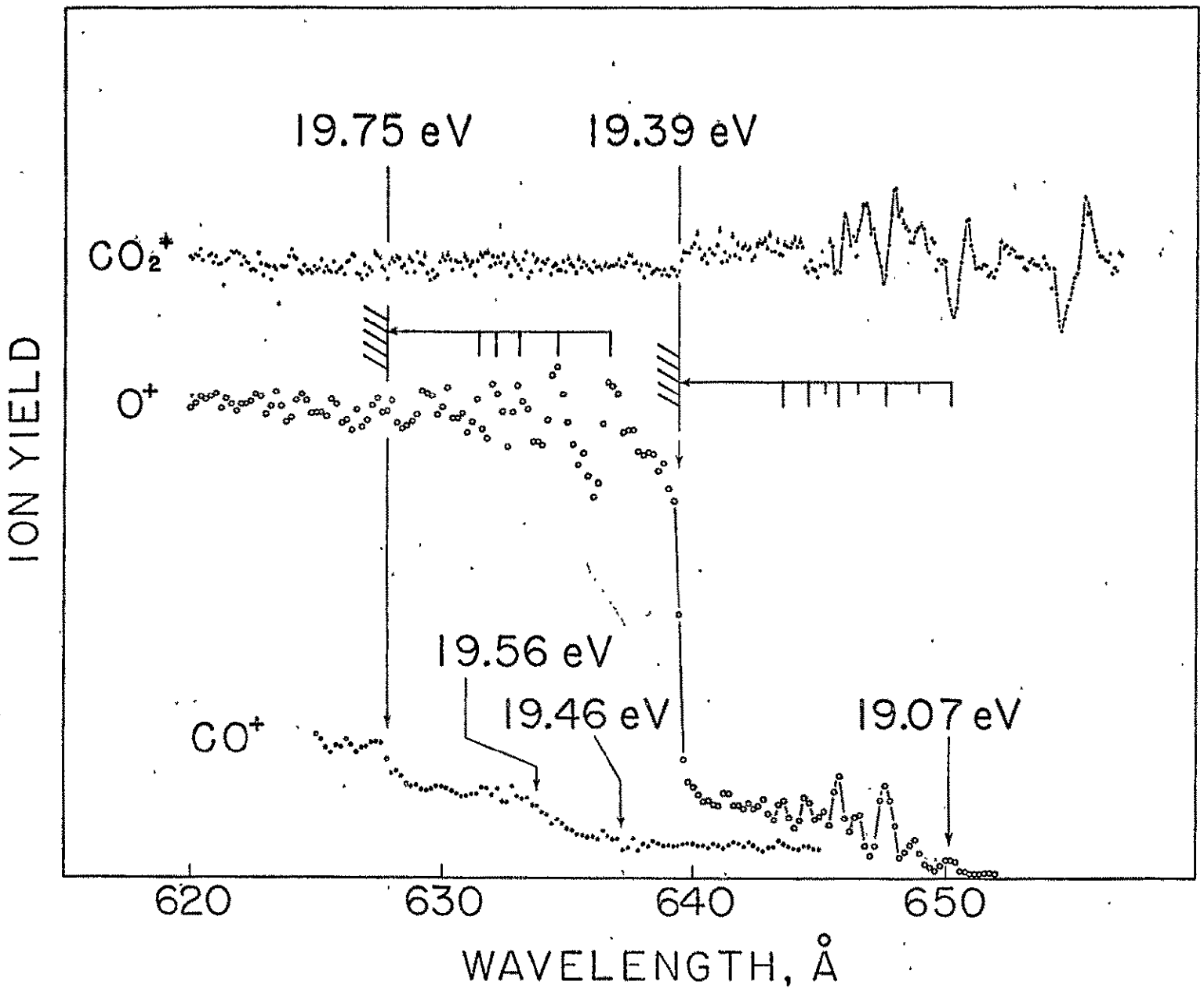
19.75 eV
19.39 eV
CO_2^+
O^+
CO^+
19.56 eV
19.46 eV
19.07 eV
ION YIELD
620
630
640
650
WAVELENGTH, Å

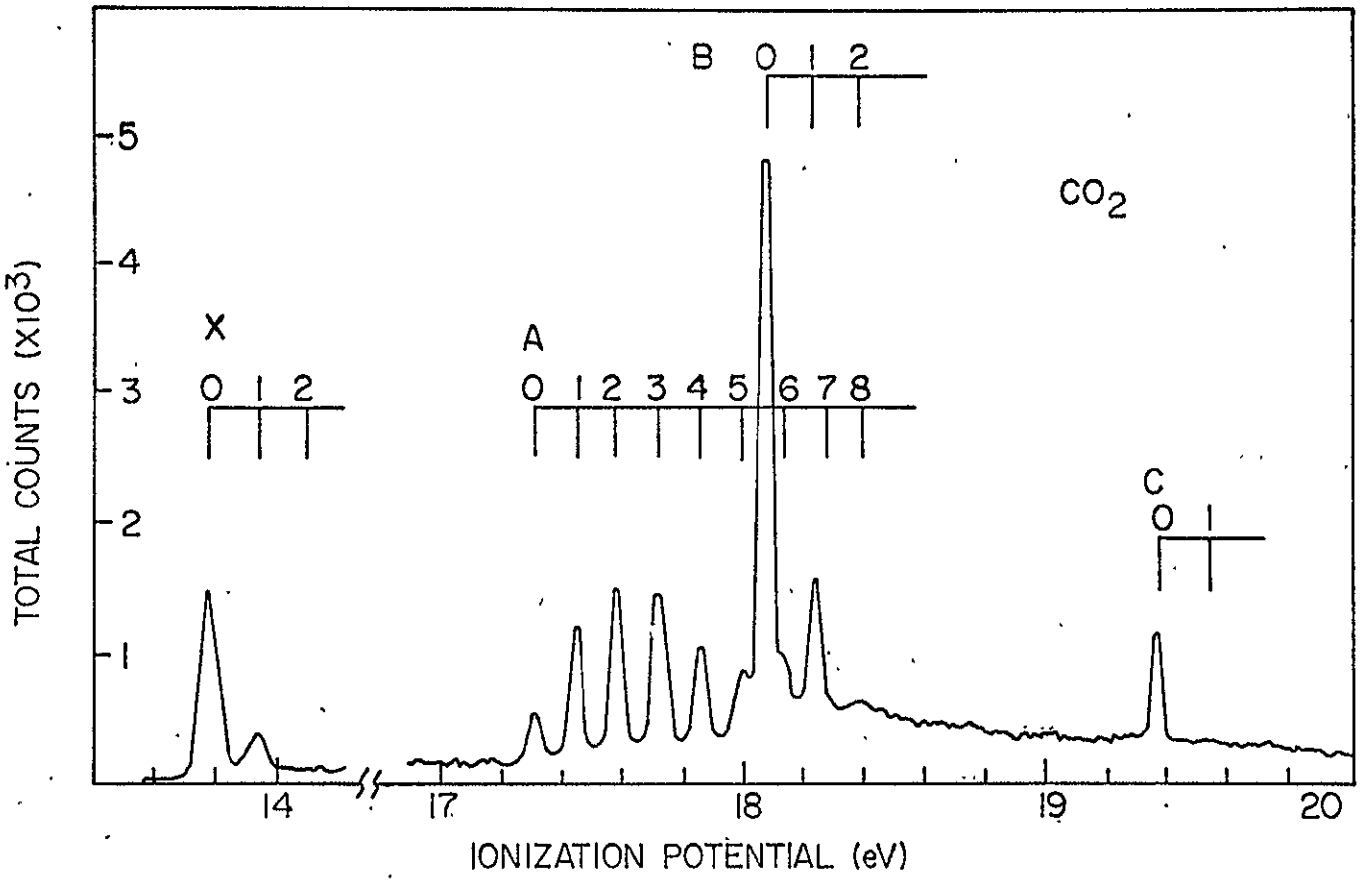
B 0 1 2
CO_2
X
0 1 2
A
0 1 2 3 4 5 6 7 8
C
0 1
TOTAL COUNTS (X10^3)
1
2
3
4
5
14
17
18
19
20
IONIZATION POTENTIAL (eV)

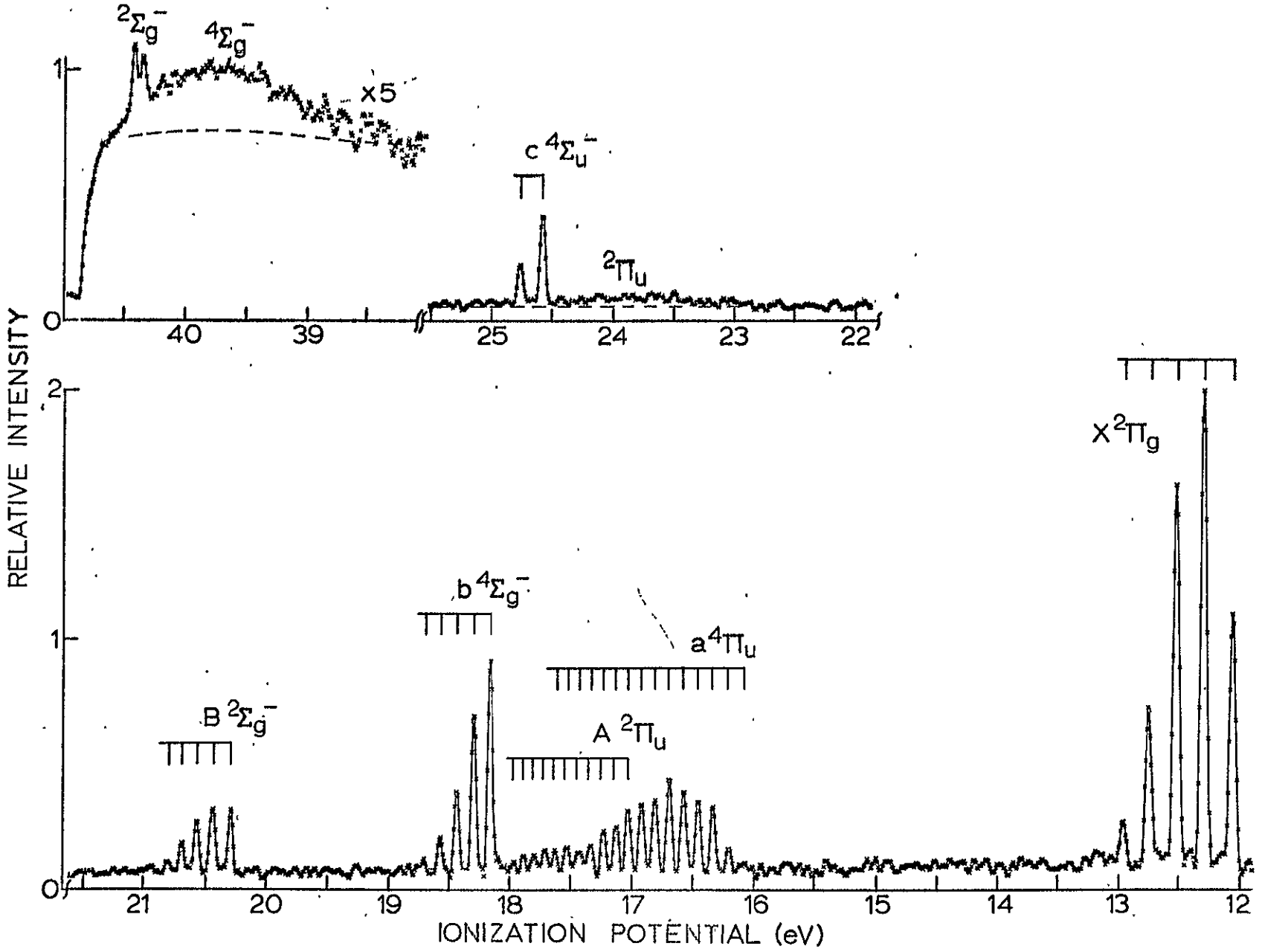

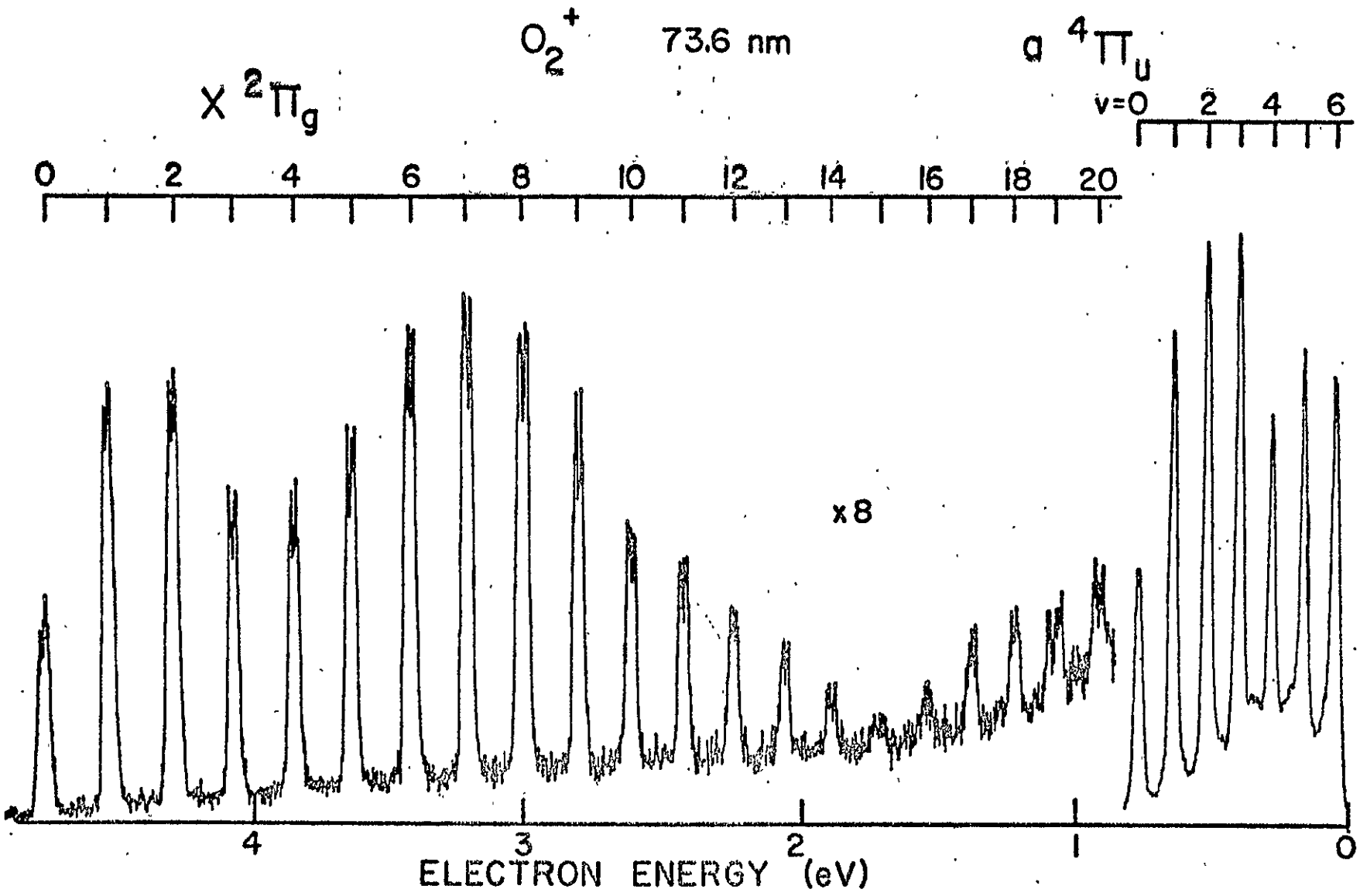
O_2^+
73.6 nm
$a\ ^4\Pi_u$
$X\ ^2\Pi_g$
v=0 2 4 6
0 2 4 6 8 10 12 14 16 18 20
x8
4 3 2 1 0
ELECTRON ENERGY (eV)

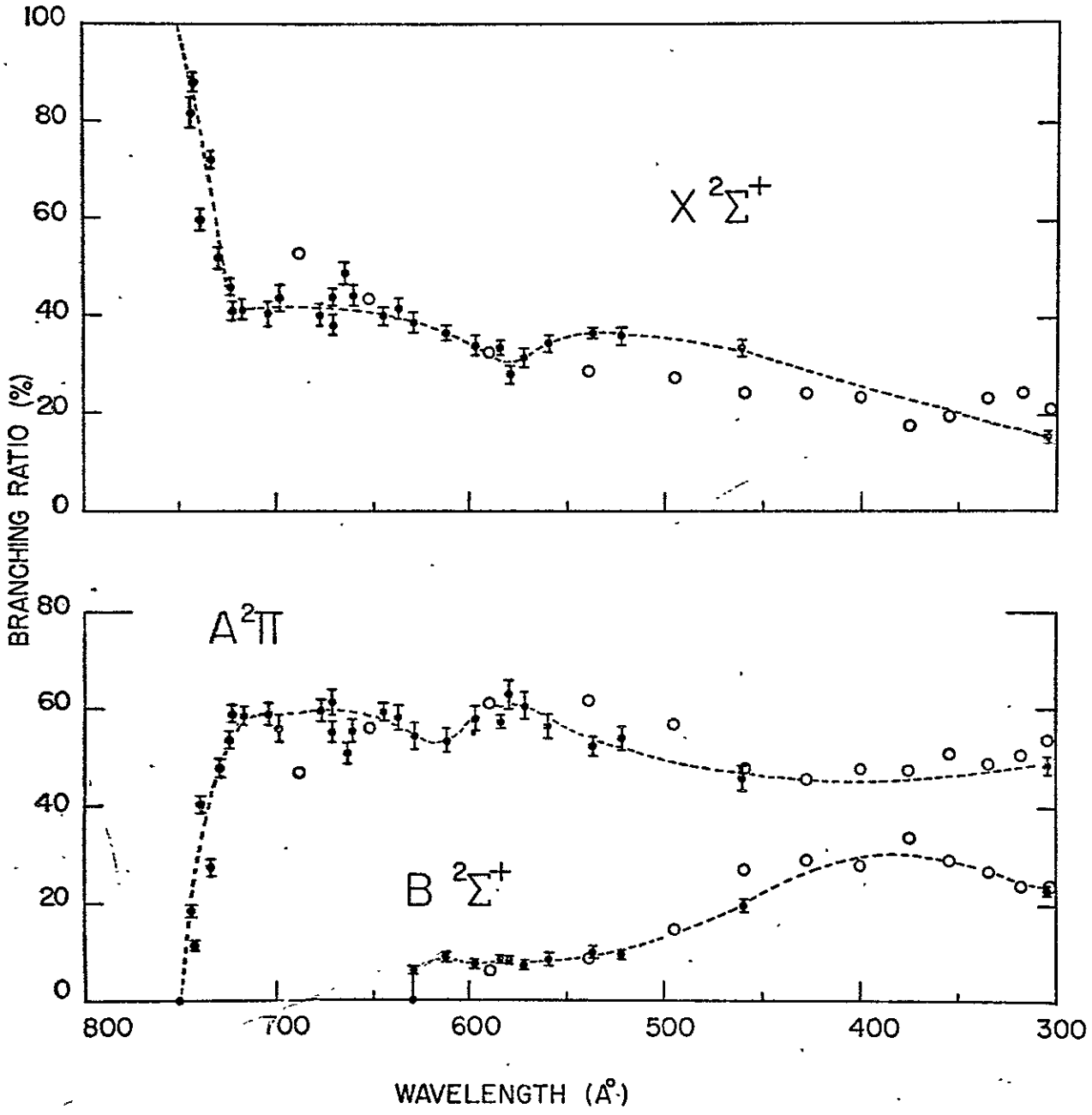
100
80
60
40
20
0
X $^2\Sigma^+$
BRANCHING RATIO (%)
80
60
40
20
0
A $^2\Pi$
B $^2\Sigma^+$
800
700
600
500
400
300
WAVELENGTH (Å)

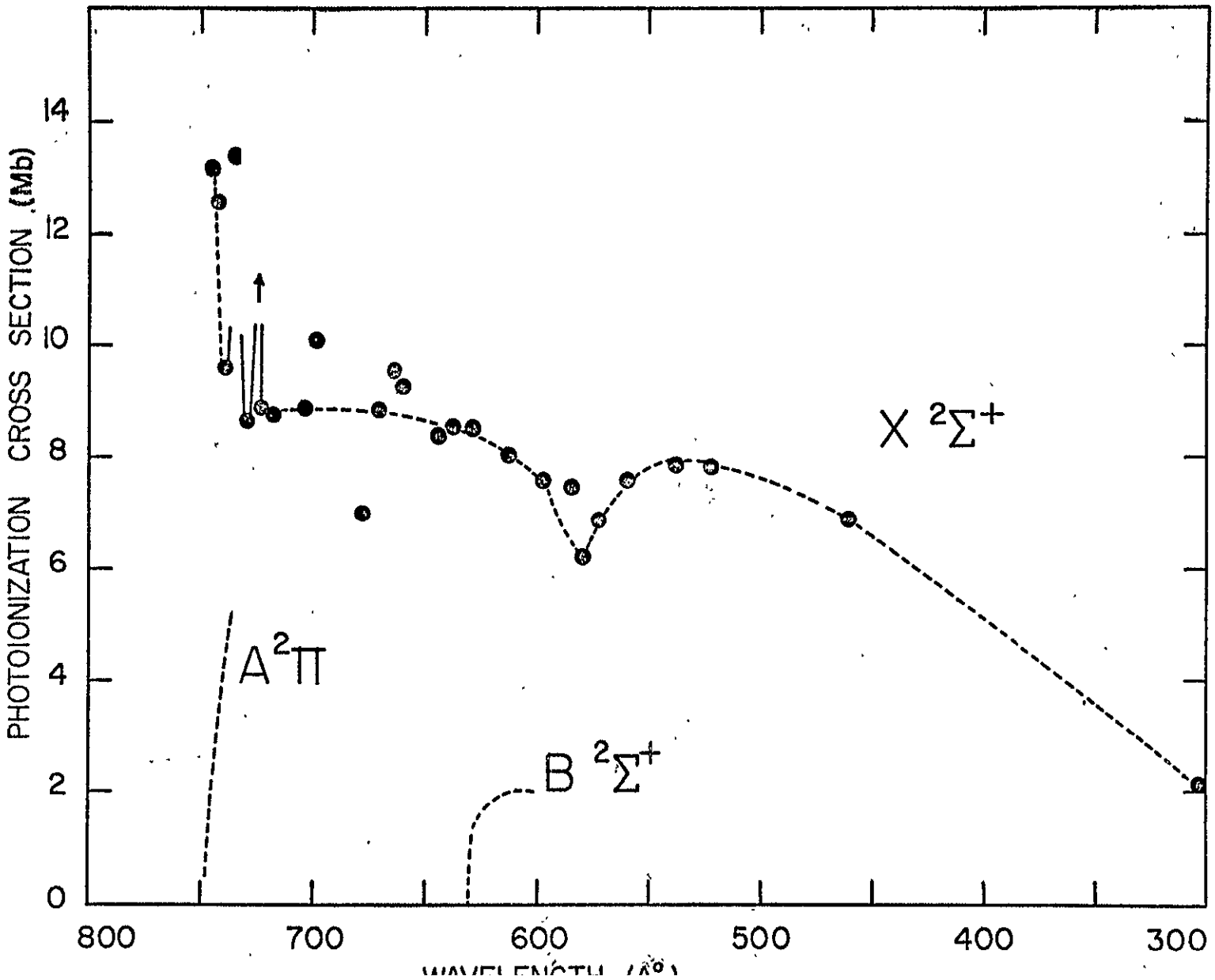
PHOTOIONIZATION CROSS SECTION (Mb)
0
2
4
6
8
10
12
14
800
700
600
500
400
300
X $^2\Sigma^+$
A $^2\Pi$
B $^2\Sigma^+$

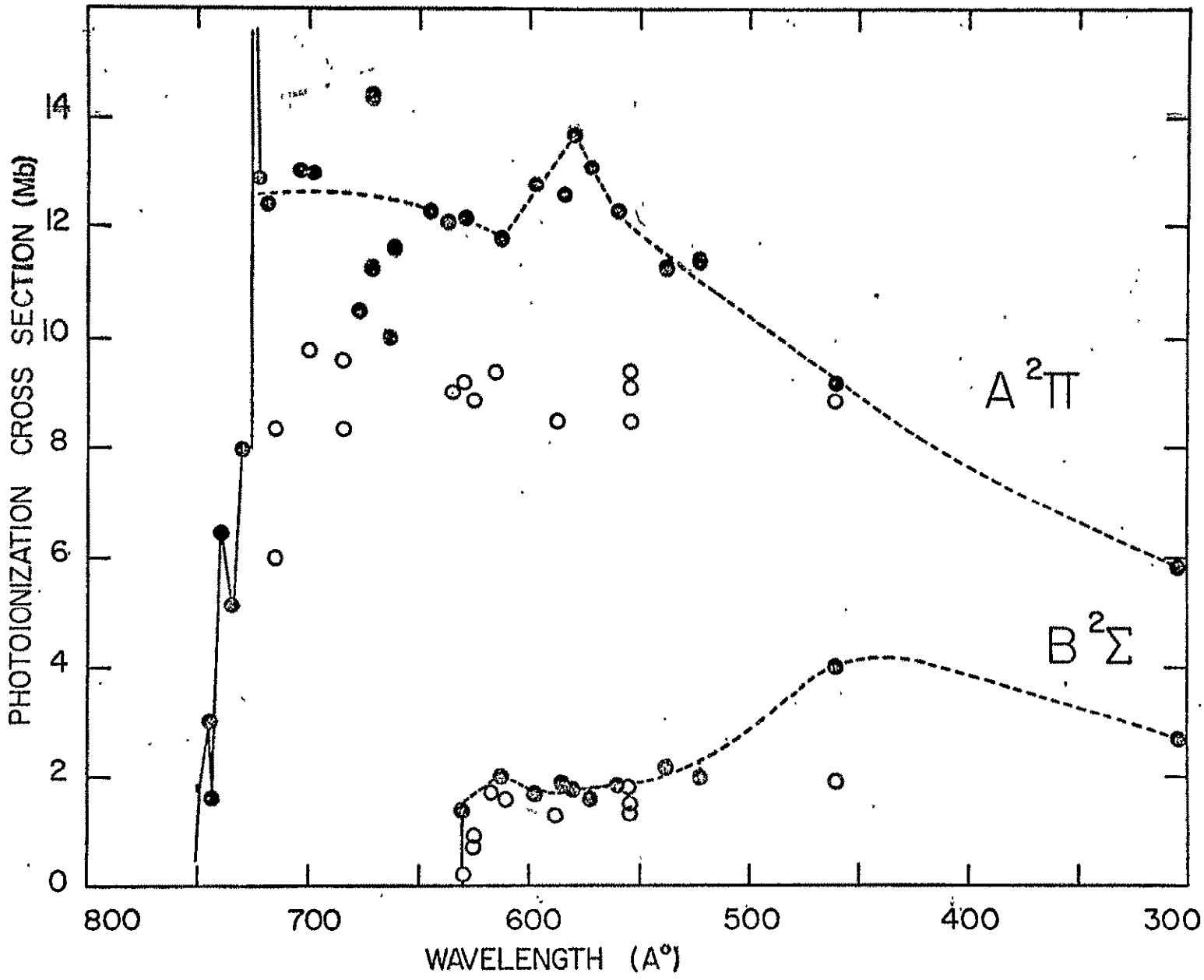
PHOTOIONIZATION CROSS SECTION (Mb)
0
2
4
6
8
10
12
14
800
700
600
500
400
300
WAVELENGTH (A°)
A ²Π
B ²Σ

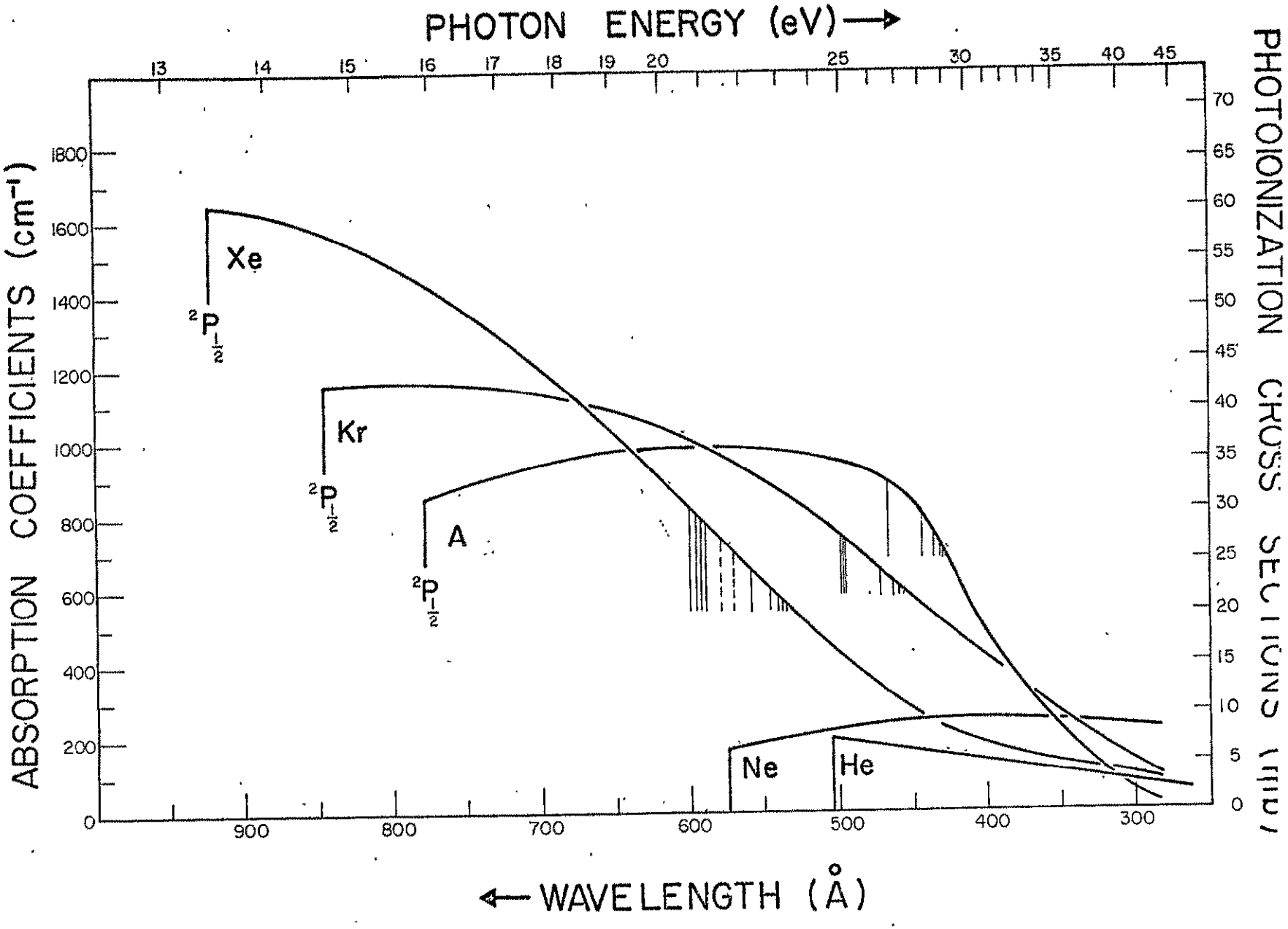

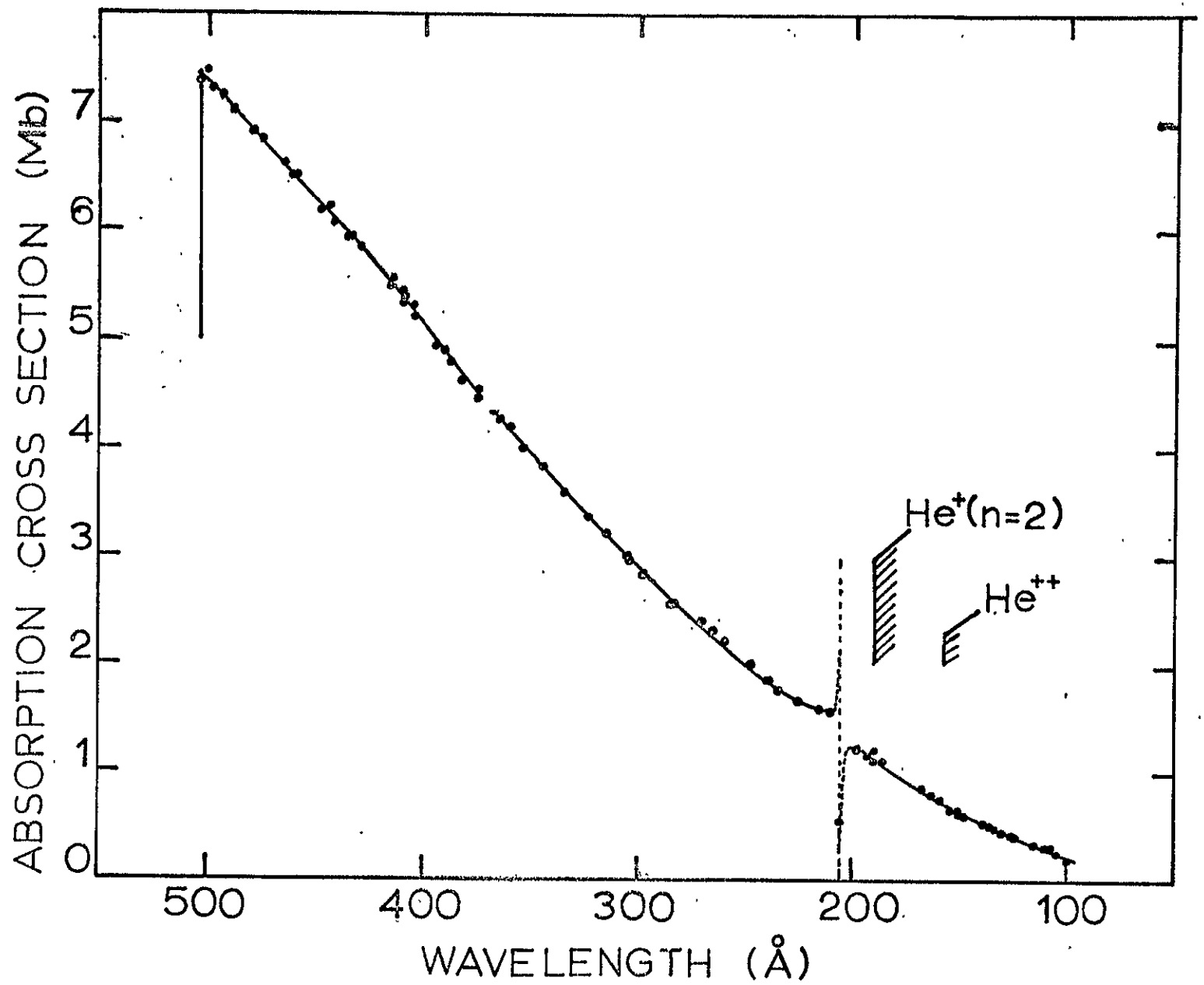
ABSORPTION CROSS SECTION (Mb)
0
1
2
3
4
5
6
7
500
400
300
200
100
WAVELENGTH (Å)
He+(n=2)
He++

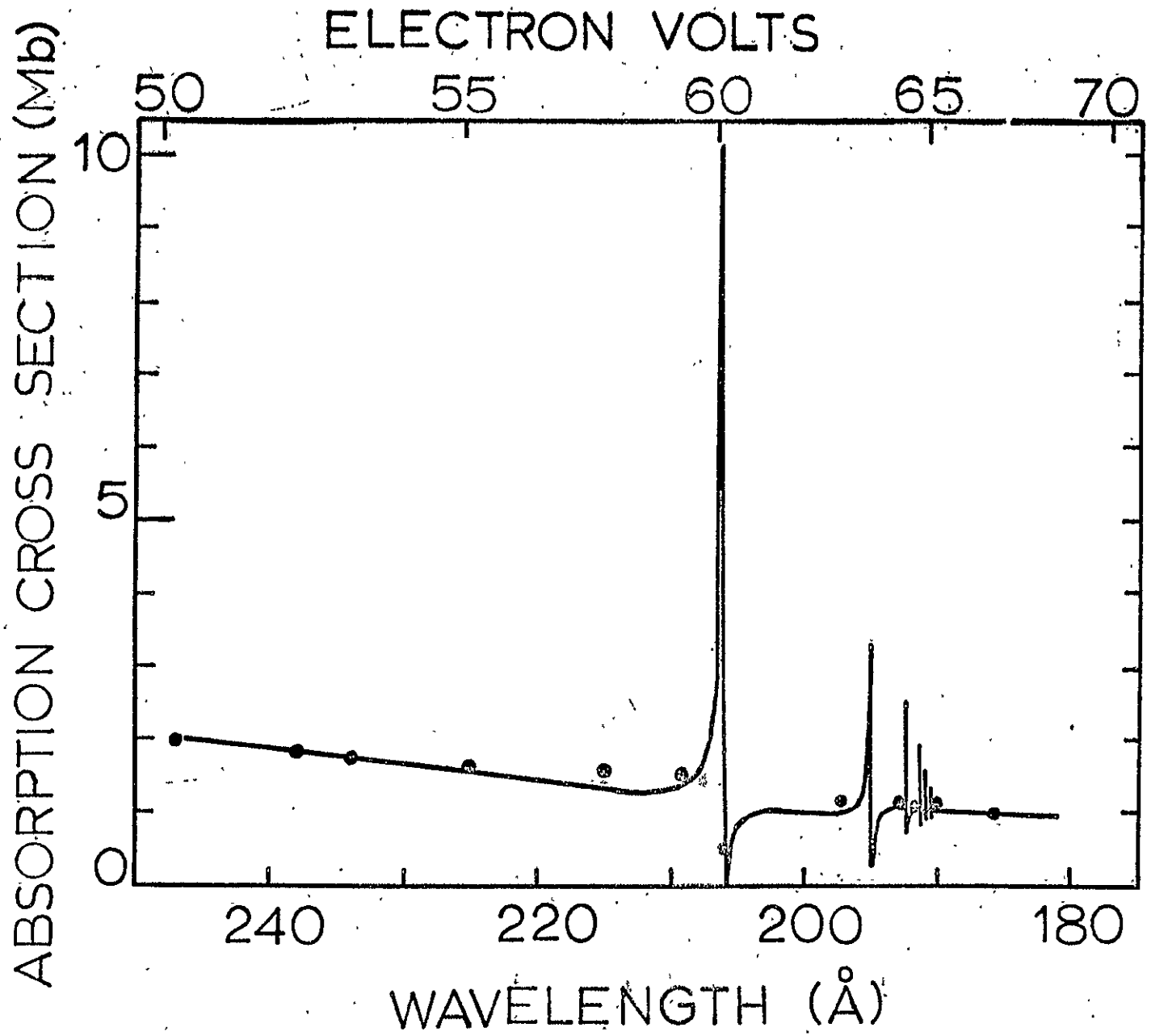
ELECTRON VOLTS
50
55
60
65
70
ABSORPTION CROSS SECTION (Mb)
10
5
0
240
220
200
180
WAVELENGTH (Å)

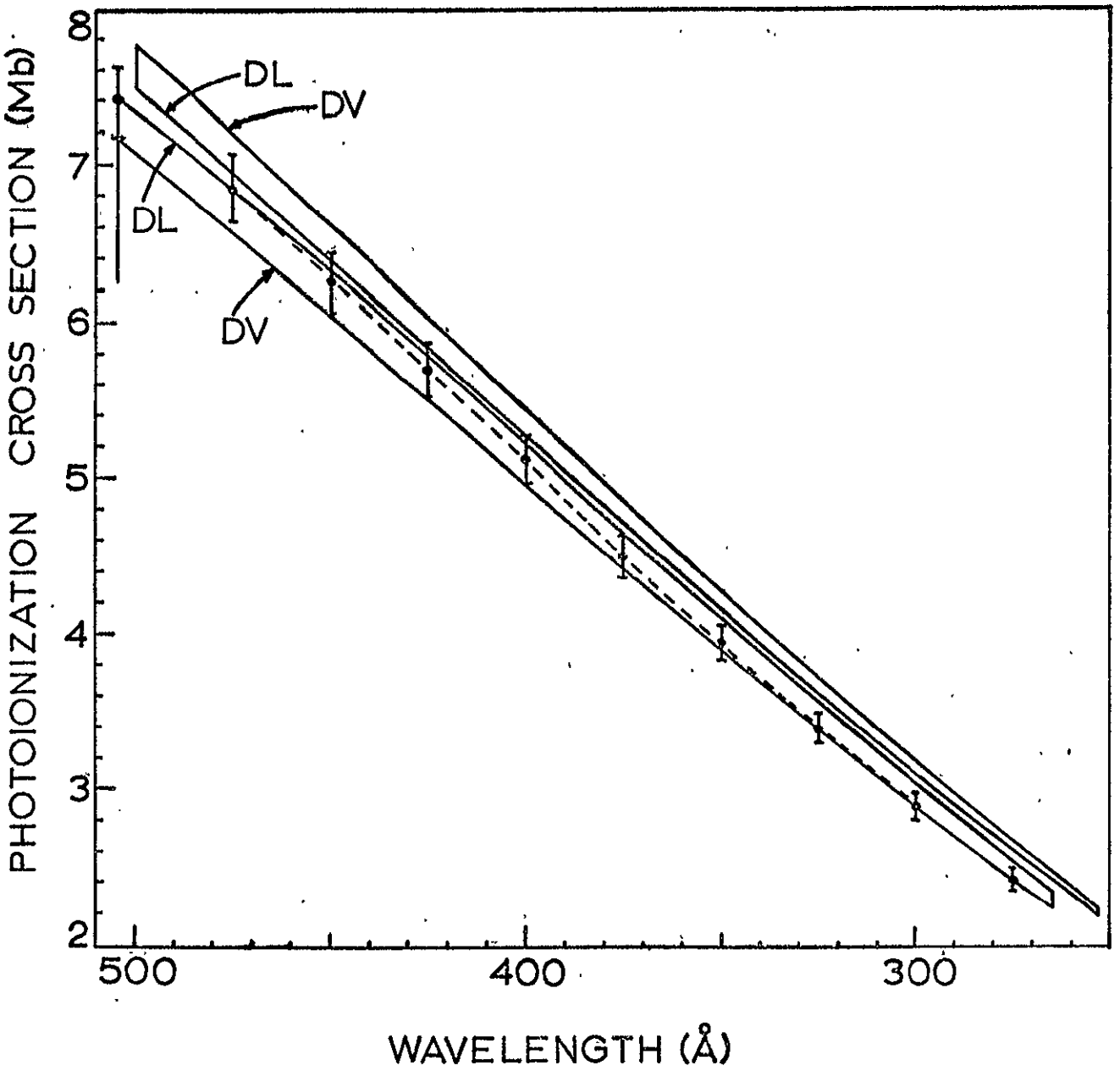
PHOTOIONIZATION CROSS SECTION (Mb)
8
7
6
5
4
3
2
DL
DV
DL
DV
500
400
300
WAVELENGTH (Å)

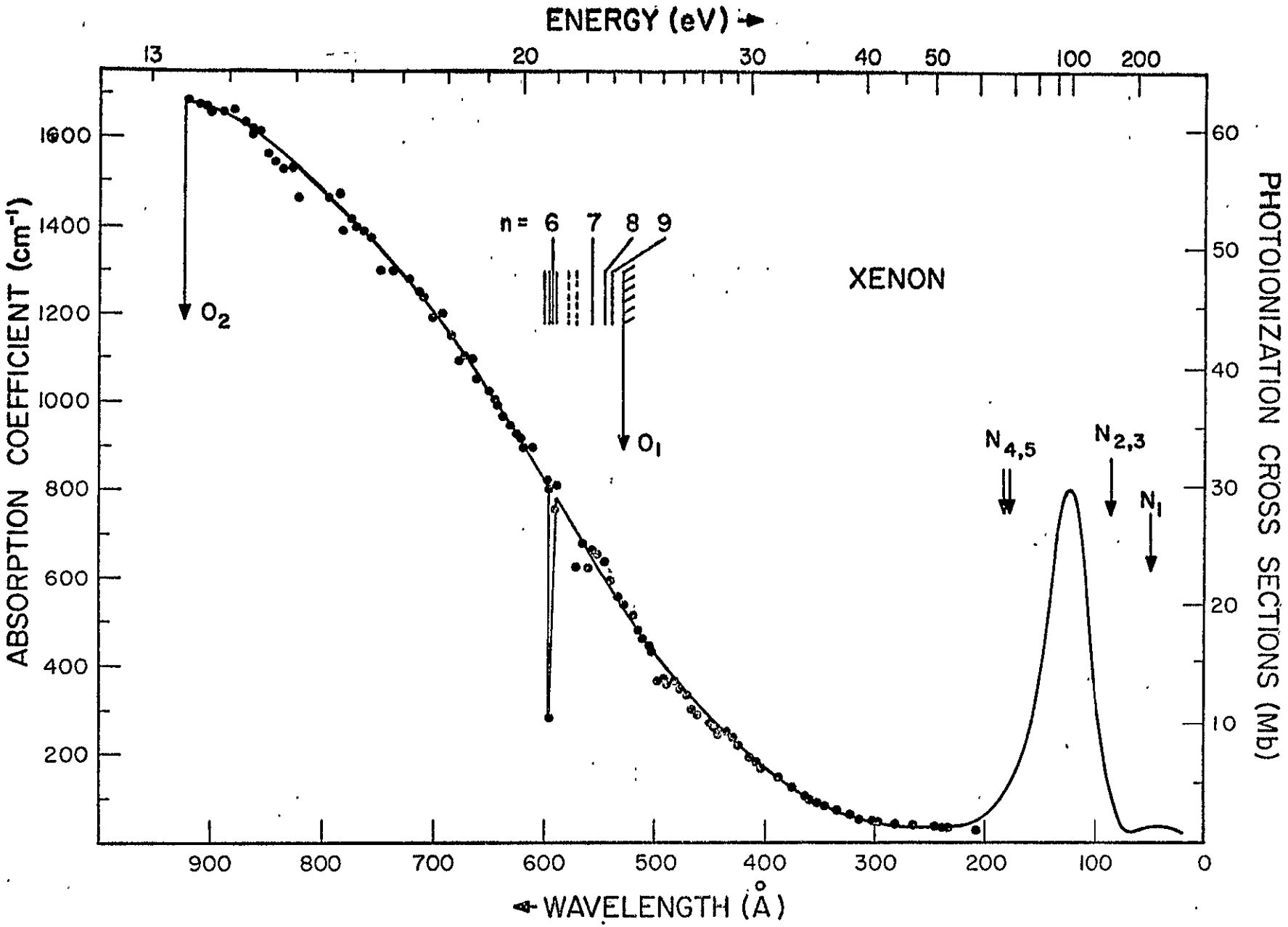

50

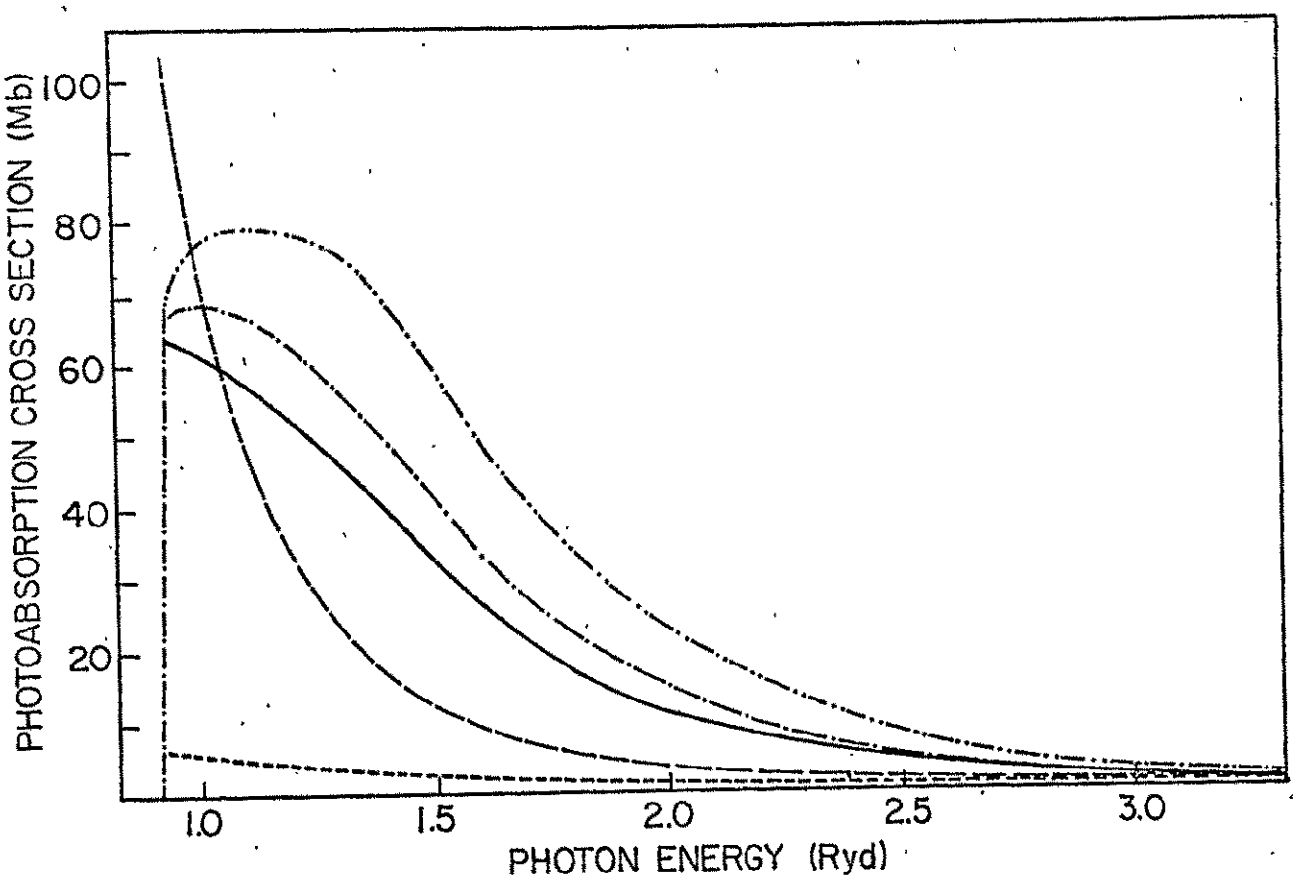
PHOTOABSORPTION CROSS SECTION (Mb)
100
80
60
40
20
1.0
1.5
2.0
2.5
3.0
PHOTON ENERGY (Ryd)

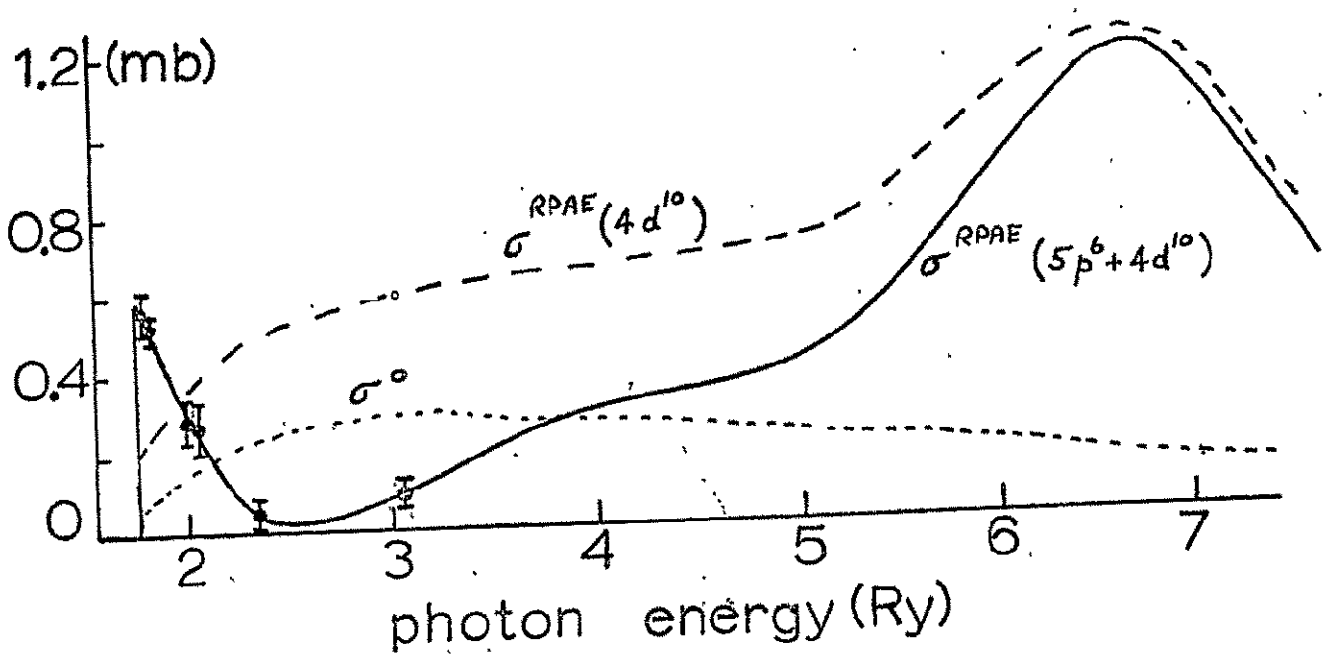
1.2
(mb)
0.8
0.4
0
$\sigma^{RPAE}(4d^{10})$
$\sigma^{RPAE}(5p^6+4d^{10})$
σ°
2
3
4
5
6
7
photon energy (Ry)

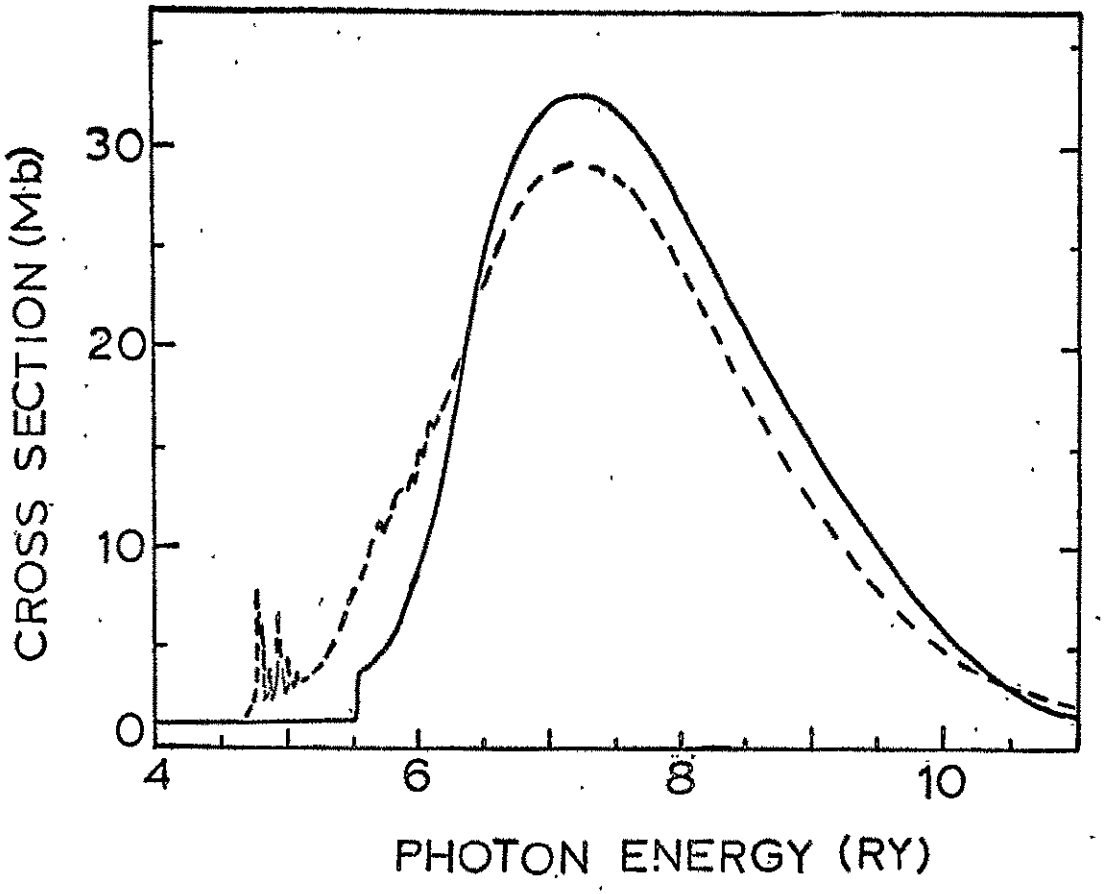
CROSS SECTION (Mb)
30
20
10
0
4
6
8
10
PHOTON ENERGY (RY)

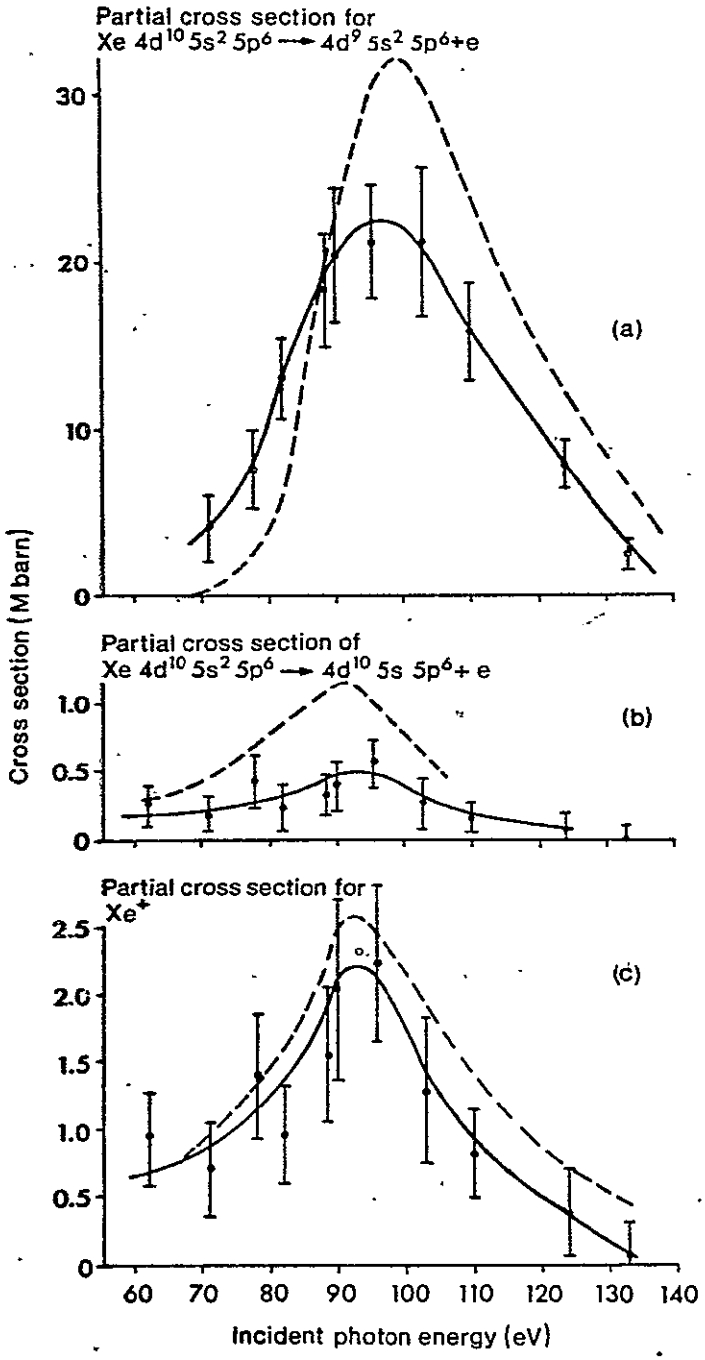

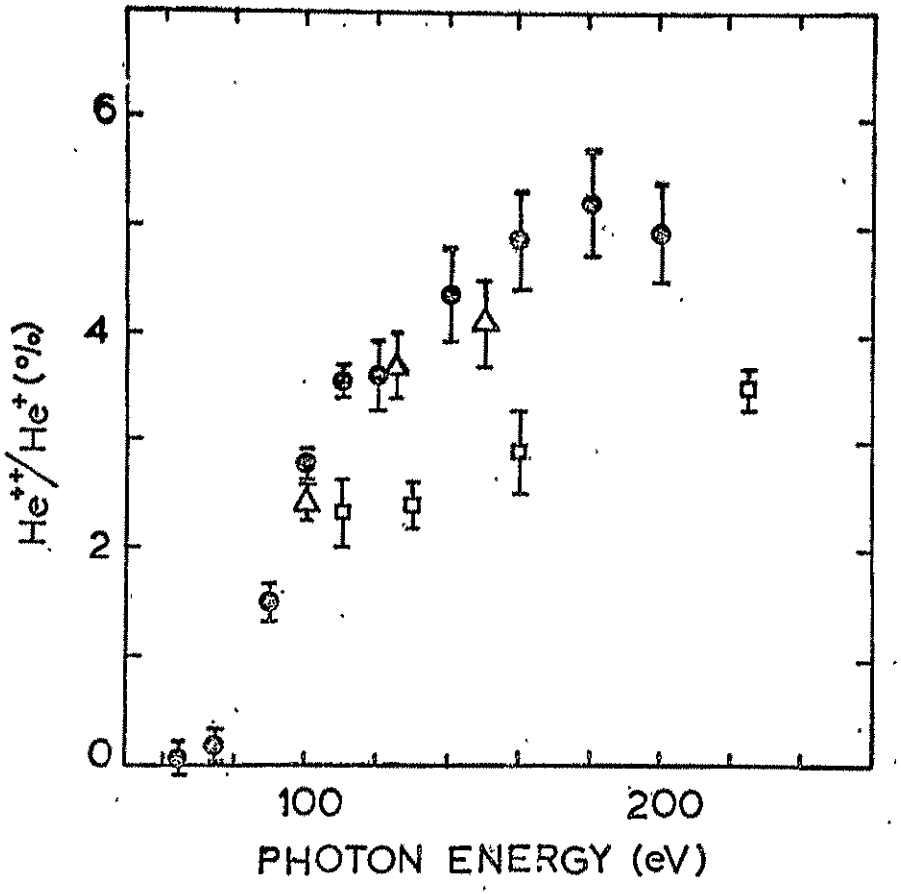
6
4
2
0
100
200
PHOTON ENERGY (eV)
He++/He+ (%)

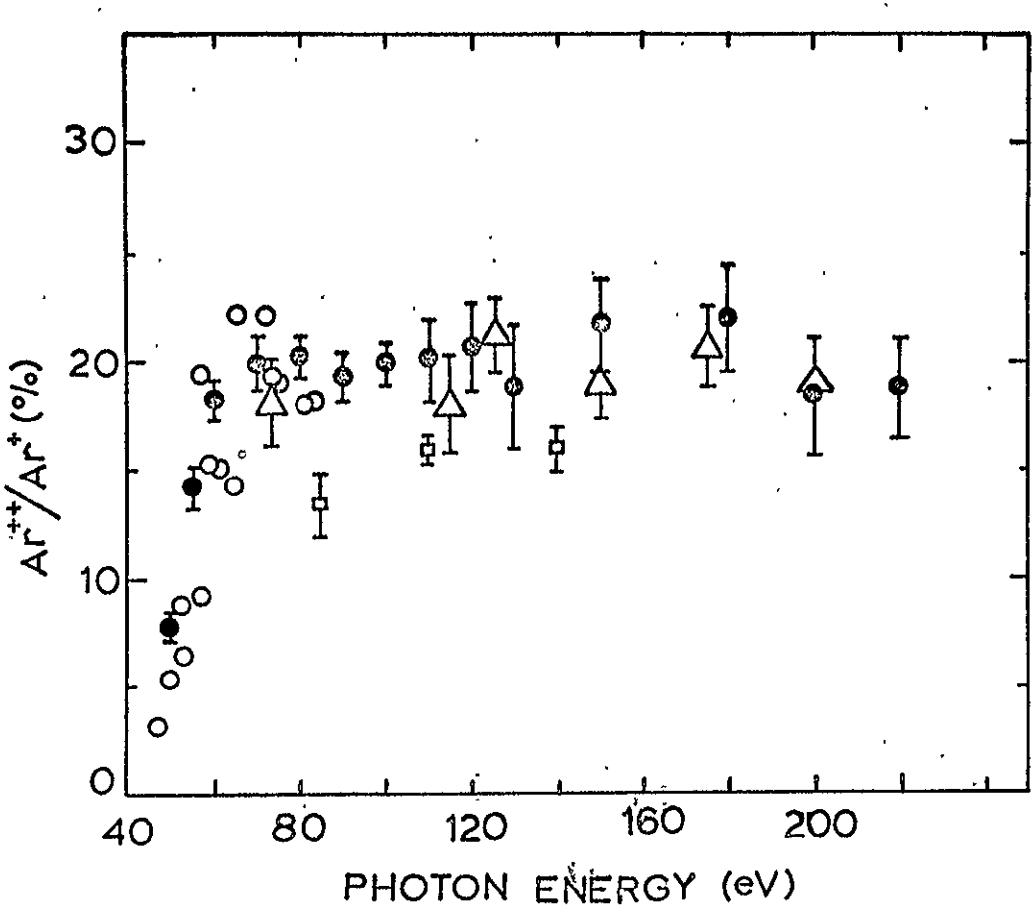
30
20
10
0
40
80
120
160
200
Ar^{++}/Ar^{+} (%)
PHOTON ENERGY (eV)

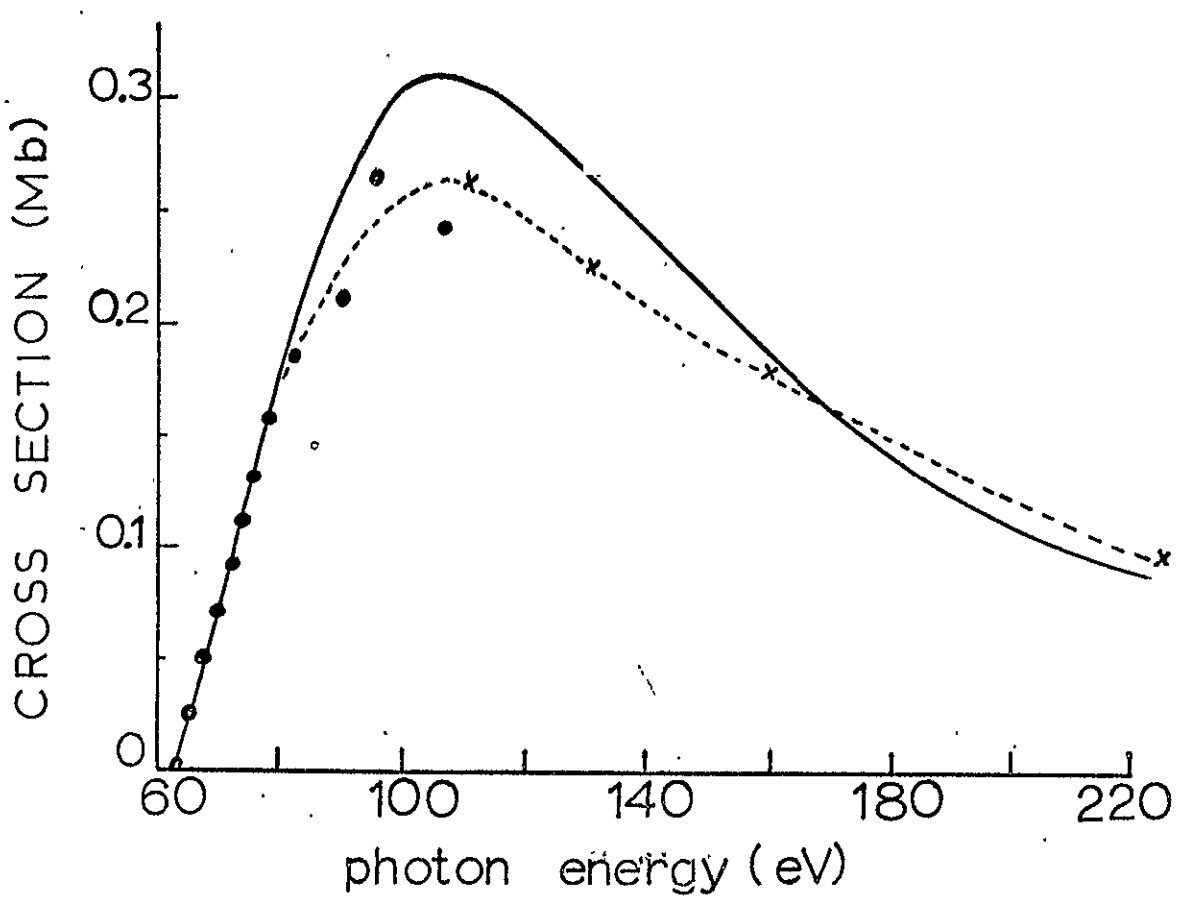
CROSS SECTION (Mb)
0.3
0.2
0.1
0
60
100
140
180
220
photon energy (eV)

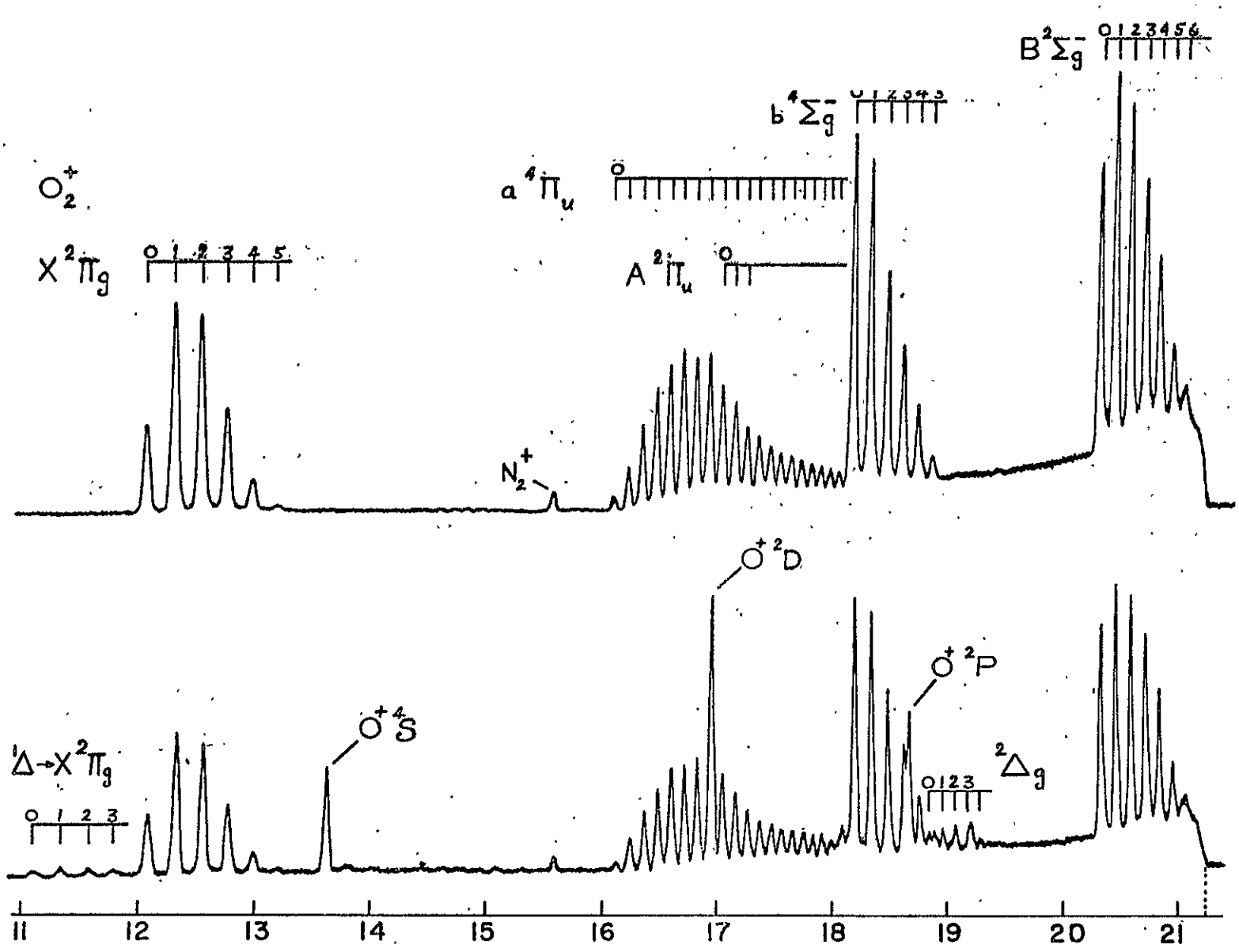

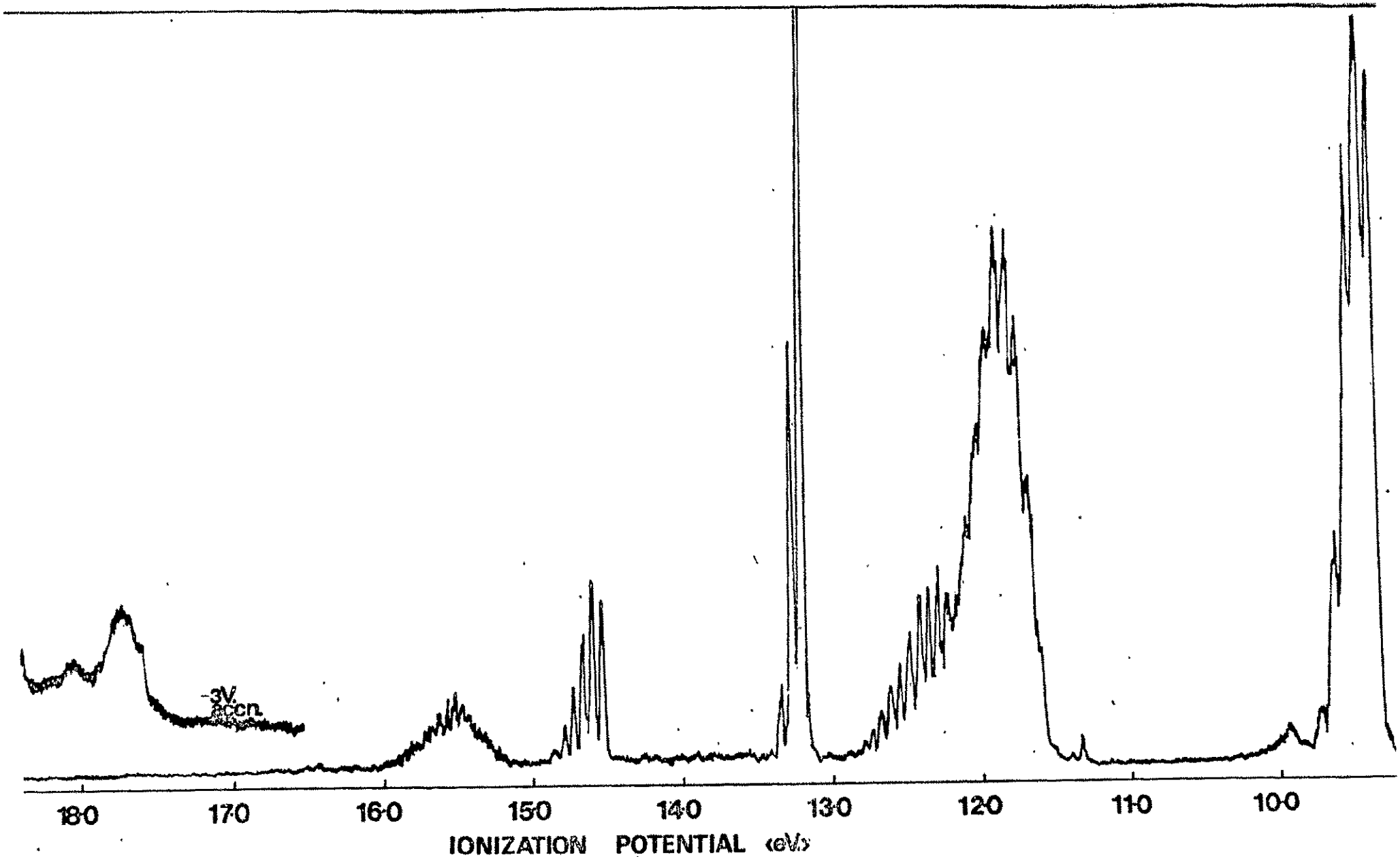
3V
Accn.
18·0
17·0
16·0
15·0
14·0
13·0
12·0
11·0
10·0
IONIZATION POTENTIAL (eV)

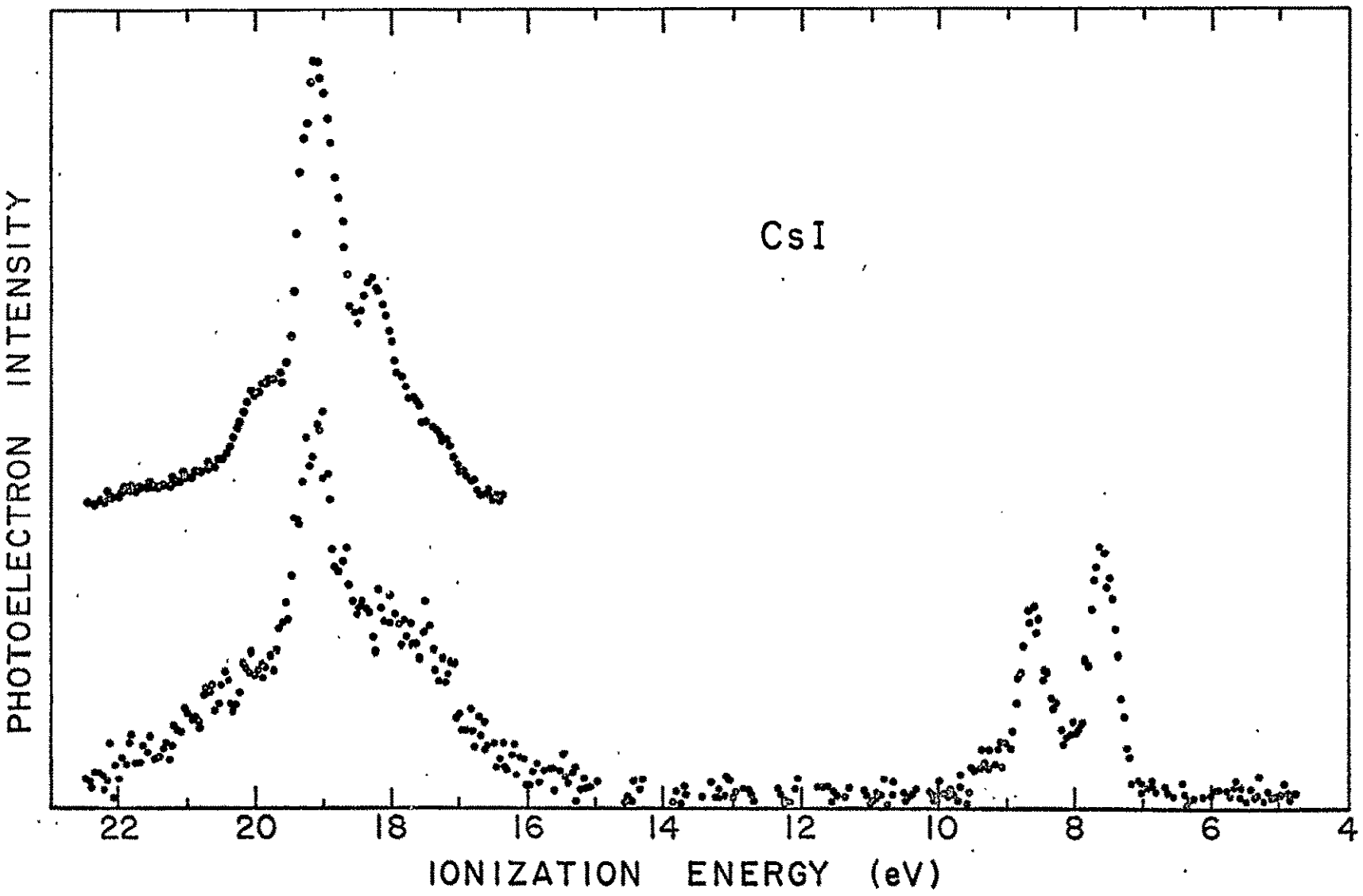
CsI
PHOTOELECTRON INTENSITY
22
20
18
16
14
12
10
8
6
4
IONIZATION ENERGY (eV)

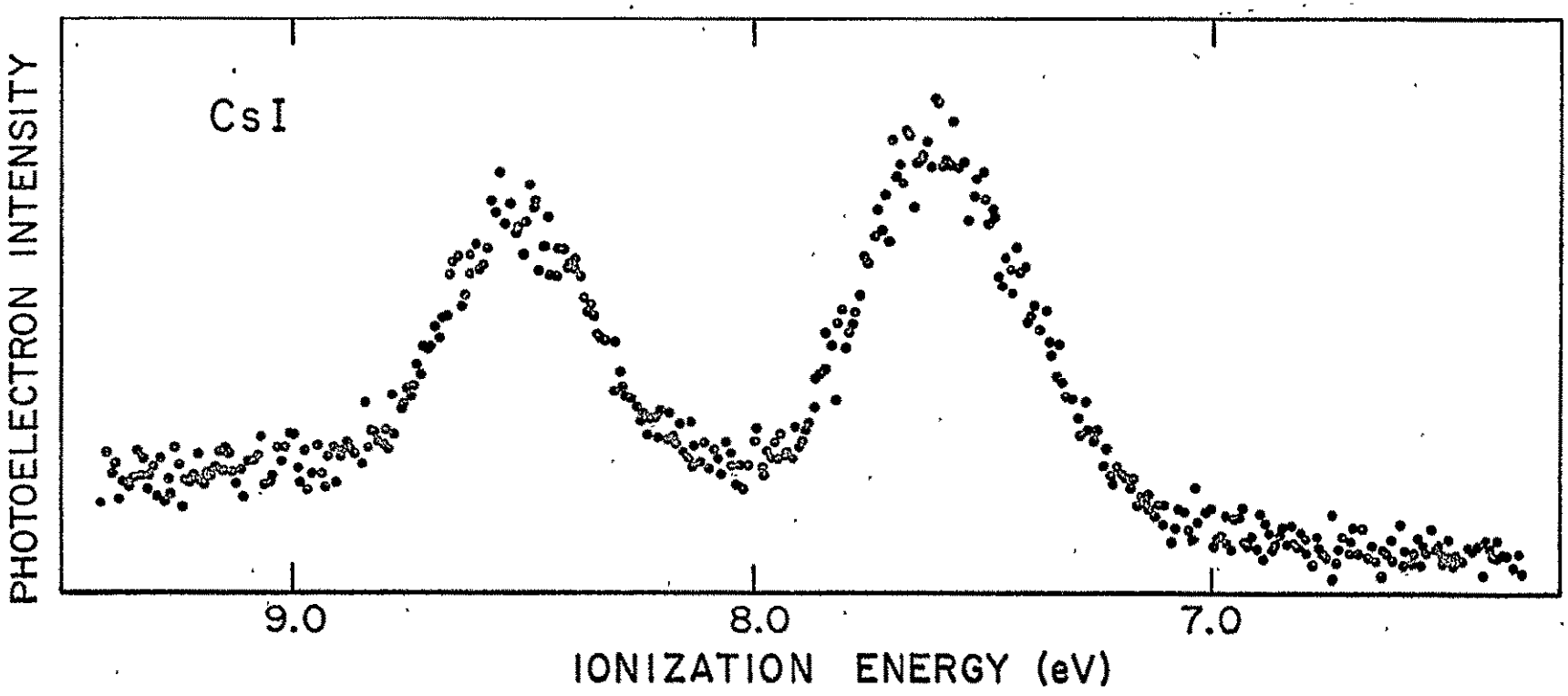
CsI
PHOTOELECTRON INTENSITY
9.0
8.0
7.0
IONIZATION ENERGY (eV)

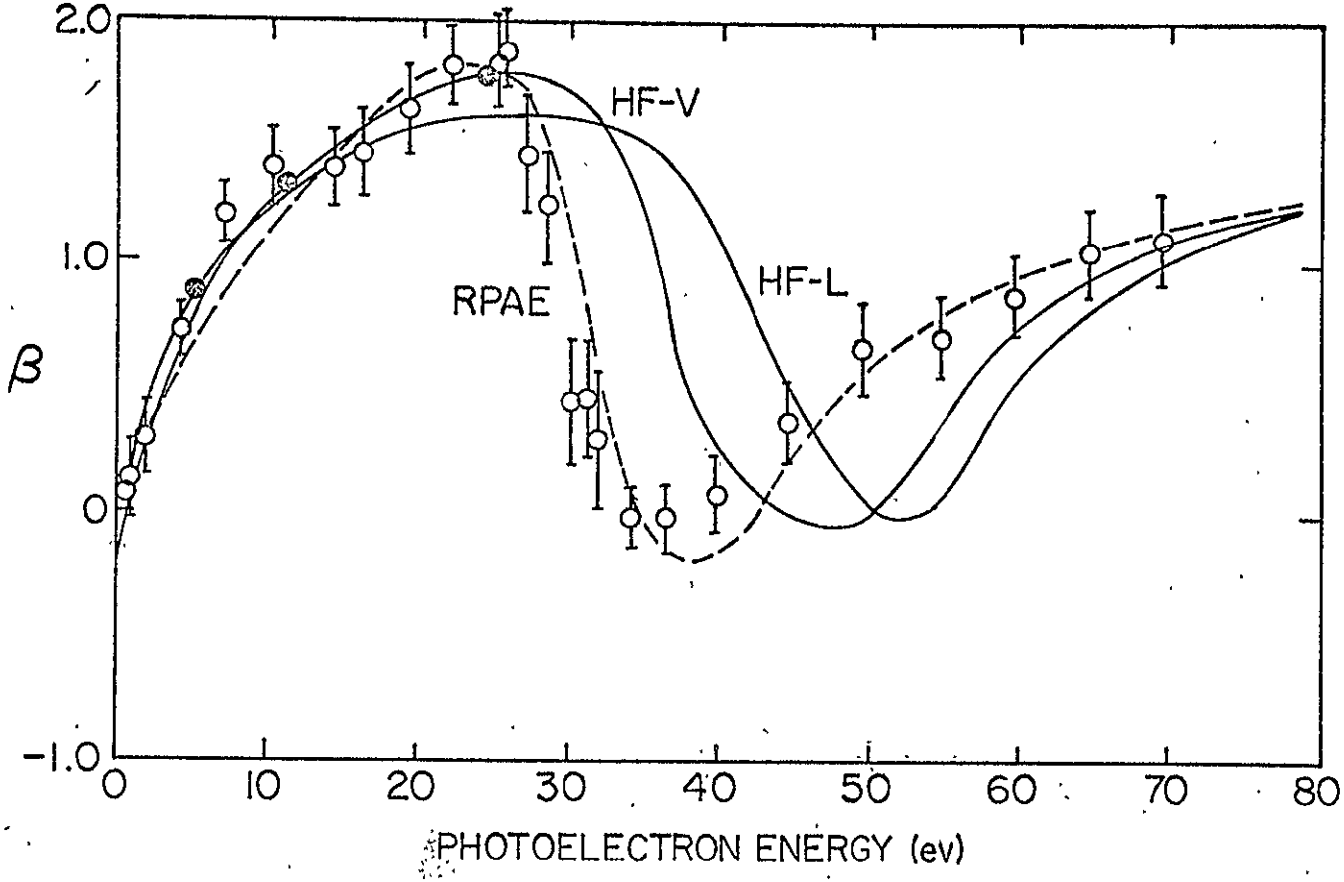
2.0
1.0
0
-1.0
β
HF-V
HF-L
RPAE
0
10
20
30
40
50
60
70
80
PHOTOELECTRON ENERGY (ev)

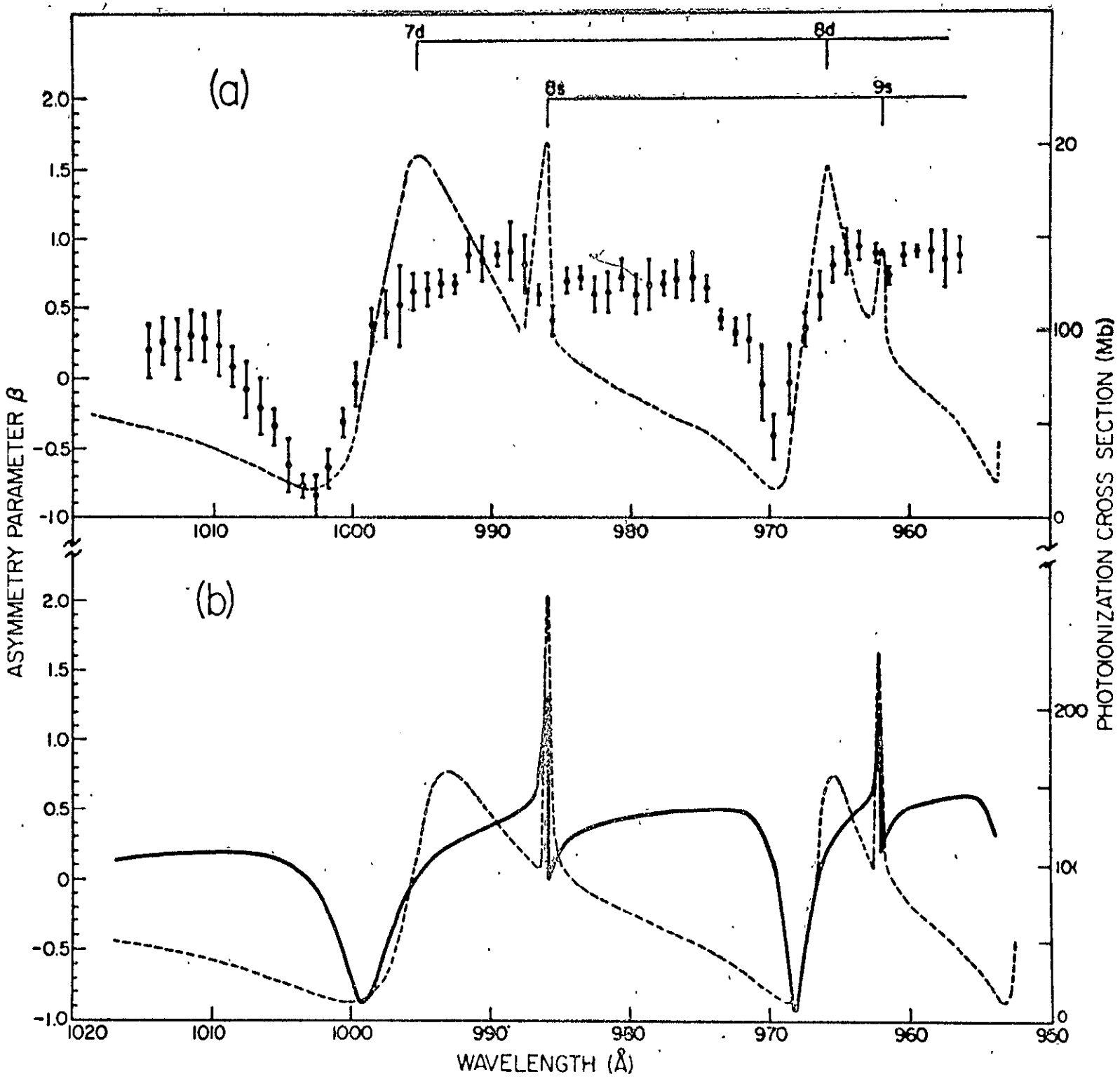
(a)
7d
8d
8s
9s
2.0
1.5
1.0
0.5
0
-0.5
-1.0
1010
1000
990
980
970
960
20
100
0
(b)
1020
950
200
WAVELENGTH (Å)
ASYMMETRY PARAMETER β
PHOTOIONIZATION CROSS SECTION (Mb)